NASA CR 72737
PWA-3933

DEVELOPMENT OF MAINSHAFT SEALS FOR ADVANCED AIR BREATHING PROPULSION SYSTEMS — PHASE II —

BY

V. P. POVINELLI AND A. H. McKIBBIN

Pratt & Whitney Aircraft
DIVISION OF UNITED AIRCRAFT CORPORATION

prepared for

NATIONAL AERONAUTICS AND SPACE ADMINISTRATION

NASA Lewis Research Center
Contract NAS3-7609
L. P. Ludwig, Project Manager

Requests for copies of this report should be referred to

National Aeronautics and Space Administration
Scientific and Technical Information Facility
P. O. Box 33
College Park, Md. 20740

NASA CR 72737
PWA-3933

FINAL REPORT – PHASE II

DEVELOPMENT OF MAINSHAFT SEALS FOR ADVANCED AIR BREATHING PROPULSION SYSTEMS

by

V. P. Povinelli
Project Manager

and

A. H. McKibbin
Assistant Project Engineer,
Analytical

PRATT & WHITNEY AIRCRAFT
DIVISION OF UNITED AIRCRAFT CORPORATION
East Hartford, Conn.

prepared for

NATIONAL AERONAUTICS AND SPACE ADMINISTRATION

23 June 1970

CONTRACT NAS 3-7609

NASA Lewis Research Center
Cleveland, Ohio
L. P. Ludwig, Project Manager
Fluid System Components Division

PREFACE

This report describes the work conducted during Phase II of contract NAS3-7609 by the Pratt & Whitney Aircraft Division of United Aircraft Corporation, East Hartford, Connecticut. Phase II was initiated on 26 July 1967 and completed on 25 May 1970. The work was performed for the Lewis Research Center of the National Aeronautics and Space Administration.

Alton J. Parks was Project Manager for Pratt & Whitney Aircraft from the initiation of Phase II until February 1969. Valentine P. Povinelli was Project Manager for Pratt & Whitney Aircraft for Phase II from March 1969 to its conclusion.

The authors wish to express their appreciation for the assistance provided by the Stein Seal Company, who manufactured the seals tested under this contract.

The following National Aeronautics and Space Administration personnel were assigned to this project:

Contracting Officer	J. E. Dilley
Contract Administrator	E. Schiopota
Project Manager	L. P. Ludwig

SUMMARY

During Phase II, two different types of mainshaft face seals for advanced gas-turbine engines were designed, fabricated, and tested. The seals were designed by NASA on the basis of experience gained during Phase I of this contract. The seal designs incorporated lift geometries which used the relative motion between the primary seal faces to provide positive separation (film lubrication). One design operated with a self-acting gas film separating the sealing faces, the other was designed for hydrodynamic oil-film separation.

Pratt & Whitney Aircraft's objectives under Phase II of this contract were to review the NASA layout drawings and design analyses, prepare detail drawings, purchase hardware, test the seals, and analyze the test results. Review of the NASA designs resulted in minor design modifications.

The gas-film seal used shrouded Rayleigh step lift pads located on the face of the carbon nosepiece to maintain separation (gas film lubrication) of the sealing surfaces. Testing of the gas-film seal demonstrated the feasibility of operation at gas temperatures up to 1200°F, pressure differentials from 50 to 250 psi, sliding speeds up to 450 ft/sec, and calculated gas-film thicknesses as low as 0.18 mil. The tests yielded excellent correlation with analytically predicted performance. A total of 911.4 hours of testing was accumulated. The testing included 320 hours at an air temperature of 1000°F, a pressure differential of 200 psi, and a sliding speed of 400 ft/sec. The average leakage for those 320 hours was 14 scfm, and the face wear was less than 0.1 mil. The performance of the gas film seal exceeded the capability of conventional contact seals and the air leakage was 1/10 that of the calculated leakage for labyrinth seals at the same condition. In another phase of the testing, 40 starts and stops caused only insignificant wear of the Rayleigh pads, indicating that positive separation of the surfaces occurred at low speeds.

The results of the testing indicate that there are three areas which require further development: 1) erosion of the sealing faces by hard particles entrained in the air leakage flow, 2) fretting wear of the secondary sealing diameters, and 3) high response amplitude of the nosepiece at conditions of high speed and low pressure. The severity of the erosion problem was not evaluated, but for systems in which the seal pressurizing air can be adequately filtered, no problem is anticipated. The nosepiece response problem at high speeds and low pressures was related to the wide range of operating conditions attempted, and will probably not be a problem when the seal is designed for a particular application. It was also observed that oil contamination of the primary sealing surfaces has an adverse effect on the seal's performance: additional attention to the windback design is needed.

The oil-film seal used outward-pumping oil-lubricated spiral grooves on the seal surface to maintain separation of the sealing surfaces. Testing indicated an inadequate seal force balance which precluded successful operation. The tests also identified the need for improved retention of the carbon nosepiece by the retaining ring, and identified the need for better dimensional stability in the nosepiece assembly.

FINAL REPORT - PHASE II

DEVELOPMENT OF MAINSHAFT SEALS FOR ADVANCED AIR BREATHING PROPULSION SYSTEMS

by

V. P. Povinelli and A. H. McKibbin

ABSTRACT

Two mainshaft face seal configurations for advanced gas-turbine engines were designed, fabricated, and tested. The seal concepts incorporated lift geometries which used the relative motion between the primary seal surfaces to provide positive separation (film lubrication). One design (self-acting) with shrouded Rayleigh step lift pads operated with a gas film separating the sealing faces. The other design (hydrodynamic) with a spiral groove geometry operated with oil-film separation. Tests of the gas-film seal demonstrated the feasibility of operation at gas temperatures to 1200°F, pressure differentials to 250 psi, and sliding speeds to 450 ft/sec. Excellent correlations with analytically predicted performance parameters were obtained. Face wear was less than 0.1 mil after 320 hours at an air temperature of 1000°F, a pressure differential of 200 psi, and a sliding speed of 400 ft/sec. Average air leakage during that test was 14 scfm. These operating conditions exceed the capability of conventional contact seals and the air leakage is 1/10 that of a labyrinth seal. Testing of the oil-film seal revealed an inadequate seal force balance.

TABLE OF CONTENTS

TABLE OF CONTENTS (Cont'd)

LIST OF ILLUSTRATIONS

LIST OF ILLUSTRATIONS (Cont'd)

LIST OF ILLUSTRATIONS (Cont'd)

LIST OF ILLUSTRATIONS (Cont'd)

LIST OF ILLUSTRATIONS (Cont,d)

LIST OF ILLUSTRATIONS (Cont'd)

LIST OF ILLUSTRATIONS (Cont'd)

LIST OF TABLES

I. INTRODUCTION

Advanced air-breathing engines require the development of mainshaft seals capable of accommodating increasingly severe environments. The intent of Contract NAS3-7609 is to develop mainshaft seals capable of operating at higher pressures, temperatures, and surface speeds than are employed in current production engines. For Phase II, the upper extremes of these parameters were a pressure differential of 250 psi, a sealed gas temperature of 1200°F, and a seal sliding speed of 450 ft/sec.

Positive-contact mainshaft seals are commonly used in current engines. A typical seal of this type is shown in Figure 1. Despite significant advances in nosepiece materials, seal-seat hardface coatings and materials, lubrication technology, heat-transfer technology, and surface finishing, several attempts to significantly extend the operating range of the present positive-contact seal have demonstrated a limited growth potential. Current practice has been to use these seals at conditions not exceeding a pressure differential of 130 psi, a gas temperature of 800°F, and a sliding speed of 350 ft/sec. It is expected that advanced engines will operate at pressure differentials over 250 psi, gas temperatures over 1200°F, and sliding speeds over 400 ft/sec. Therefore, conventional positive-contact seals are entirely inadequate for these advanced conditions.

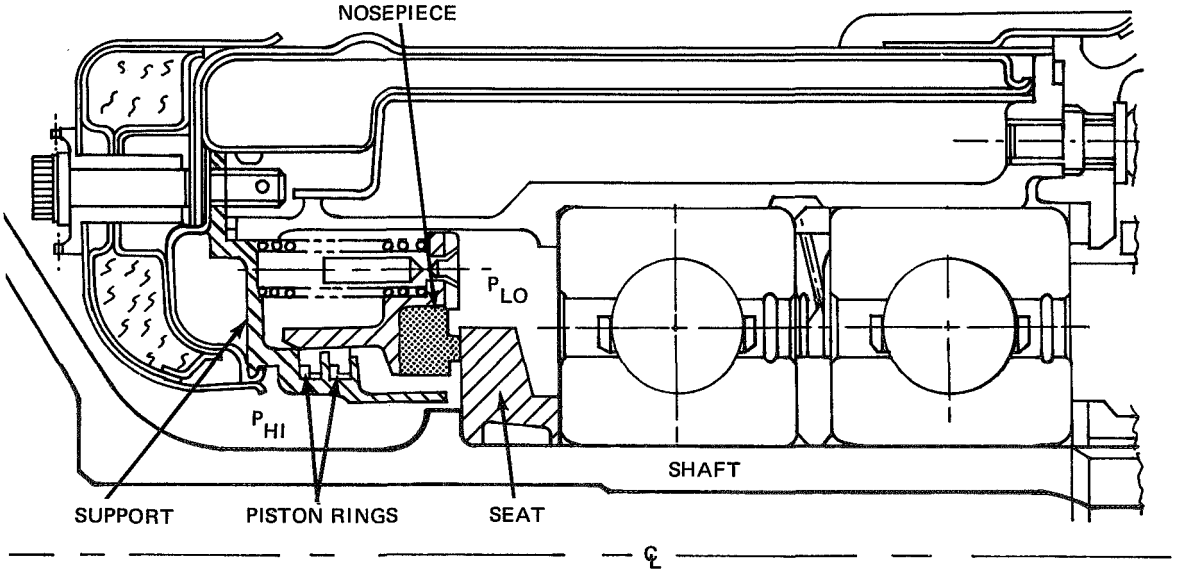

Figure 1 Typical Positive-Contact Seal

The most common alternative to the positive-contact seal is the labyrinth seal; however, once certain limitations on temperature and pressure differential are reached, the simple, lightweight labyrinth seals must give way to complicated multi-labyrinth designs similar to the one shown in Figure 2. Such designs require pressure bleed-off and cold air pressurization. The seal becomes heavy and bulky, with an undesirably high leakage at high pressure differentials.

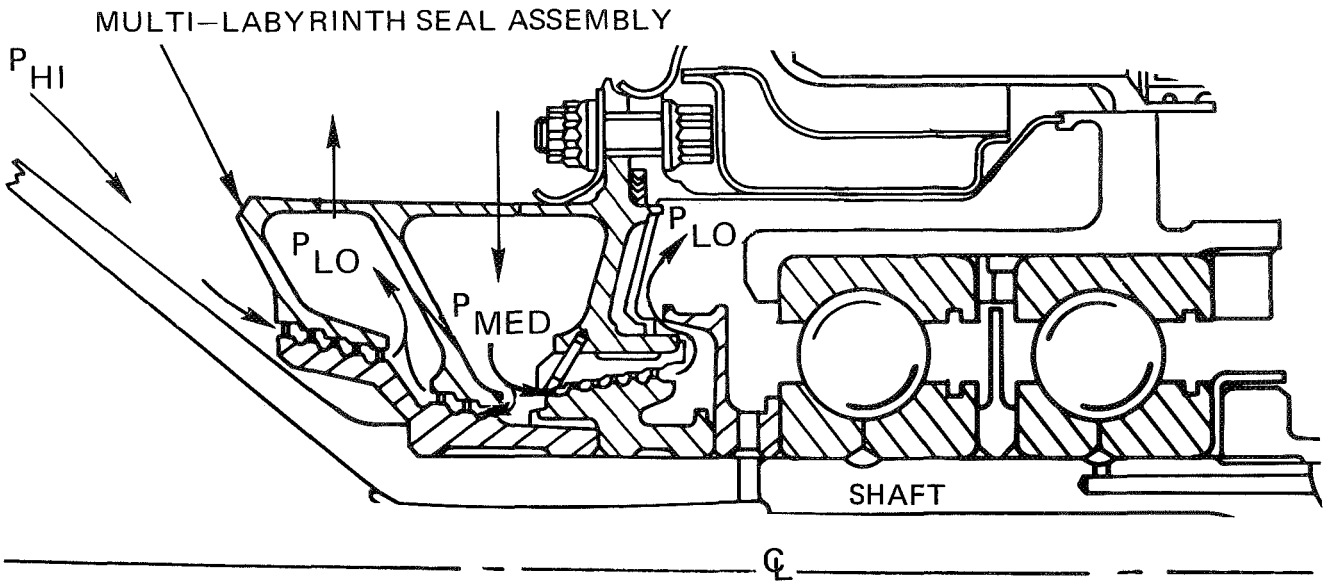

Figure 2 Typical Multi-labyrinth Seal

Development testing under Phase I of this contract indicated that film-lubricated face seals would not have the high wear rates of positive-contact seals under the harsh conditions of advanced engines, and could reduce air leakage to about one tenth of that experienced with multilabyrinth seals. Thus those seal designs in which positive separation of the sliding surfaces was obtained by externally pressurized and self acting means were candidates for advanced engine applications. Based on the results of Phase I, two seals using self-acting (gas) and hydrodynamic (oil) geometries were designed by NASA for testing in Phase II. In one face seal the sliding faces were separated by a gas film produced by shrouded Rayleigh step lift pads. The other face seal had oil-lubricated spiral grooves to maintain separation.

Three gas-film seals accumulated a total of 911.4 hours of testing at conditions typical of advanced engines. Low wear and acceptable leakage rates were obtained. Testing of the oil-film seal revealed an inadequate seal force balance.

The objectives of the Phase II study were to:

1. Determine the feasibility of operating self-acting and hydrodynamic seals at advanced engine conditions.

2. Determine wear and leakage rates of self-acting and hydrodynamic seals operating under advanced engine conditions.

3. Reveal design weaknesses by running endurance tests of several hundred hours.

The test rig used in Phase II simulated the roller bearing sump at the turbine location in an advanced gas-turbine engine. The test seal provided the separation between the high-pressure hot gas (turbine side) and the low-pressure mixture of oil and air (sump side). The test seals for this program had a maximum face diameter of 7.02 inches.

The rig was operated at seal sliding speeds up to 450 ft/sec (15,345 rpm), sealed gas temperatures up to 1200°F, and pressure differentials up to 250 psi. The maximum oil inlet temperature was 350°F.

II. CONCLUSIONS

The test series conducted under Phase II has provided considerable information about the feasibility of using gas film-lubricated face seals in mainshaft locations to accommodate the increasingly severe environments found in advanced engines. Specific conclusions reached as a result of the Phase II work are listed below:

- The self acting gas-film seal can be operated at conditions expected in advanced gas-turbine engines.
- Operation of a gas-film seal at calculated film thicknesses as low as 0.18 mil is possible.
- Shrouded Rayleigh lift pads can be used on the seal nosepiece to provide positive face separation between the primary sealing faces.
- A successful gas-film seal design requires a detailed accounting of all thermal and mechanical distortions in order to obtain parallelism between the primary sealing faces.
- The wear rate, of the self-acting gas-film seal, due to starting and stopping was found to be insignificant.
- The leakage rate, of the self-acting gas-film seal, is lower than 1/10 that of conventional labyrinth seals.
- Unlike the externally pressurized seals of Phase I, in the self acting gas-film seal, loss of the self-acting geometry does not result in a catastrophic failure.
- The force balance at the primary sealing faces of the hydrodynamic oil-film seal was inadequate for successful operation over the intended operating range.
- Additional design data is needed to accurately predict the load capacity of oil-lubricated spiral grooves.

III. RECOMMENDATIONS

Based on the experience obtained during the Phase II tests, the contractor recommends that:

- Experimental evaluations of the self-acting gas-film seal be continued to determine its operational limits in terms of temperature, speed, and pressure differential.
- Further development of the self-acting seal be directed toward investigating the sealing dam's resistance to erosion by hard particles entrained in the leakage air, and the secondary seal ring's resistance to fretting.
- The relationship between seal seat vibration and the tracking ability (response) of the self-acting seal nosepiece be investigated.
- Effort be expended on the present gas-film configuration with the intent of simplifying the design and reducing the cost and weight.
- Effort on the oil-film seal design be directed toward defining the optimum film-producing hydrodynamic geometry and improving dimensional stability through the use of more of the design features found in the gas-film seal.

IV. TASKS I AND II MAINSHAFT SEAL DESIGN ANALYSIS AND SEAL DETAIL DESIGN

A. BACKGROUND

The seals fabricated and tested in Phase II were produced from layout drawings prepared by NASA and from detail drawings prepared by Pratt & Whitney Aircraft. Preparation of the layouts was guided by experience gained from Phase I and by extensive design analysis conducted jointly by NASA and the contractor. NASA began work on preliminary layout drawings and design analysis before the Phase II amendment went into effect, so that preliminary layouts were ready for review by the contractor one week after the start of the Phase II program.

In Task I of the Phase II program, the contractor reviewed NASA's design analysis and layout drawings, and conducted studies to substantiate the design approach and to determine the need for design refinements. All engineering disciplines relating to the construction and operation of the gas-film seal (Type A) and the oil-film seal (Type B) were examined by the contractor. Although the analysis of the oil-film seal was much less extensive than that of the gas-film seal, it followed generally the same pattern. In addition, Pratt & Whitney Aircraft performed the detail design for a variation of the Type A seal, designated Type A-1.

The sequence in which Task I design review topics are presented generally follows the sequence in which the work was carried out. Further description of the seal designs and an outline of NASA's contribution to the design analysis is found in Appendices A through D.

Under Task II, Pratt & Whitney Aircraft completed the detail design of the two seals designed by NASA, and supplied prints and reproducible drawings to NASA.

B. GENERAL DESIGN, GAS-FILM SEAL AND OIL-FILM SEAL

The design features included in the gas-film Type A seal (shown in Figure 3) and the oil-film Type B seal (shown in Figure 4) resulted mainly from experience gained from the Phase I tests. Design highlights common to both seals are listed below: (Also see Appendices A and B)

- The seal seats were center-pilot mounted, with keys connecting them to the shaft spacer. A machined bellows provided a static seal between the shaft and the seal seat to accommodate differential expansion of the parts and to mitigate seat deformation due to clamping.

- Cooling oil was passed through the shaft spacer and then through the seat to reduce thermal gradients.

- Heat shields were used on both sides of the seal seat to minimize thermal gradients and seal seat deformation.

- A resilient piloting ring was used to minimize the eccentricity between the sealing dam and the secondary sealing diameter.

- Some of the same parts were used in both designs. A few parts such as the piston ring, seal carrier, and seal seat were dimensionally similar in both designs, but were made of materials having significantly different physical properties.

- A static seal that allowed radial movement between the mating faces of the carrier and the nosepiece precluded carrier deformation affecting the nosepiece.

Design features peculiar to the gas-film seal are listed below:

- Shrouded Rayleigh step lift pads were used on the face of the carbon nosepiece for self-acting support.

- Outward-pumping spiral grooves were used on the outer half of the face of the seal seat to prevent inward oil leakage from the bearing compartment.

Design features peculiar to the oil-film design are listed below:

- Outward-pumping oil-film spiral grooves were provided on the seal seat's face to maintain the seal clearance.

- Oil for the spiral-groove oil film was supplied through passages in the seal seat.

In addition to reviewing the Type A and Type B seals designed by NASA, Pratt & Whitney Aircraft performed the detail design for a variation on the Type A seal, designated Type A-1 as a backup design. The principal difference between the Type A seal and the Type A-1 seal is that the Type A-1 seal uses a ceramic nosepiece ring rather than a carbon nosepiece ring in

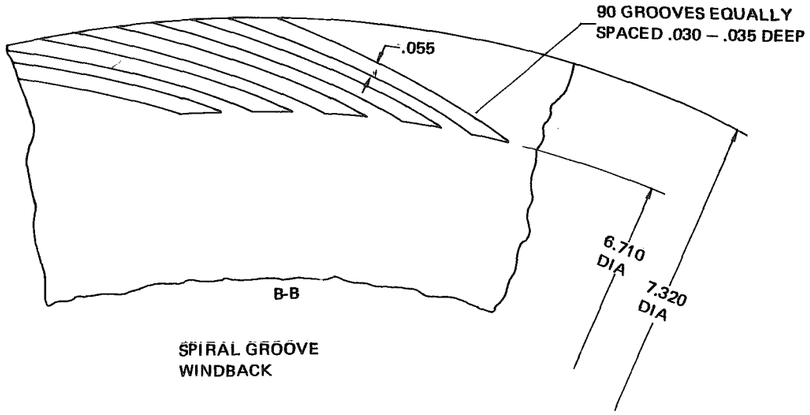

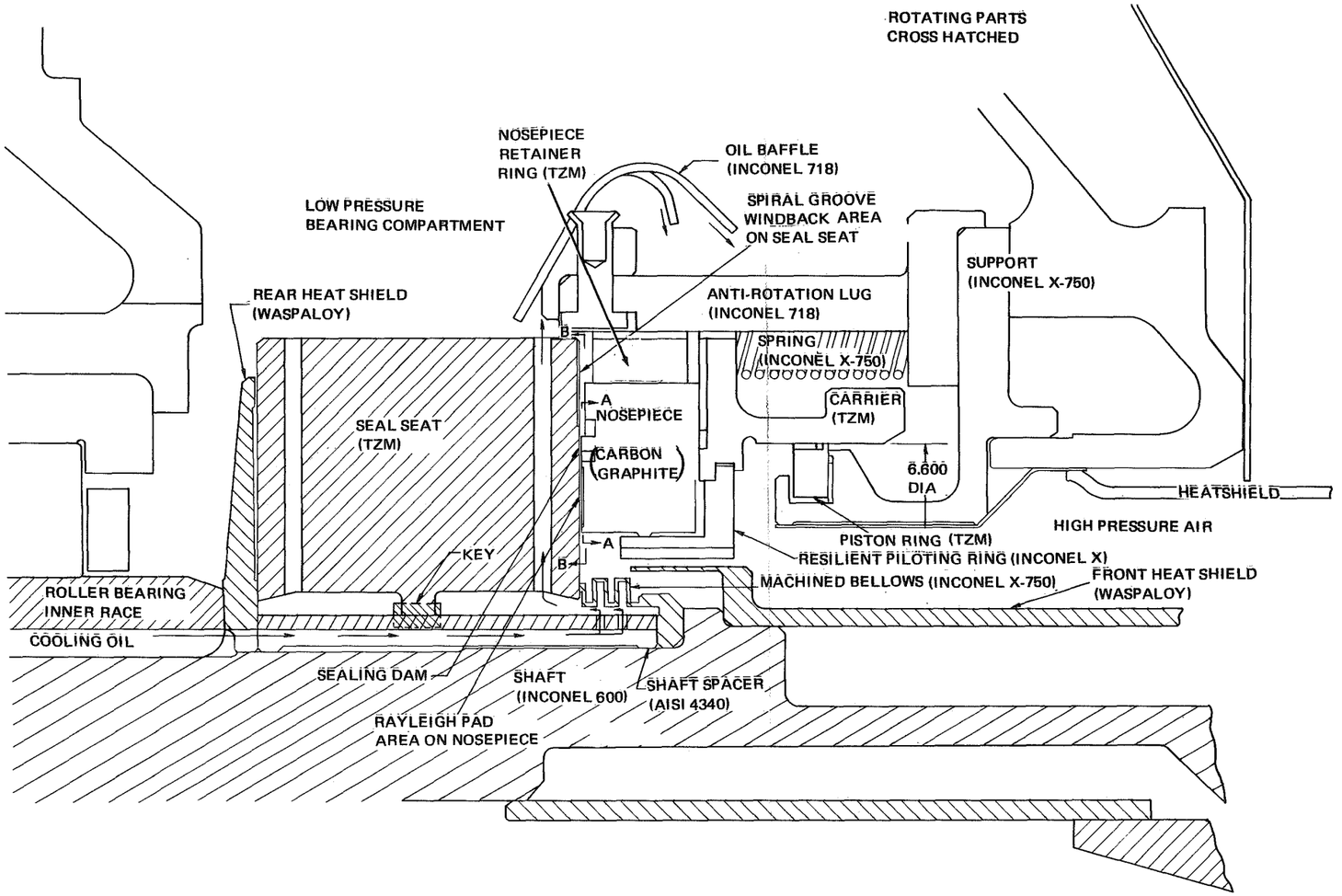

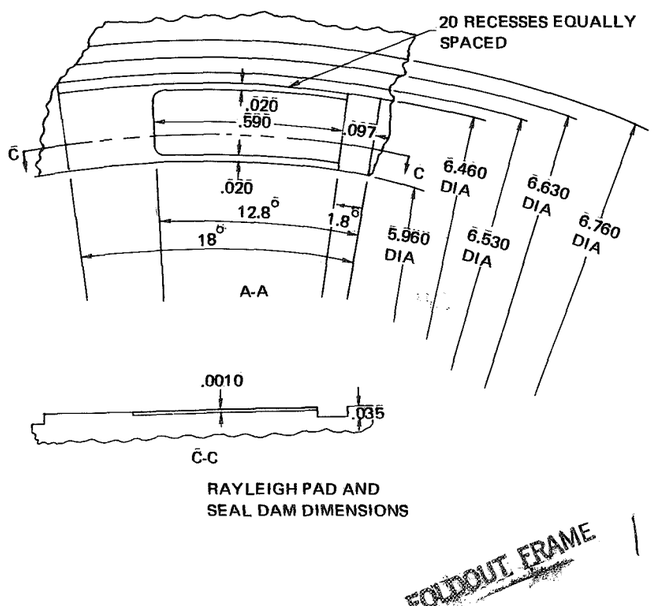

Figure 3 Gas-Film Seal (Type A) Design Features

FOLDOUT FRAME 1

FOLDOUT FRAME 2

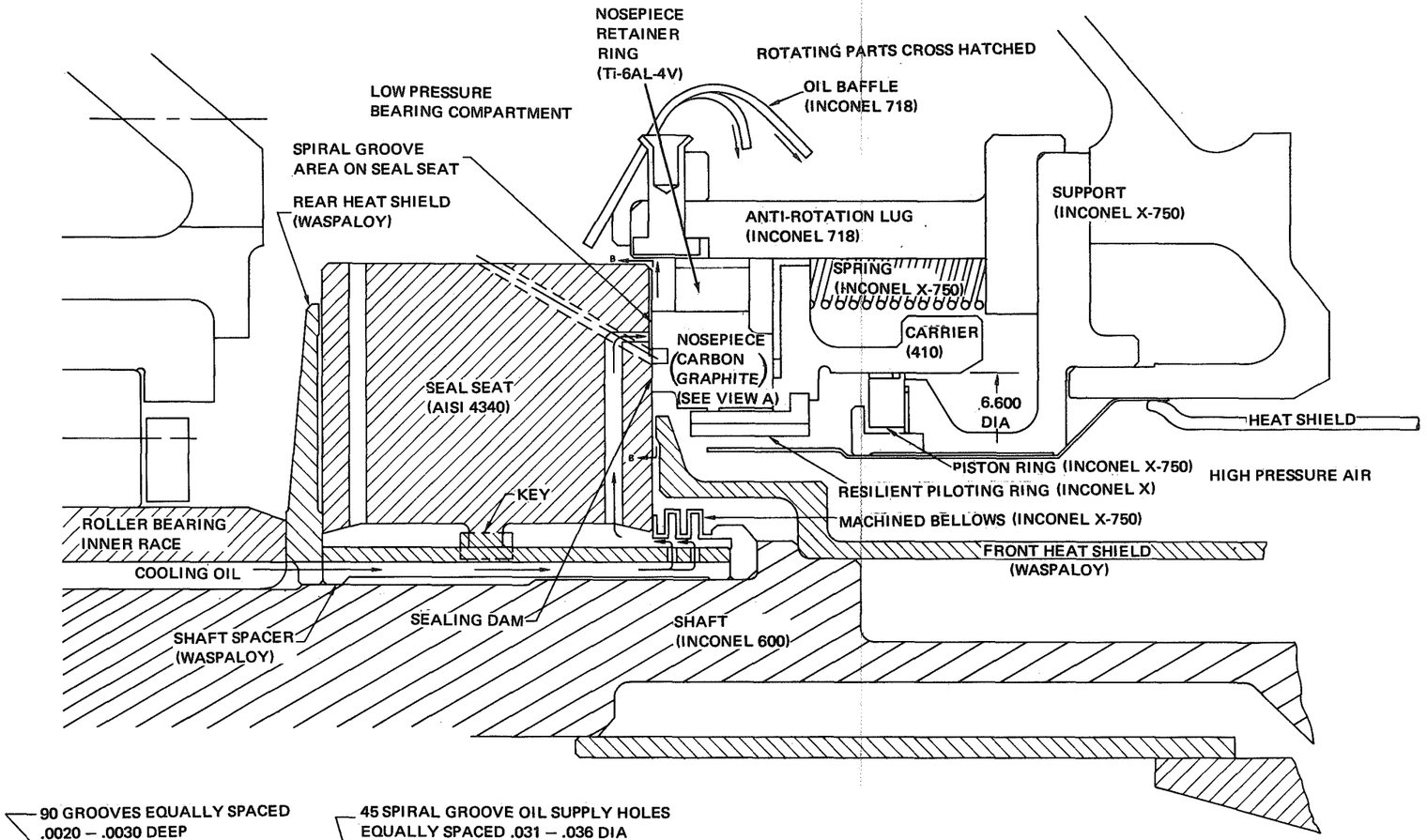

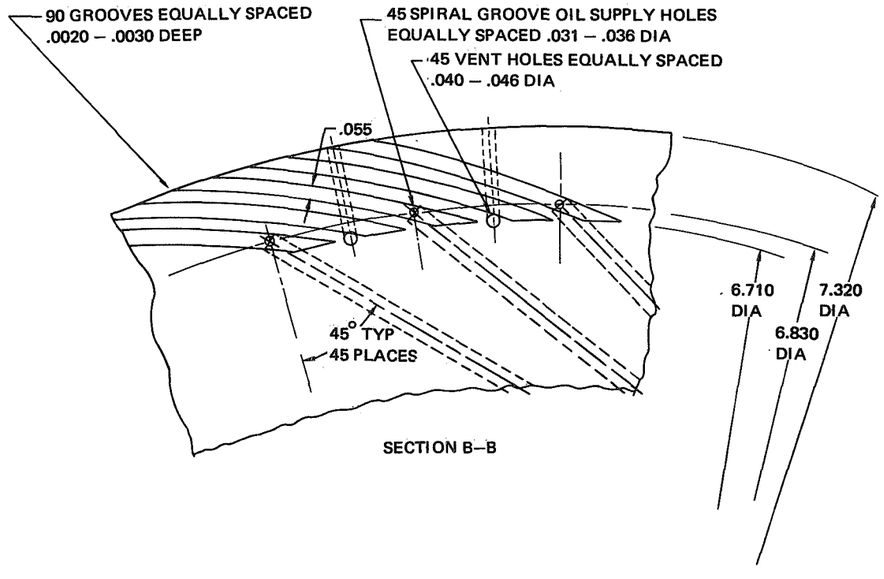

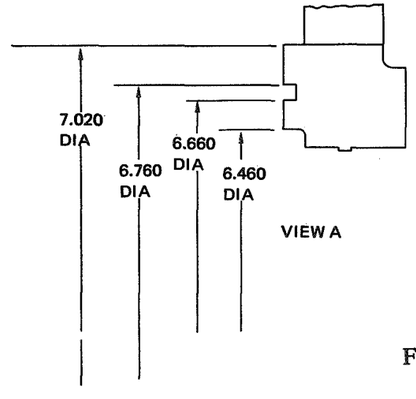

Figure 4 Oil-Film Seal (Type B) Design Features

FOLDOUT FRAME 1

FOLDOUT FRAME 2

the nosepiece assembly. As shown in Figure 5, the seal face configuration is different from the Type A configuration. Fabrication of the Type A-1 seal was completed during Phase II, and inspection revealed no significant deviations from the blueprint requirements. The ceramic nosepiece ring assembly and a close-up of the nosepiece are shown in Figure 6. The ceramic nosepiece was not tested in Phase II of the contract, as the Type A seal proved satisfactory. The ceramic nosepiece assembly will be evaluated in Phase III.

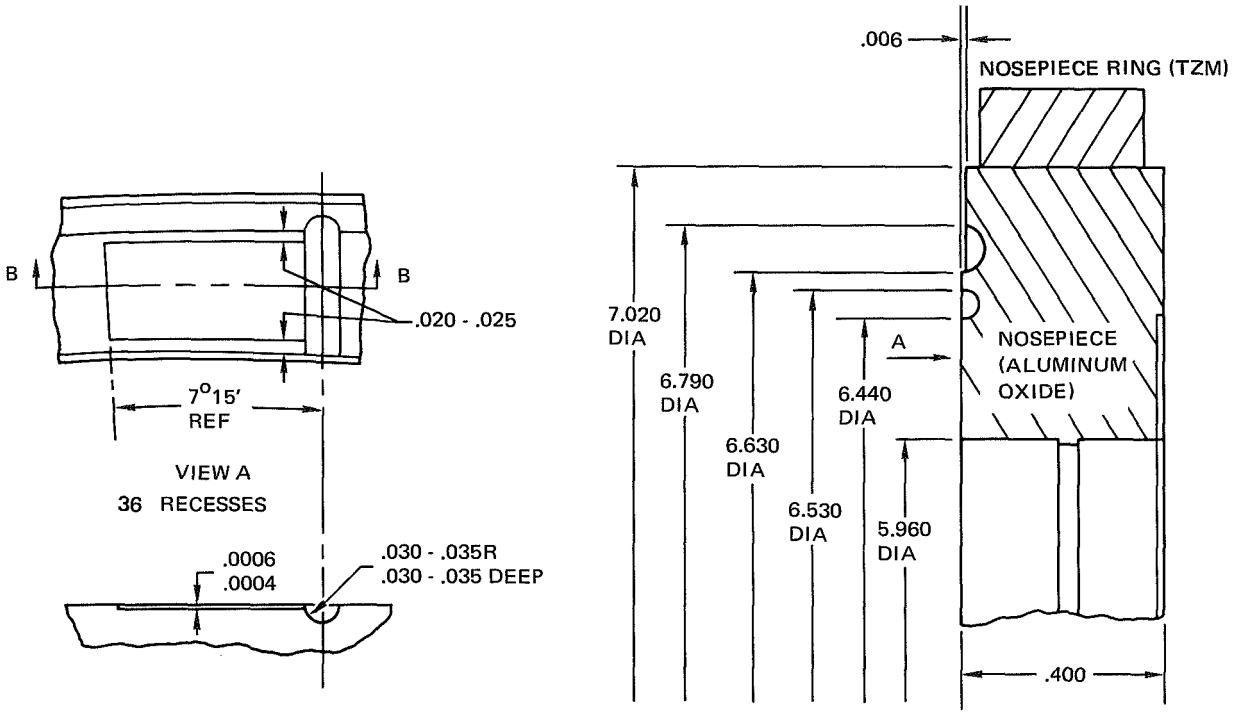

Figure 5 Ceramic Nosepiece Face Dimensions for the Gas-Film Seal (Type A-1)

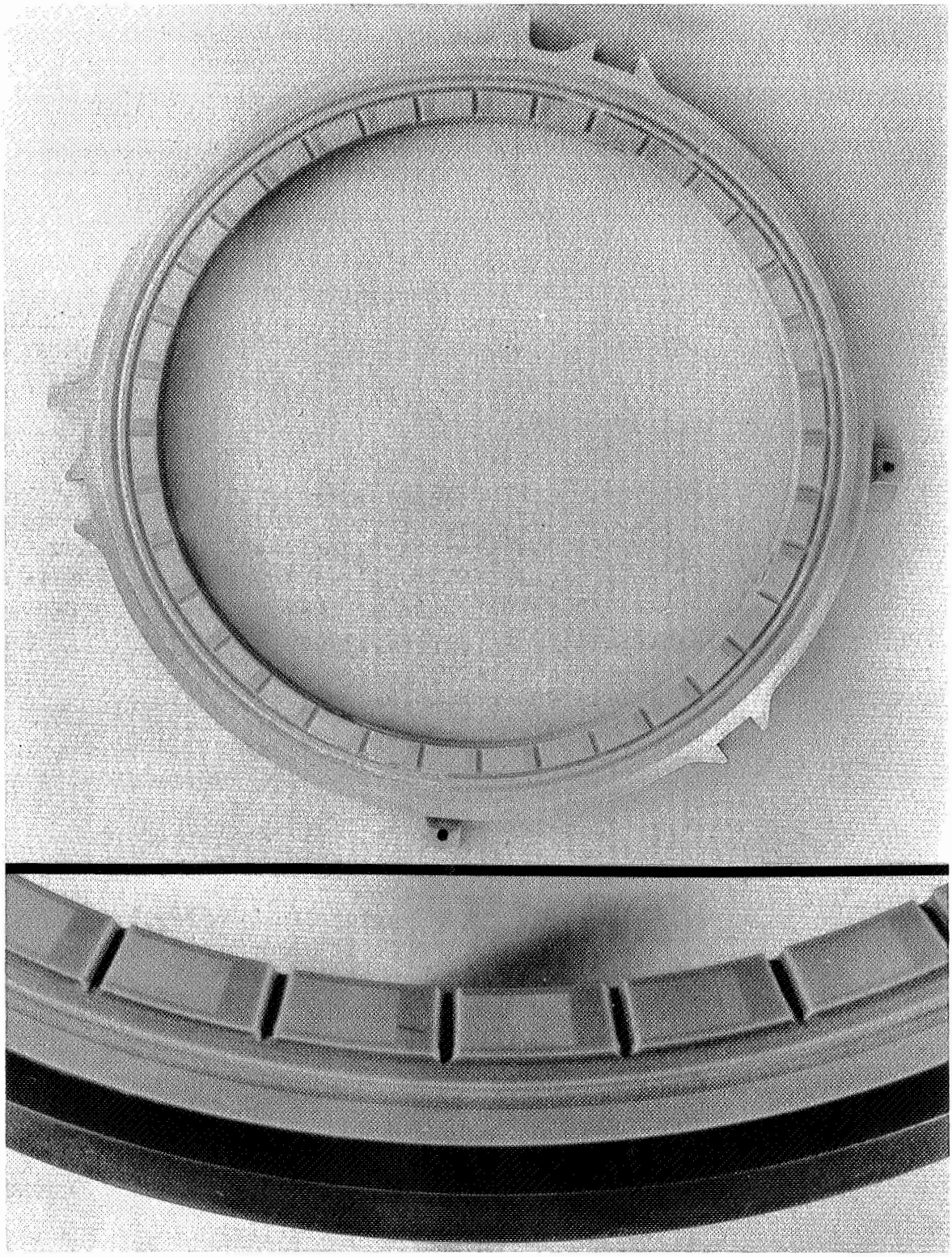

Figure 6 Completed Ceramic Nosepiece Ring Assembly with Close-Up of Ceramic Ring (CN-23132 & 23133)

C. PRIMARY FILM ANALYSIS, GAS-FILM SEAL

The self-acting seal was selected for development in the Phase II program. This type of seal employs self-acting Rayleigh step pads to precisely control the separation of the primary sealing faces. In Phase I a self-acting seal was found to be less sensitive to the surface distortions than the externally pressurized seals.

NASA and the contractor agreed that the Rayleigh pads would be selected for the self-acting geometry. Pad geometry (see Figure 3) was optimized with the selection of 20 pads, each recessed 0.001 inch deep, 0.210 inch wide, and 0.590 inch long. Lands 0.020 inch wide shrouded the inner and outer edges of each recess. The NASA analysis of load capacity and tolerance to angular displacement was verified by the contractor. The details of the NASA self acting gas film analysis are given in Appendix C.

The other major design feature of the primary seal is the narrow land, or sealing dam, which controls the rate of air leakage through the seal. The details of the leakage calculations are given in Appendix D. The sealing dam was originally designed to be 0.100 inch wide. Further analysis conducted jointly by NASA and the contractor indicated that reduction of the dam width to 0.050 inch provided a needed increase in tolerance to angular coning of the seal surfaces without causing an excessive increase in leakage. Surface coning alters the pressure distribution and opening force in the primary seal (dam). A decrease in seal dam width reduces opening force variation, while it increases leakage. The 0.050-inch dam width was chosen as an acceptable compromise.

D. AXIAL FORCE BALANCE CALCULATIONS AND THERMAL ANALYSIS, GAS-FILM SEAL

A quantitative analysis of the primary film thickness and leakage rate requires the calculation of steady-state axial forces on the seal nosepiece. For a given seal design, steady-state axial forces are controlled by the seal surface speed, air pressure differential, air temperature, primary sealing surface deviation from true parallelism, and by the relationship between the diameters of the sealing dam and the secondary seal. These relationships require extensive knowledge of temperature patterns and structural displacements within the seal assembly. The analysis of circumferential film thickness variation and local minimum film thickness requires the calculation of dynamic forces on the nosepiece. The dynamic forces depend on secondary seal friction, nosepiece mass, and seal seat face runout.

The steady-state axial force calculations performed by NASA were based on a thermal analysis which indicated that the air temperature between the primary sealing faces should be nearly equal to the temperature of the sealed air. A thermal map produced by the contractor, however, indicated that air temperature between the primary sealing surfaces is significantly affected by the cooling oil temperature. Figure 7 summarizes the results of the contractor's thermal analysis. This lower leakage air temperature results in lower calculated steady-state film thicknesses and higher air leakage rates. The contractor's analysis correlating leakage data with theory was based on leakage air temperatures which were assumed to equal a temperature measured near the center of the carbon nosepiece. The results of the leakage calculations are presented in Section V., along with the test data. Satisfactory correlation between the theoretical and measured leakage rates has established the validity of the theoretical approach.

The NASA force balance analysis was based on the further assumptions that the sealing face deviations from parallelism would be negligible and that the position of the secondary sealing diameter relative to the seal dam would not vary from the nominal fabricated dimensions. The results of the force balance are discussed in Appendix D. The thermal map of Figure 7 indicates that thermal distortions are not great enough to interfere with these assumptions. The contractor recommended two changes in mechanical design to provide further assurance that these assumptions would be valid. These changes are discussed in Section IV. E, below.

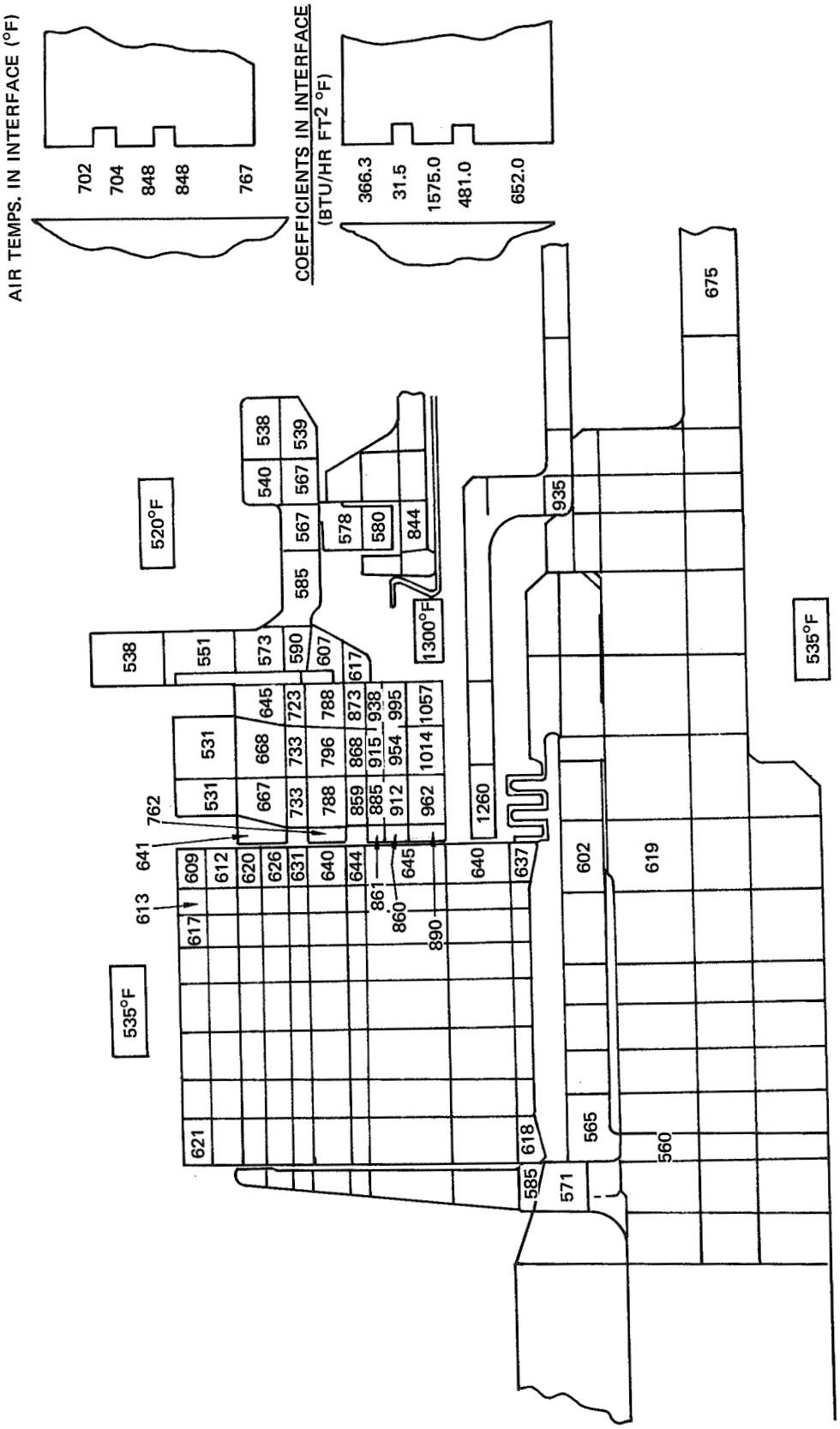

Figure 7 Calculated Thermal Map of the Gas Film Seal with Oil Cooling at an Air Temperature of 1300°F, a Pressure Differential of 300 psi, and a Speed of 500 ft/sec (17,000 rpm)

E. MECHANICAL DESIGN AND ANALYSIS, GAS-FILM SEAL

When the mechanical design of the gas-film seal was planned, the preservation of seal surface flatness at extreme operating conditions was placed above all other considerations. Of nearly equal importance, however, was the requirement that the concentricity between the seal dam and the piston-ring diameter be precisely maintained.

The nosepiece and the seal seat were closely examined (analytically) by NASA and the contractor for evidence of surface distortion due to pressure loads, thermal growth, or dynamic effects. Nosepiece pressure and thermal distortions were judged to be negligible after the axial thickness of the TZM (0.5 Ti, 0.008 Zr, Mo Alloy) retainer ring was increased to approach the thickness of the carbon nosepiece ring. Variations from seal-seat flatness were also reduced to near zero by increasing the thickness of the seal seat from the original 0.800 inch to 1.125 inches and by using TZM material for the seat. The 40-percent increase in axial thickness was responsible for a 65-percent decrease in angular displacement under the worst operating conditions. At worst conditions, the angular displacement of the sealing face was 0.09 milliradian, or 35 microinches.

Tolerance control on the concentricity between the seal dam and the piston ring secondary sealing diameter was complicated by the use of separate parts for the nosepiece ring assembly and the carrier. The piston-ring (secondary seal) acts against the carrier bore. It was necessary to provide a shear connection between the nosepiece ring assembly and the carrier, and the connection had to be resilient enough so that thermal distortions were not transmitted from the carrier to the nosepiece. An Inconel piloting ring (see Figure 3) contacting both parts at six evenly spaced points around its circumference proved to be an adequate solution to the problem.

V. TASK III
MAINSHAFT SEAL EVALUATION

A. BACKGROUND

Under Task III, Pratt & Whitney Aircraft procured the gas-film seal (Type A) and oil-film seal (Type B) and tested them in the full-scale test rig developed under Phase I. The testing consisted of preliminary dynamic checkouts, simulated engine operation, and endurance testing. The preliminary dynamic checkouts were performed with room-temperature air, an oil-in temperature of 250°F, seal pressure differentials up to 200 psi, and seal velocities up to 400 ft/sec. Simulated engine operation was carried out with air temperatures up to 1000°F, oil-in temperatures up to 350°F, seal pressure differentials up to 200 psi, and seal velocities up to 400 ft/sec. The endurance tests consisted of steady-state testing; cyclic testing to simulate take-off, cruise, and approach conditions; and a series of short-duration start-ups and shutdowns. The lubricant used during the testing was Type II turbine oil.

At the direction of NASA, testing on the oil-film seal was discontinued when the preliminary dynamic checkouts revealed the need for improved retention of the carbon nosepiece by the retaining ring and the need for better balance between the load capacity of the oil film and the hydraulic closing force. The effort which would have been applied to testing the oil-film seal at elevated temperatures was allotted to tests of the gas-film seal, which successfully completed more than 900 hours of dynamic testing. A summary of the testing on the gas-film seal is shown in Table I, and a test summary for the oil-film seal is shown in Table II.

B. TEST EQUIPMENT

1. Test Rig

Evaluation of the seals was carried out in a full-scale test rig. The rig was mounted on a bed plate and driven by a Ford industrial engine through a five-speed truck transmission and a 12:1 ratio gearbox. Facilities for heating the oil required for testing were located in the test cell, and the air was heated by an electrical heater. A schematic diagram of the test facility is shown in Figure 8 and a photograph is shown in Figure 9.

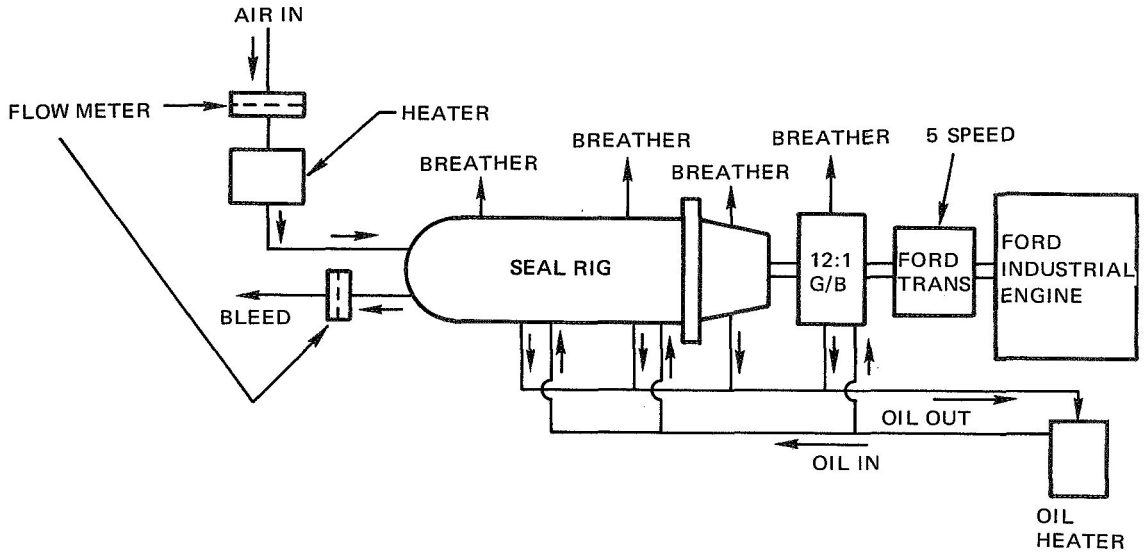

Figure 8 Schematic Diagram of Seal Test Facility

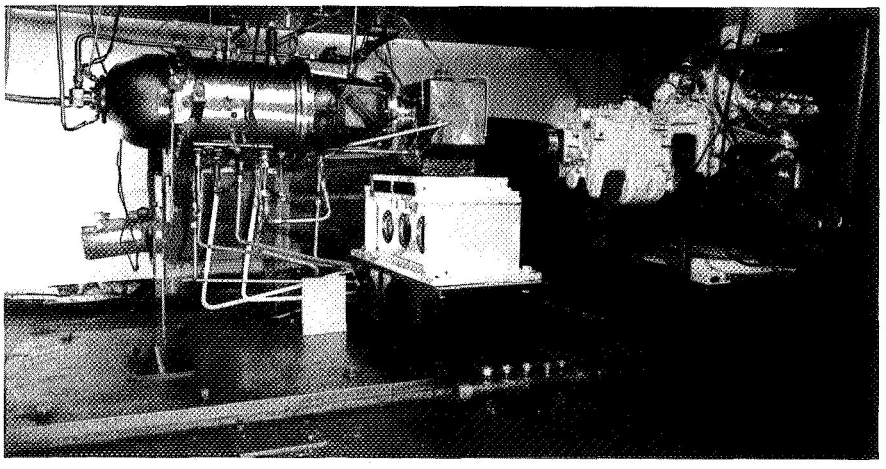

Figure 9 Overall View of X-119 Stand Showing Mainshaft Seal Rig, Gearbox, and Drive Engine (CN-6928)

TABLE I

GAS FILM SEAL TEST SUMMARY

Build No.	Carbon Nosepiece	Seal Seat	Spring Load (lbs)	Other Special Features	Type of Test PDCP	SEO	END	Reason For Test Termination	Condition After Test Carbon Nosepiece	Seal Plate	Start/ Stop	Test Hrs.	Total Bld. Start/Stops	Total Bld. Hrs.
1	New	New	7.8	Instrumented with Thermo-couples and Accelerometers	X			Excessive Air Leakage Due to Carbon Shifting in Retainer Ring	Out-of-flat 0.8 mil.	New	0	.0	0	0
1-1	New	New From Bld. 1	7.8		X	X		Excessive Air Leakage Hub Stackup Loose	0.1 mil. Wear on Outer Edge	Good	9	31.2	9	31.2
1-1	Used From Bld. 1-1	New	7.8	Increased Stackup Locking Torque		X	X	Nosepiece in Rubbing Contact with Seal Plate	Worn - 15 of 20 Pads Worn Off	Good	14	144.9	23	176.1
2	Repaired Nosepiece From Bld. 1	Used From Bld. 1-1	7.8	Increased Radial Torque Pin Clearance			X	Completed Program	Avg. Pad Wear 0.07 mil. Seal Dam Scored and Tapered	Good	11	171.2	11	171.2
2-1	Used From Bld. 2	Used From Bld. 2	15.6	Increased Spring Load			X	Completed Program	Avg. Pad Wear 0.07 mil. Seal Dam Scored and Tapered	Good	3	60.7	14	231.9
3	New	Used From Bld. 2-1	15.4				X	Completed Program	Good, Wear Less than 0.05 mil.	Good	5	338.5	5	338.5
3-1	Used From Bld. 3	Used From Bld. 3	15.4	Substituted New TZM Piston Ring in Assembly			X	High Air Leakage	Seal Dam Scored, Scratches 1 mil. deep	Good	2	18.4	7	356.9
3-2	Used From Bld. 3-1	Used From Bld. 3-1	15.4	Substituted New 410 Carrier and Inconel Piston Ring with 24-mil Gap			X	Completed Program	Pad Wear Less than 0.05 mil.	Good	40	7.6	47	364.5
3-3	Used From Bld. 3-2	Used From Bld. 3-2	7.8	Reduced Spring Load			X	Completed Program	Seal Dam Wear Particle Erosion	Good	8	78.9	55	443.4
3-4	Used From Bld. 3-3	Used From Bld. 3-3	7.8	New Piston Ring with 34-mil. Gap			X	Completed program	Seal Dam Wear Particle Erosion	Good	4	26.5	59	469.9
3-5	Used From Bld. 3-4	Used From Bld. 3-4	15.4	Increased Spring Load			X	Completed program	Pad Wear 0.09 mil., Wear on Dam 0.24 mil.	Fair	5	33.5	64	503.4

TABLE II

OIL FILM SEAL TEST SUMMARY

Build No.	Carbon Nosepiece	Seal Seat	Spring Load (lbs)	Other Special Features	Type of Test PDCP	SEO	END	Reason For Test Termination	Condition After Test Seal Plate	Carbon Nosepiece	Test Hours
1	New	New	27.8	Instrumented with Thermo-couples and Accelerometers	X			Excessive Air Leakage Due to Cracked Bellows Spacer	New	New	0.00
1-1	New From Build 1	New From Build 1	27.8	Replaced Cracked Bellows from Build 1	X			Unstable Operation	Good	Fair - .1 to .3 mils Wear on Dam Inner Diameter	0.05
2	Reoperated Build 1-1	Used From Build 1-1	27.8	Build 1-1 Seal Modified to Reduce Spiral Groove Load Capacity and Increase Seal Venting Capability	X			Seal Leakage Increased Rapidly	Good	Coned and Warped Displaced Within Nosepiece Retainer Ring	1.05

PDCP = Preliminary Dynamic Checkout Program
SEO = Simulated Engine Operation
END = Endurance

FOLDOUT FRAME 1

FOLDOUT FRAME 2

A layout of the test rig is shown in Figure 10. The pressure dome was insulated to cut heat losses during testing. Pressurized and heated air entered the conical manifold attached to the inside of the pressure dome. Air temperatures at the seal were continually monitored and adjusted by means of a bleed valve. Oil was introduced to the thrust bearings by means of calibrated jet and scoop arrangement. Oil was brought to the test seal from a jet via a scoop and passageways which allowed under-race cooling of the roller bearing. This oil was centrifugally thrown out of the seal plate through 45 radially drilled holes, providing cooling for the seal seat. The roller bearing was lubricated with mist and spray in the seal compartment. The flight-weight parts used in the rig were:

- Duplex ball thrust bearings
- Inner and outer bearing supports
- Thrust-bearing support mount
- Roller bearing, inner race, and support mount
- Test seal seat
- Test seal assembly

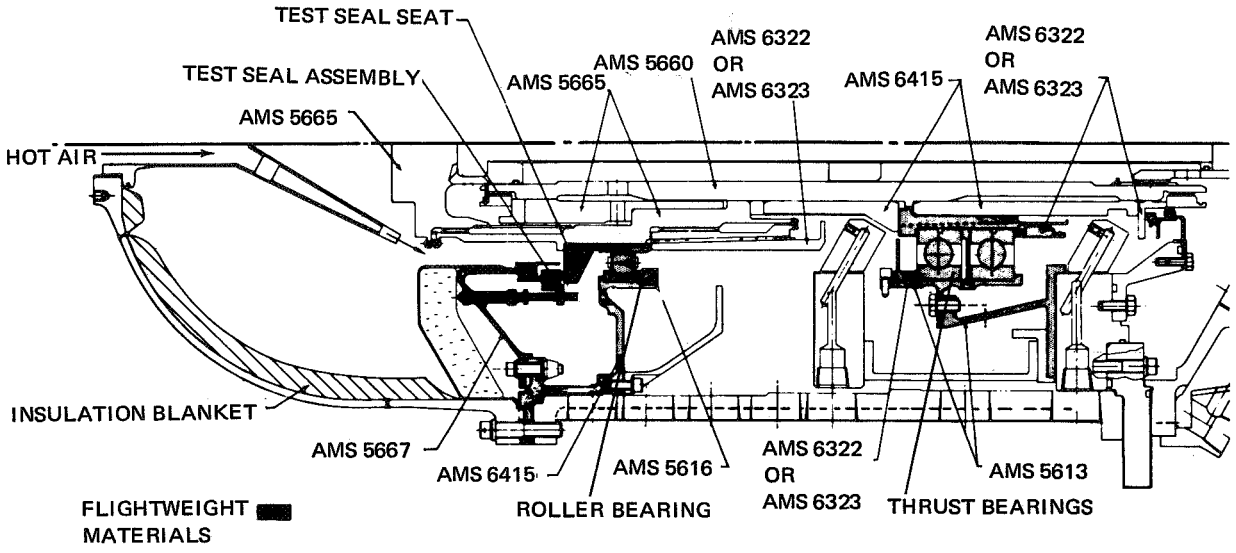

Figure 10 Rig Layout Showing Test Seal Location and Materials Used

2. Pressure Check Fixtures

Two pressure check fixtures were designed and fabricated to permit thorough checks of both the test seals and the test rig. Both the seal fixture and the rig fixture are shown in Figure 11. The seal fixture consisted of a pressure vessel which positioned the seal assembly against a simulated seal seat. The seal was pressurized through the bore and the air leakage into the low-pressure compartment was collected and measured. Additionally, removal of the fixture's cover allowed observation of the air leakage paths.

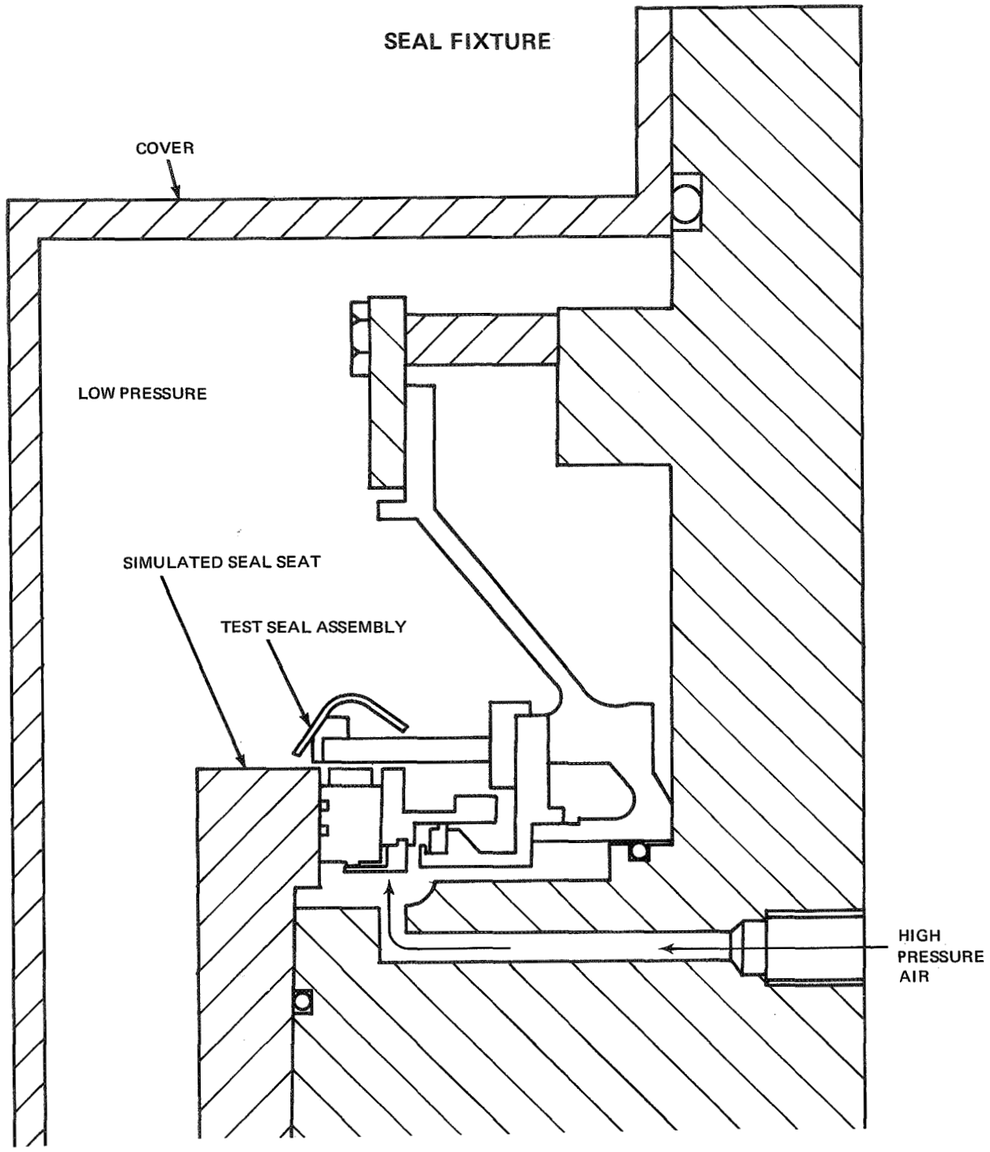

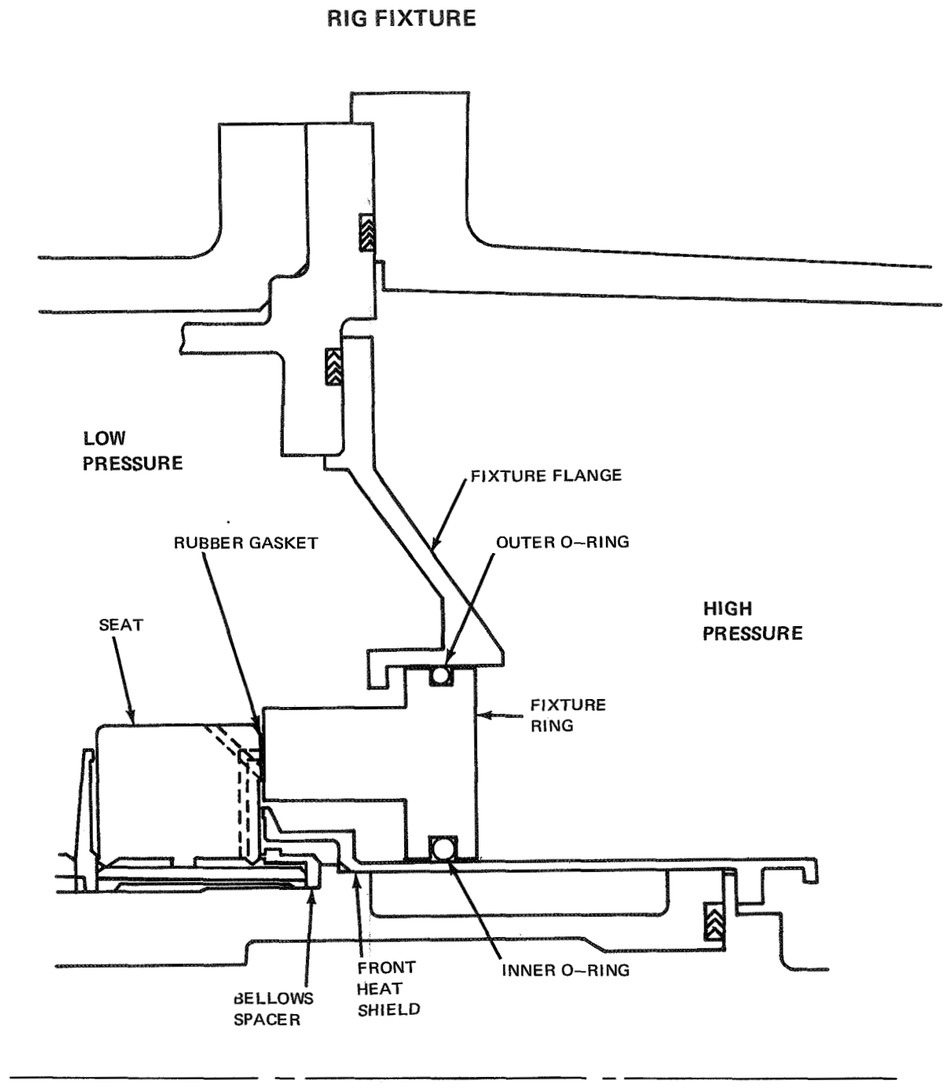

Figure 11 Schematic Diagrams of Pressure Check Fixtures

FOLDOUT FRAME 1

FOLDOUT FRAME 2

The rig fixture replaced the entire seal assembly in the test rig, and allowed a systematic check of possible leakage paths in the rig and rotor assembly. With the rubber gasket and both O-rings in place, it was possible to pressurize the static rig gaskets. Removal of the inner O-ring allowed pressurization of the bellows spacer.

C. EXPERIMENTAL EVALUATION OF THE GAS-FILM SEAL (TYPE A)

1. Preliminary Dynamic Checkout - Build 1

The initial static air leakage calibration was halted when the leakage past the seal increased rapidly at pressure differentials above 50 psi. The test results indicated that the carbon nosepiece was lifting off the carrier at the mating surface. Disassembly of Build 1 revealed an area of severe distortion in the carbon nosepiece. The rear face of the nosepiece had a raised area over an arc length of approximately 30°, with a maximum height of 0.8 mil. The front face had a depression corresponding to the raised area on the back face. The shifting of the carbon within the retainer ring may have been caused either by the relaxation of residual stresses resulting from the installation of the carbon into the TZM retainer ring, or by localized heating from the installation of the thermocouples on the retainer ring.

2. Preliminary Dynamic Checkout - Build 1-1

For Build 1-1 the distorted nosepiece assembly was replaced with a spare assembly. Tests were run with ambient air, an oil-in temperature of 250°F, seal pressure differnetials ranging from 50 to 200 psi, and seal sliding speeds ranging from 0 to 400 ft/sec. The results of this testing are summarized in Figure 12.

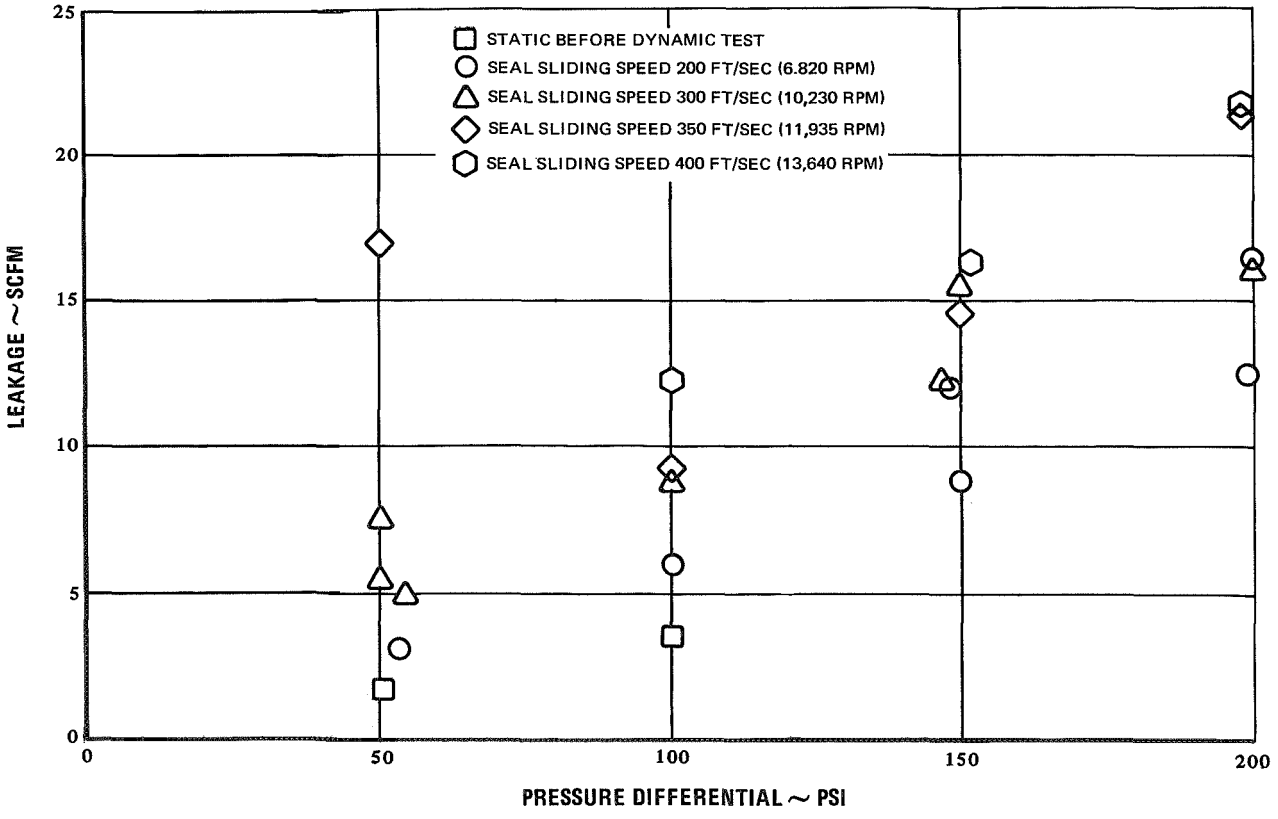

Figure 12 Air Leakage Past Build 1-1 of the Gas-Film Seal with Air at Ambient Temperature

Twice during the testing it was noted that there was a carbonaceous residue on the seal seat. The residue was in the form of two bands that matched the locations and widths of the seal dam and the Rayleigh pads on the carbon nosepiece. The deposit was heaviest at the outer edge and faded toward the inner edge. The residue was easily removed with a solvent. The second time this condition was found, a complete inspection of the seal was performed. The inspection revealed that there were no changes from the pretest condition, and the flatness and runout of the seal seat were unchanged. In the first case, residual oil from previous testing had drained across the primary sealing faces. The oil had apparently been trapped in the spiral-groove windback on the seal seat. In the second case, low gas-film stiffness (which would be expected at a pressure differential of 50 psi and a sliding speed of 350 ft/sec) may have resulted in a loss of seal tracking ability. In addition, operation at a pressure differential of 50 psi across the seal results in a thrust load which is in the skid regime of the rear thrust bearings. Either the loss of tracking or the bearings' skidding might have caused the nosepiece to rub momentarily against the seal seat.

A comparison of theoretical and actual leakage for Build 1-1 of the gas-film seal is presented in Figures 13 and 14. The theoretical curves were obtained by combining the calculated leakage past the seal dam (primary sealing faces) with the static leakage obtained from initial static calibration testing (assumed to be idential with the leakage past the secondary seal during dynamic testing). The leakage past the seal dam was obtained by calculating the air film thickness at the seal dam for each operating condition. With this information and the assumption that both seal surfaces were flat and parallel, the leakage past the primary seal was calculated. There was excellent agreement between the theoretical and actual leakages.

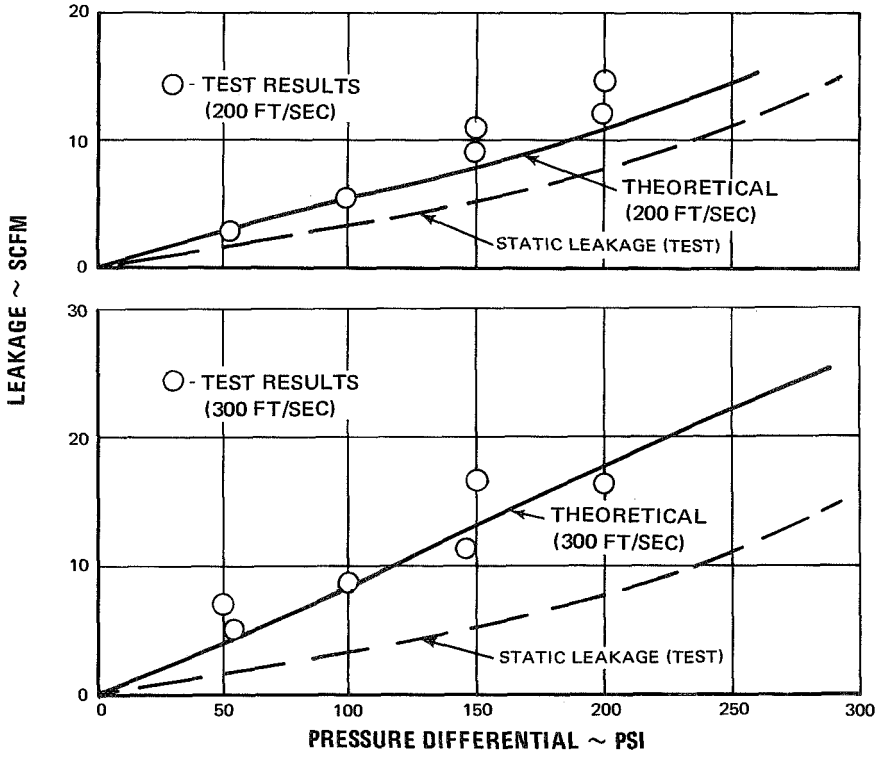

Figure 13 Air Leakage Past Build 1-1 of the Gas-Film Seal at Sliding Speeds of 200 and 300 ft/sec

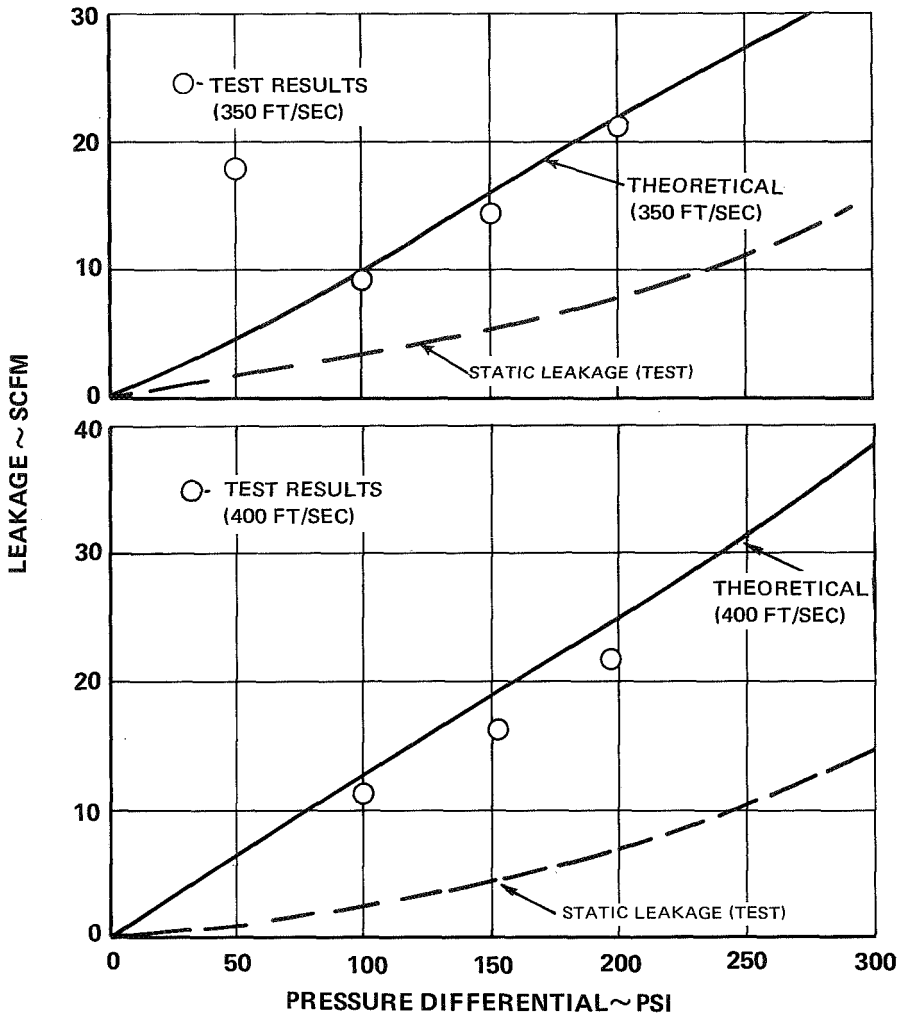

Figure 14 Air Leakage Past Build 1-1 of the Gas-Film Seal at Sliding Speeds of 350 and 400 ft/sec

Curves of calculated primary film thickness for Build 1-1 are shown in Figure 15. Plotted on the curves are points where the seal was operated, or where operation was attempted. Build 1-1 was operated at apparent film thicknesses between 0.18 and 0.35 mil.

3. Simulated Engine Operation – Build 1-1

Build 1-1 of the gas-film seal was subjected to simulated engine operation over a period spanning nearly three months. The simulated engine conditions are tabulated below:

Air Temperature (°F)	400, 600, 800, 1000
Oil Temperature (°F)	250, 350
Seal Pressure Differential (psi)	100, 150, 200
Seal Velocity (ft/sec)	300, 350, 400

The leakage results of the entire 72-point simulated engine operation program are summarized in Table III.

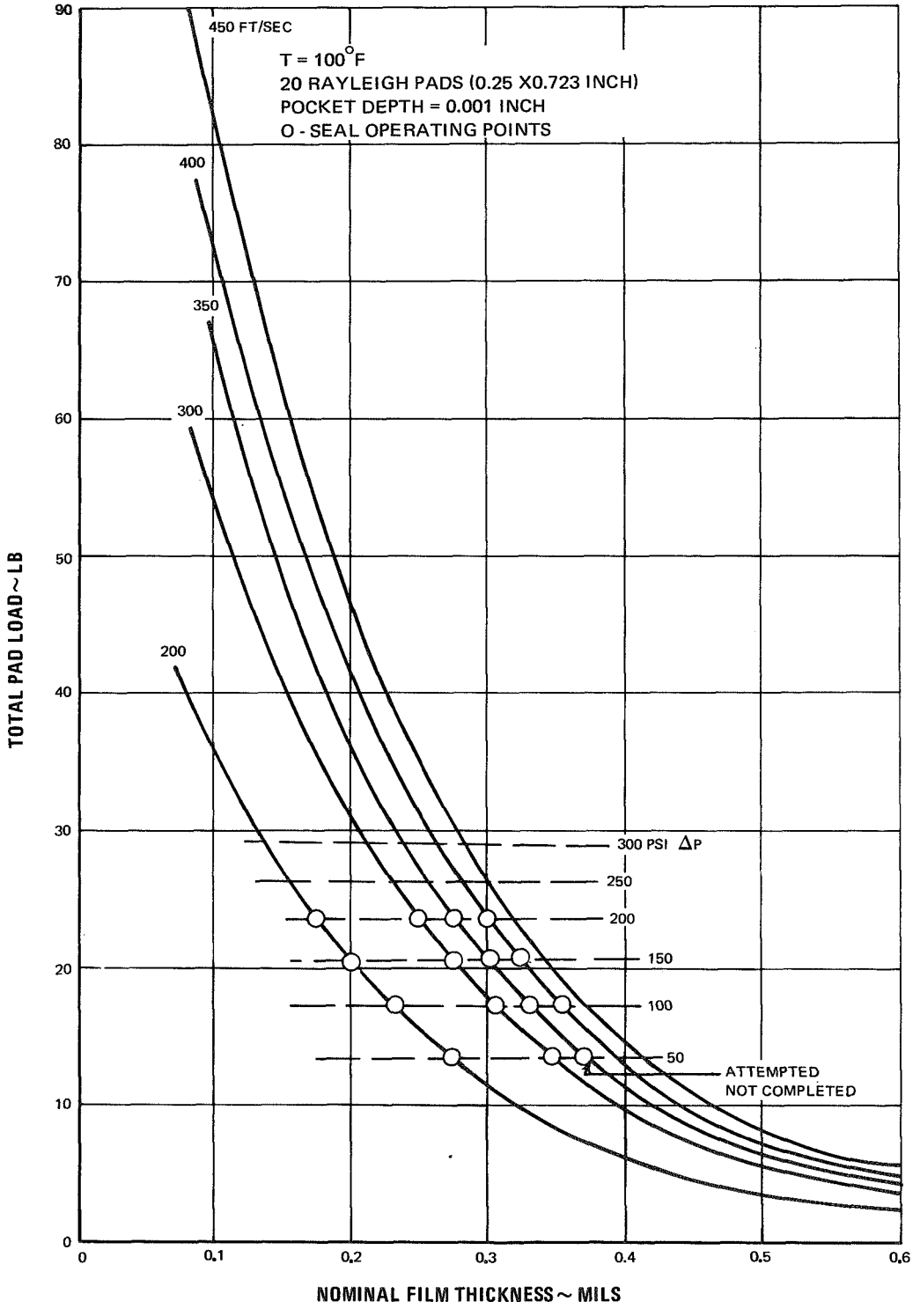

Figure 15 Calculated Primary Film Thickness for the Gas-Film Seal

TABLE III
LEAKAGE (IN SCFM) DURING SIMULATED ENGINE TESTING

Oil-In Temp. (°F)	Seal Sliding Speed (ft/sec)	Seal Pressure Differential (psi)	Leakage (in scfm) at Various Air Temperatures 400°F	600°F	800°F	1000°F
250	300	100	14.8	16.3	14.7	16.9
		150	21.0	26.2	19.4	23.6
		150		20.9		
		200	25.5	31.8	28.9	27.2
		200	32.8			
	350	100	16.7	18.2	17.6	17.5
		150	23.2	25.3	26.6	24.8
		150	22.4	35.0		
		200	25.5	22.8	35.5	32.1
		200	23.4	36.2		
	400	100	12.0	29.0	28.8	26.9
		100	36.2			
		150	23.3	38.0	33.5	32.8
		150	15.8			
		150	23.0			
		200	32.1	48.5	41.6	39.0
		200	27.9	45.1		
		200	51.5			
350	300	100	19.3	13.8	13.3	12.3
		100	14.0			
		150	21.5	24.4	19.3	17.8
		200	27.2	30.2	25.9	23.6
		200	32.1			
	350	100	21.6	17.2	15.2	15.1
		150	22.4	25.0	21.8	19.1
		150	31.6	26.5		
		200	26.8	30.9	27.9	26.8
		200	35.4			
	400	100	22.0	29.0	24.0	26.5
		150	26.2	30.2	30.2	33.5
		200	29.6	40.5	38.2	27.0
		200				39.7

During the initial simulated engine testing with 350°F oil, a sudden increase in seal air leakage was observed, and the seal was removed from the rig to determine the cause for the increase. Profile traces across the carbon nosepiece indicated a small amount of wear. The wear tapered from approximately 0.1 mil on the outer edge of the sealing dam to a negligible amount at the inner edge of the self-acting geometry.

After inspection the seal was cleaned, reinstalled in the test rig, and tested further. Both static and dynamic testing at room temperature yielded high air leakages. A systematic check of the rig indicated that air was leaking through the bore of the seal seat. A subsequent inspection revealed that the seat assembly had loosened axially during operation, allowing the parts to rotate relative to the shaft. The resulting wear created an additional leakage path through the bore of the seal seat. The heaviest wear occurred on the parts adjacent to the roller bearing.

Two steps were taken to reduce this problem. The shaft was chrome plated to reduce the clearance between the roller bearing's inner race and the shaft, and the torque on the locking nut was increased from 5000 in-lb to 10,000 in-lb. Later visual inspections of the seal revealed that the parts were no longer rotating relative to the hub. At the end of the simulated engine testing the seal, nosepiece and seal seat, were in good condition. Operation of the seal was generally satisfactory; however the data indicated a change in the leakage characteristics of the seal as the test progressed.

4. Endurance Testing - Build 1-1

After the simulated engine operation, Build 1-1 of the gas-film seal was subjected to a 20-hour endurance test at the following conditions:

Air Temperature	1000°F
Oil-in Temperature	350°F
Seal Pressure Differential	200 psi
Seal Sliding Speed	400 ft/sec

The air leakage remained at approximately 38.5 scfm throughout the test. Visual inspection at the end of the test revealed that both the seal nosepiece and seal seat were in good condition, with no signs of severe contact between the nosepiece and seal seat. The average Rayleigh pad recess depth was 0.8 mil. Figures 16 and 17 show the condition of the seal after the steady-state endurance test.

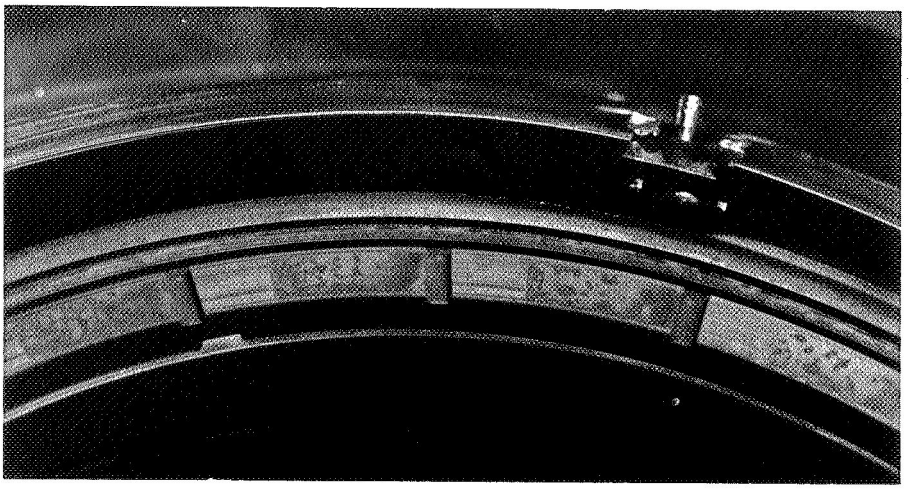

Figure 16 Rayleigh Pads After Endurance Testing in Build 1-1 (CN-20794)

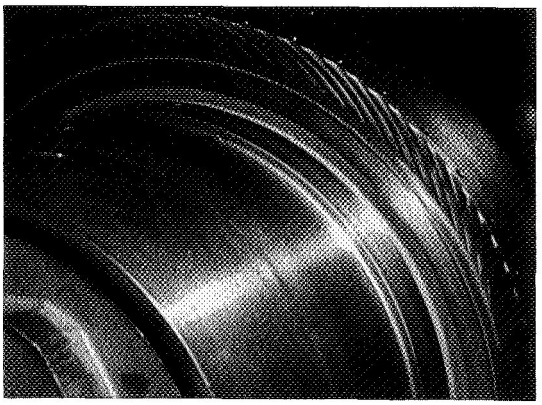

Figure 17 Seal Seat After Endurance Testing in Build 1-1 (CN-20792)

During the preliminary dynamic checkouts of Build 1, Build 1-1, and in the early stages of engine simulation testing accelerometer data was taken and sent to NASA for analysis. The accelerometers were attached to the seal nosepiece and measured nosepiece accelerations in the axial and radial directions. Analysis indicated that the accelerometer output waveform was complex at all dynamic conditions. However it was evident that the primary component of the accelerations was axial and occurred at shaft rotational frequency. Thus the nosepiece was responding primarily to the axial runout of the seat face. Accelerometer data could not be taken during later tests because temperatures at the accelerometer locations exceeded values permissible for the accelerometers.

Cyclic endurance testing followed the steady-state endurance test. Ten cycles were completed under the following conditions:

Takeoff (1/2 hour):	
Air Temperature	1200°F
Oil-in Temperature	350°F
Seal Pressure Differential	250 psi
Seal Sliding Speed	450 ft/sec
Cruise (4 hours):	
Air Temperature	1200°F
Oil-in Temperature	350°F
Seal Pressure Differential	200 psi
Seal Sliding Speed	400 ft/sec
Approach (1/2 hour):	
Air Temperature	800°F
Oil-in Temperature	350°F
Seal Pressure Differential	100 psi
Seal Sliding Speed	250 ft/sec

Air leakage during the cyclic endurance testing is summarized in Table IV.

TABLE IV
AIR LEAKAGE DURING CYCLIC ENDURANCE TESTS

Cycle	Takeoff Air Leakage (scfm)	Cruise Air Leakage (scfm)	Approach Air Leakage (scfm)
1	50.3	35.6	16.1
2	38.9	23.4	12.5
3	40.4	23.4	12.1
4	43.8	21.7	9.6
5	37.9	19.5	8.0
6	41.3	19.6	7.4
7	38.8	21.4	9.7
8	33.7	21.2	9.9
9	33.6	21.1	9.6
10	36.3	21.2	11.8

The test seal was removed from the rig for a visual inspection after completing ten cycles. Visual inspection of the carbon nosepiece revealed that the seal had been rubbing in a cocked position. Fifteen of the 20 Rayleigh pads were worn below the recess depth, as shown in Figure 18. The LCIC-coated TZM seal seat was in good condition (see Figure 19), with no signs of excessive heat generated by the rubbing.

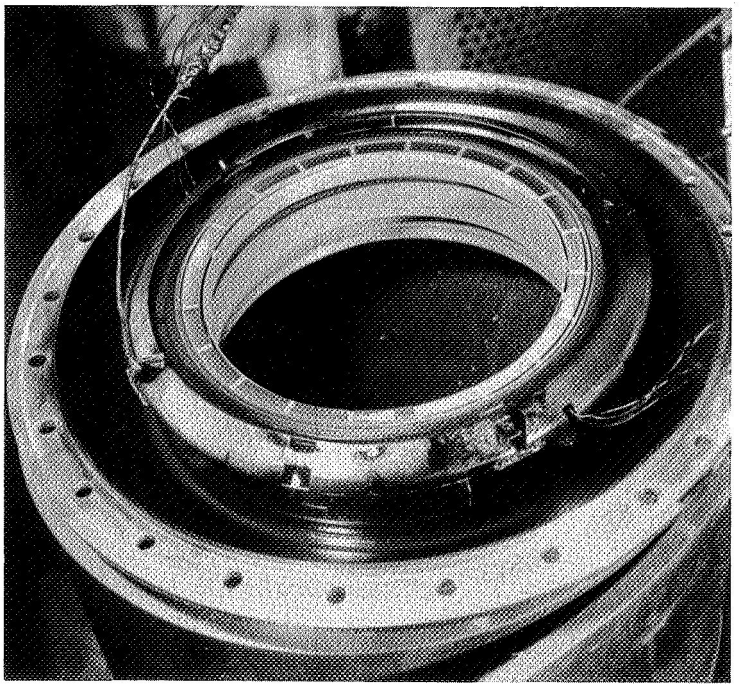

Figure 18 Carbon Nosepiece After Ten Five-Hour Endurance Cycles (CN-21256)

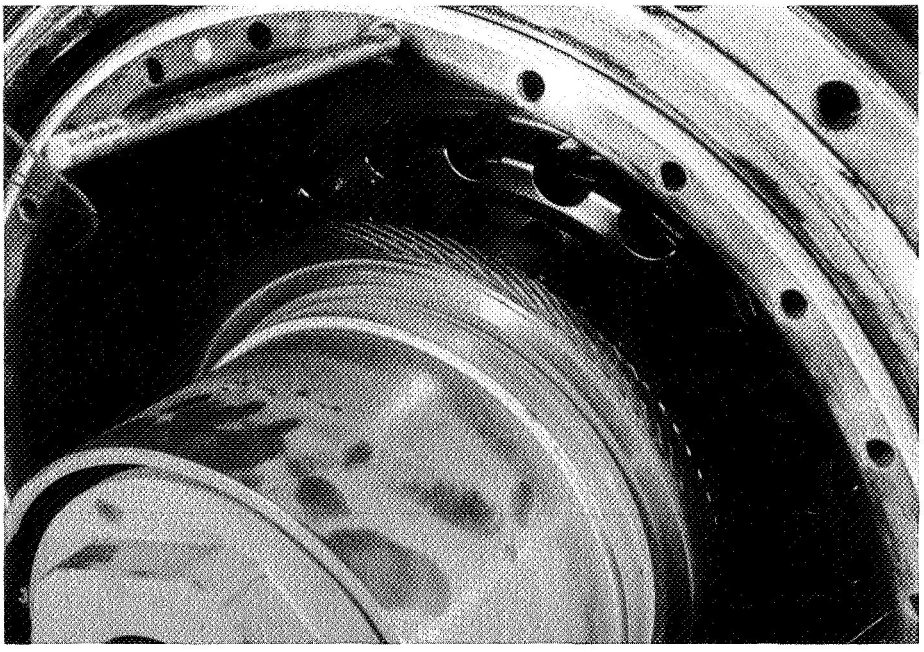

Figure 19 Seal Seat After Ten Five-Hour Endurance Cycles (CN-21257)

As a result of the visual inspection, cyclic endurance testing on Build 1-1 was terminated. The seal assembly was pressure checked in the static fixture, and as expected, showed an excessive leakage of 3.7 scfm at 20 psi. After the static check, the seal was disassembled and the components were inspected in detail.

Inspection of the nosepiece ring assembly showed that it was worn in a cocked position. The recess depth of the least worn of the Rayleigh pads was 0.7 mil deep. Approximately 180° away, the face had worn 7.5 mils. The rear face of the carbon nosepiece had assumed a conical shape, with the inner edge lower than the outer edge by eight helium light bands. The bottom surface of the three anti-rotation slots showed signs of contact with the anti-rotation lugs.

When the carrier was inspected, it was found that the surface which had been in contact with the piston ring had been damaged by fretting. A profilometer reading across the surface revealed that the wear marks were as much as 0.3 mil deep. The area next to the nosepiece and the high-pressure areas remained clean, while the other areas were heavily coated with oil deposits as shown in Figure 20. With the nosepiece ring installed on the carrier, the seal dam was concentric with the balance diameter within 1.6 mils.

The wear pattern on the piston ring corresponded to the cocked position of the carrier (caused by the cocked nosepiece wear). The maximum piston ring sealing-land wear was 0.1 mil, and the maximum piston ring support-land wear was 0.3 mil. The most significant factor contributing to nosepiece wear was the radial interference caused by differential thermal expansion between the retainer ring and the anti-rotation lugs. The heaviest wear on the carbon nosepiece was at the location of one of the three lugs. Therefore, the radial clearance between the nosepiece ring and the anti-rotation lugs was increased: no further problem due to interference was experienced.

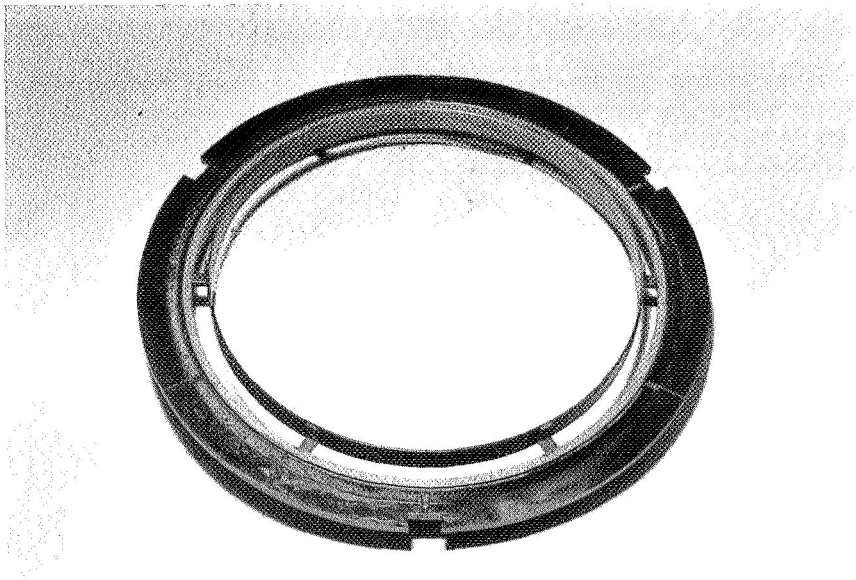

Figure 20 Front View of Carrier. Note Heavy Oil Deposits (CN-21330)

5. Endurance Testing - Build 2

Build 2 of the gas-film seal used the repaired carbon nosepiece from Build 1, and incorporated an increased torque-pin clearance. Build 2 was subjected to a 200-hour endurance test which was split into a 50-hour segment, a 100-hour segment, and a final 50-hour segment. The test conditions for the three segments are listed below:

	First Segment	Second Segment	Third Segment
Air Temperature (°F)	1000	1000	800
Oil-in Temperature (°F)	350	350	350
Seal Pressure Differential (psi)	200	200	100
Seal Velocity (ft/sec)	400	400	250
Spring Load (lbs)	7.8	7.8	15.6

During the first 50-hour segment, the air leakage gradually increased as the test progressed, as shown in Figure 21. During the first segment, the seal was frequently removed from the rig for visual inspection. These inspections showed that the Rayleigh pad land area was being progressively polished from the outer edge toward the inner edge. It was also noted that the seal dam became scratched as the testing progressed.

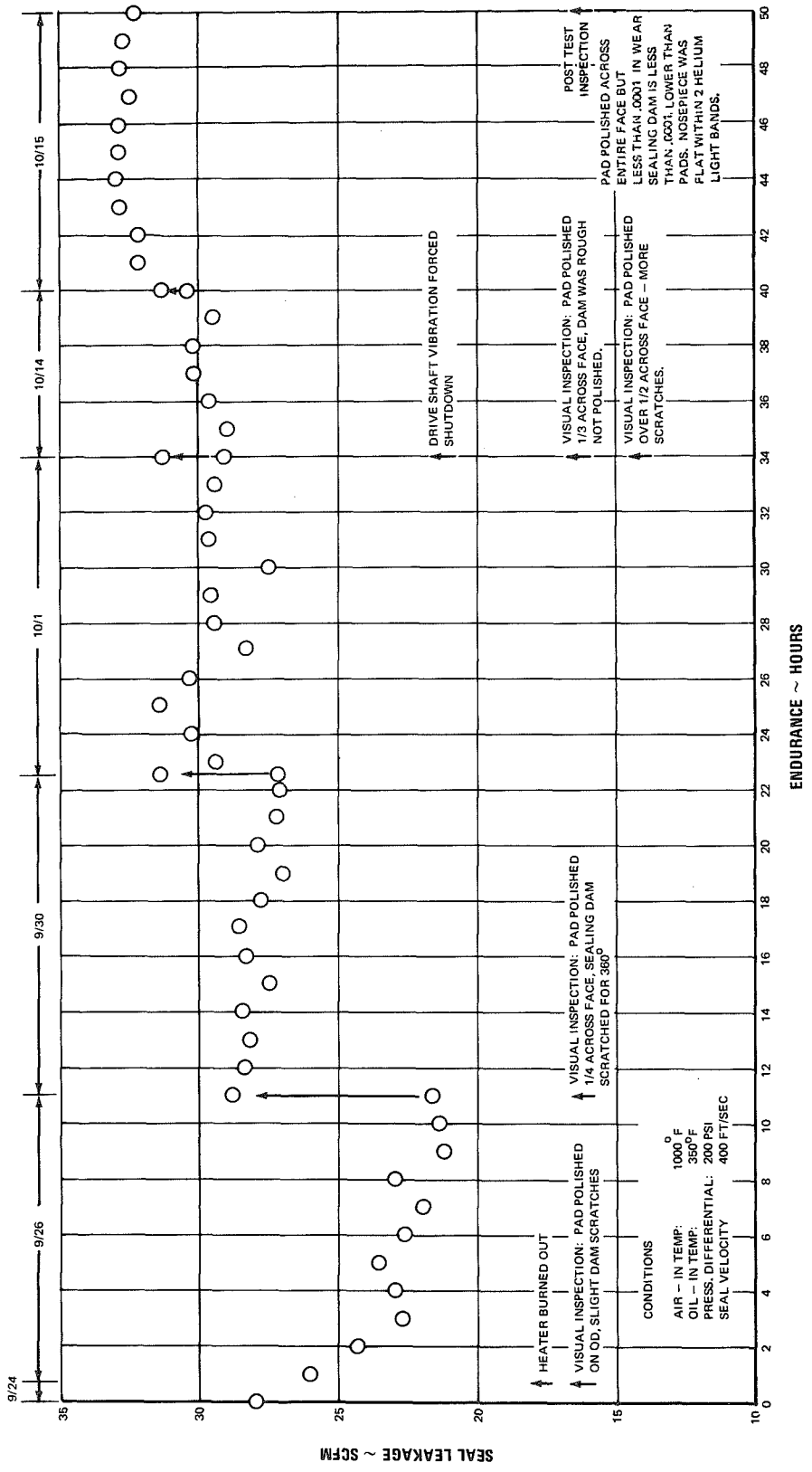

Figure 21 Air Leakage Past Build 2 of the Gas-Film Seal During a 50-Hour endurance Test

At the end of the first 50 hours, the seal was disassembled for inspection. The Rayleigh pad recess depth was measured with a 0.0001-inch dial indicator, and it was found that the seal face had worn less than 0.1 mil. The seal dam was scratched and slightly lower than the Rayleigh pads. The nosepiece remained flat within two helium light bands in the area of the Rayleigh pad lands. After inspection, the seal was reassembled and reinstalled in the test rig for the second test segment.

The 100-hour segment of endurance testing on Build 2 was run continuously, except for a half-hour shutdown caused by an ignition failure in the drive engine. The sudden shutdown and startup had no apparent adverse effects on the seal. The initial air leakage of 40 scfm decreased to 32 scfm (the final leakage of the first test segment) after 12 hours of running, and gradually decreased to 28 scfm by the end of the second segment. The air leakage data recorded during the 100-hour segment are presented in Figure 22.

After the 100-hour test, before the seal was removed from the rig, the static leakage was checked. This check showed a significant increase over pretest static leakage. A further test in the static pressure check fixture showed a leakage of 3.7 scfm at a pressure differential of 10 psi. Prior to the 100-hour endurance segment, static leakages in the fixture had been 1.6 scfm at 20 psi, 2.4 scfm at 30 psi, 3.1 scfm at 40 psi, and 4.0 scfm at 50 psi.

The condition of the seal after disassembly is shown in Figure 23. The Rayleigh pad land surfaces were polished, but the sealing dam was not. The sealing dam, however, had circumferential scratches. The chromium carbide coated molybdenum alloy (TZM) seal seat shown in Figure 24, was in excellent condition, with no signs of severe contact between the seat and the nosepiece.

A flatness check of the seal face showed that each Rayleigh pad land was flat within three helium light bands, and overall flatness of the 20 Rayleigh pads was within six helium light bands.

Profile traces were taken across the face of the carbon nosepiece at several circumferential locations with a Clevite surface analyzer. Representative traces are shown in Figures 25 and 26. Figure 25 shows the nosepiece in the as-received condition, while Figure 26 shows that the sealing dam was tapered and scored during testing. At the particular location shown in Figure 26, the trace shows a scratch 1.5 mils deep, and a 0.4-mil taper across the sealing dam. The inner edge of the seal dam was lower than the outer edge. It is believed that the damage to the sealing dam was caused by ceramic particles which broke loose from the electric air heater and were carried into the rig by the air flow. To reduce the amount of particles carried into the rig, the shutdown procedure was revised and a trap was installed in the air line.

The profile trace in Figure 26 also shows that the average Rayleigh pad recess depth at that location was 0.86 mil. (The original Rayleigh pad recess depth was 0.92 mil). Thus, after a total test time of 171 hours, of which 150 hours were endurance testing, the Rayleigh pad wear was 0.06 mil at this location. Surface traces taken at 5 of the 20 Rayleigh pads showed that the average wear was 0.07 mil.

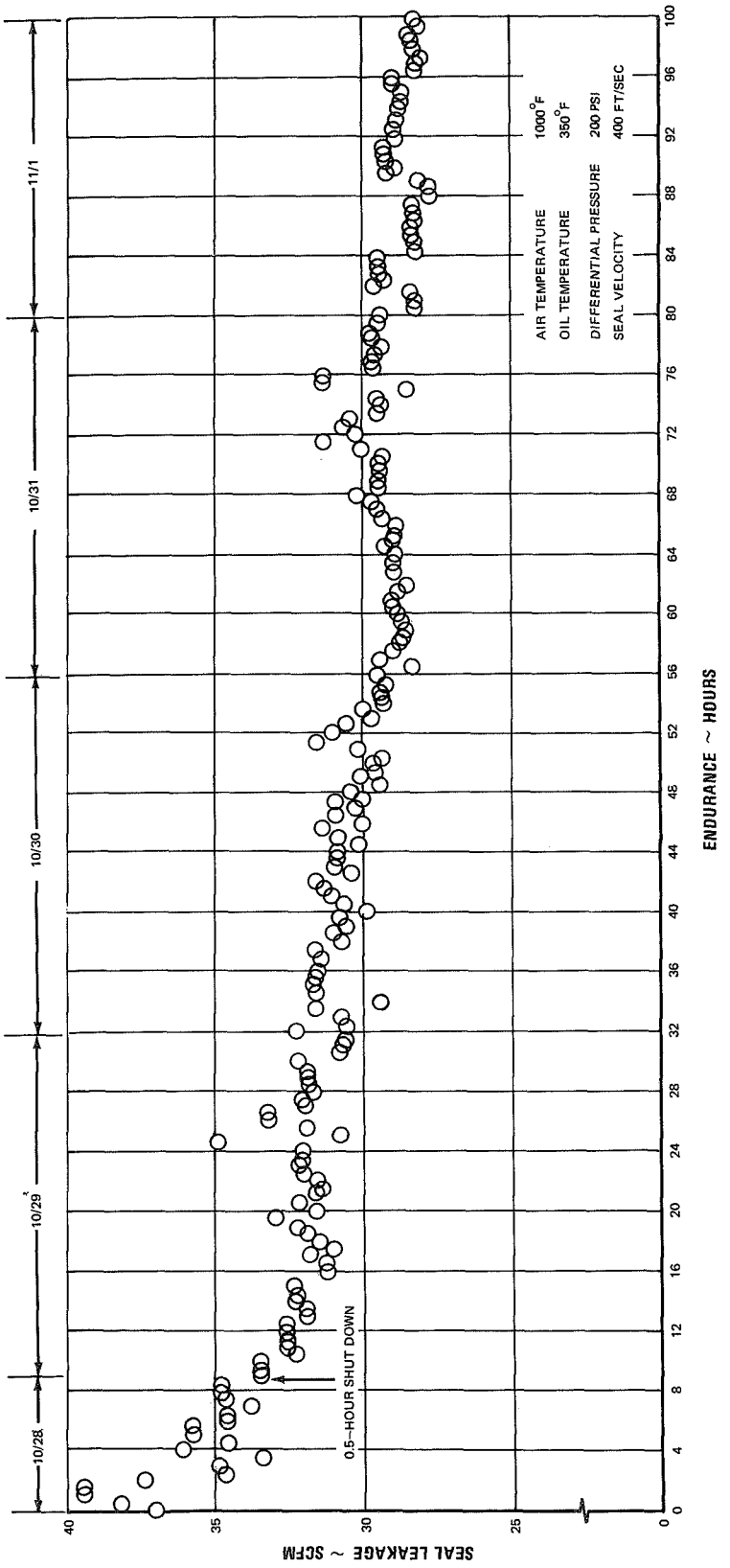

Figure 22 Air Leakage Past Build 2 of the Gas-Film Seal During the First 100-Hour Endurance Test

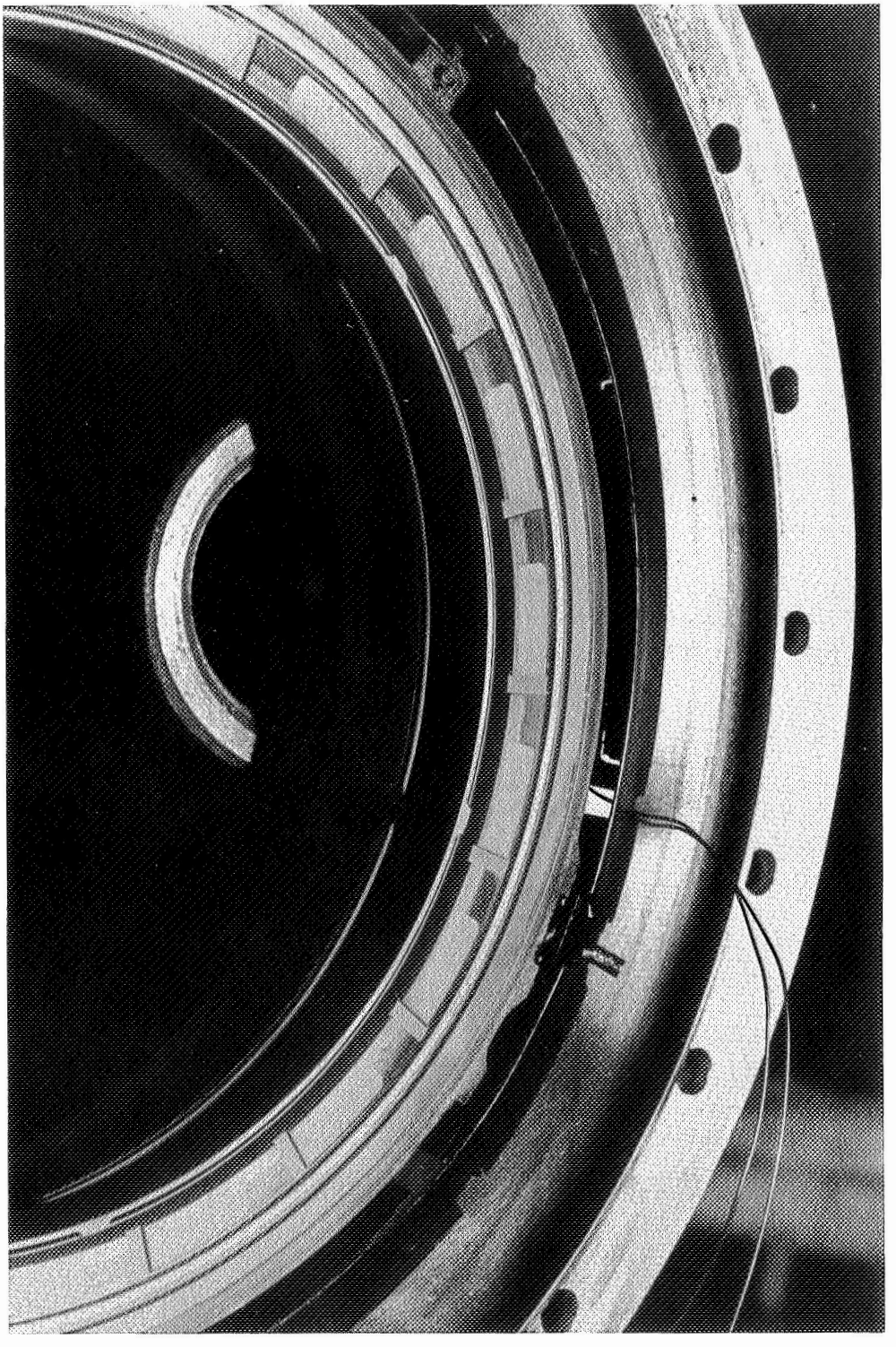

Figure 23 Build 2 of the Gas-Film Seal Assembly After 100-Hour Endurance Test. Total Time on Seal 171.2 Hours (CN-22282)

Figure 24 Condition of Chromium-Carbide-Coated Molybdenum Alloy Gas-Film Seal Seat Used in Build 2 After a Total Test Time of 315 Hours (CN-22281)

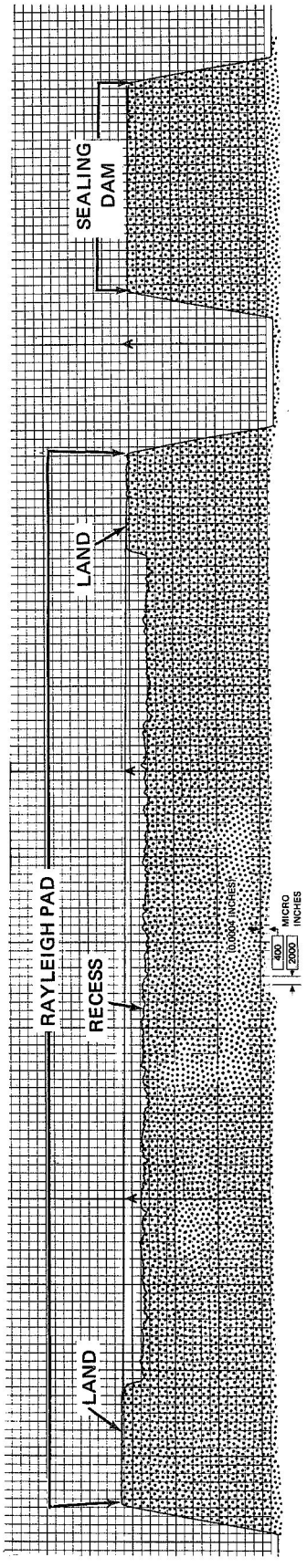

Figure 25 Representative Profile Trace Radially Across a Rayleigh Pad from Build 2 Before Testing

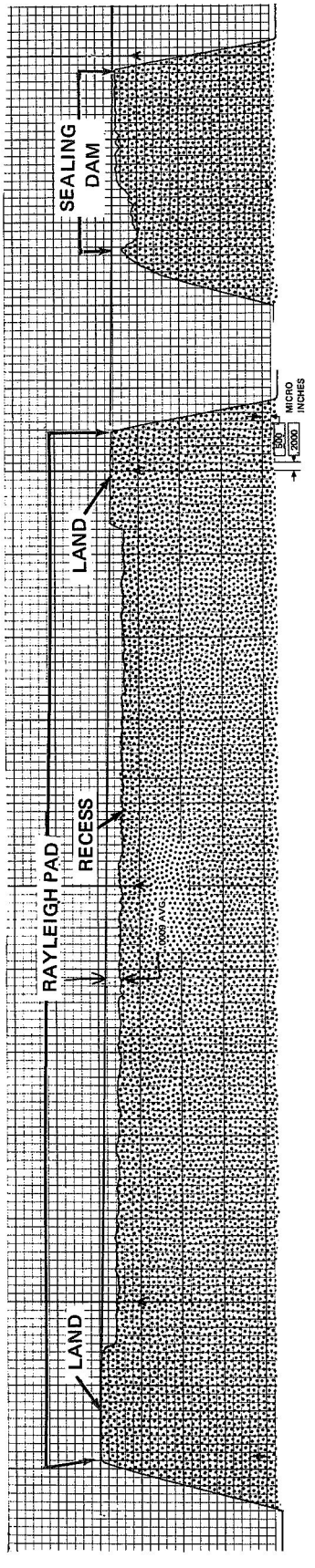

Figure 26 Representative Profile Trace Radially Across a Rayleigh Pad from Build 2 After a Total of 150 Hours

After inspection, the back face of the carbon nosepiece was lightly hand lapped to remove the oil deposits that had coked on during operation. The test seal was reassembled with 18 springs (double the previous number). It was hoped that the additional spring force would decrease the operating film thickness and reduce the air leakage. A static leakage calibration was taken and compared with a calibration performed before the 100-hour segment. The effect of the tapered dam is more pronounced at the higher pressures, as shown in the tabulation below.

Pressure Differential (psi)	Leakage With 9 Springs Before 100-Hour Segment (scfm)	Leakage with 18 Springs After 100-Hour Segment (scfm)
50	6.3	6.7
100	12.1	18.2
150	21.2	40.4
200	40.5	77.0

Because the static leakage measurements indicated a high leakage rate and because the profile traces of the carbon nosepiece indicated a highly tapered flow passage at the sealing dam, an effort was made to correlate flow passage taper angle with equilibrium film thickness and leakage rate. To calculate the leakage, an existing computer program was modified to account for entrance losses and film friction with a tapered flow path. However, the profile traces showed that the leakage path was not constant around the circumference of the nosepiece. To account for this variation, the sealing dam was divided into five sections and an average slope and a mean depth below the Rayleigh pads were found for each section. From the load capacity of the Rayleigh pads, and curves of gas leakage versus film thickness, an equilibrium film thickness and leakage could be obtained for each section of the dam. The calculations were performed for an air temperature of 400°F, a nosepiece temperature of 360°F, a seal pressure differential of 150 psi, a seal velocity of 300 ft/sec, and a spring force of 15.6 pounds which resulted from use of 18 springs. A test point was run at those conditions just prior to the last segment of the 200-hour endurance test. The predicted leakage at those conditions was 29.1 scfm, while the measured leakage was 29.8 scfm.

At the start of the final 50-hour segment of the endurance test, the air leakage was 13.5 scfm. It remained nearly constant during the entire segment, as shown in Figure 27. A power failure after approximately 44 hours shut the rig down, but did not significantly affect seal operation.

At the end of the final 50-hour segment, surface traces were taken across the same Rayleigh pads that had been checked earlier. Figure 28 shows a trace at the same circumferential location as the traces of Figures 25 and 26. Figure 28 shows that the maximum scratch depth and taper in the sealing dam had increased slightly, to 1.6 and 0.6 mils respectively. The average Rayleigh pad recess depth from this trace is 0.78 mil. Thus, the Rayleigh pad wear after 200 hours of steady-state endurance testing was 0.14 mil in this location. The average wear at five pads was also found to be 0.14 mil.

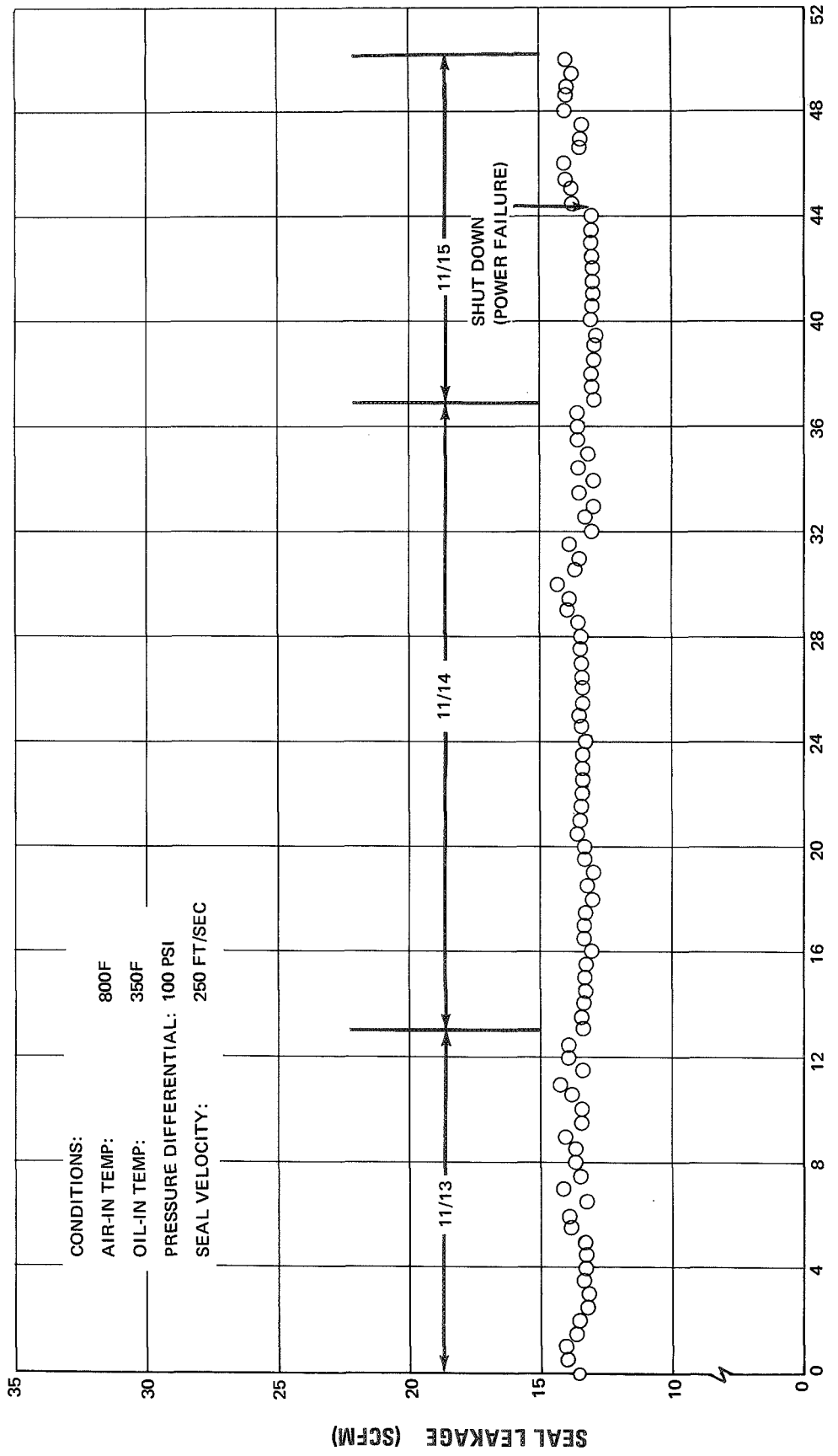

Figure 27 Air Leakage from Build 2-1 of the Gas-Film Seal for the Second 50-Hour Endurance Test

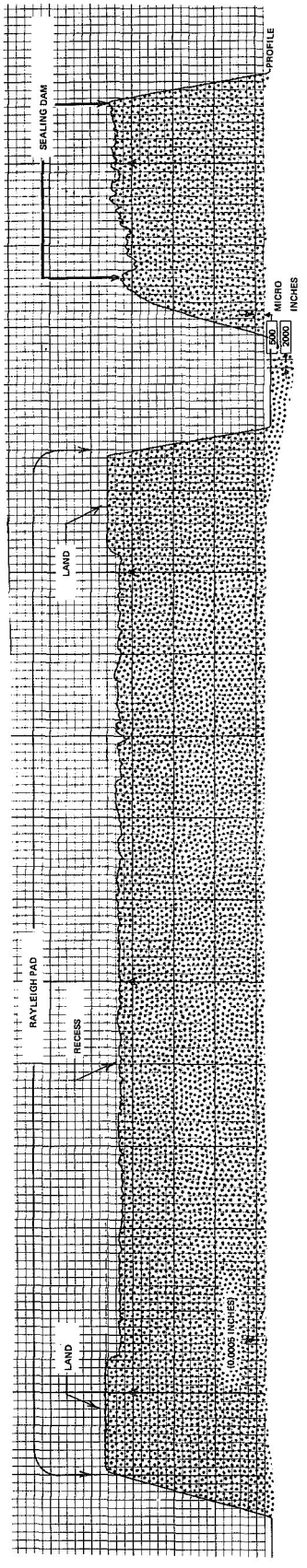

Figure 28 Representative Profile Trace Radially Across a Rayleigh Pad from Build 2-1 After a Total of 200 Hours of Endurance

6. Endurance Testing - Build 3

Build 3 of the gas-film seal used a new nosepiece installed in the support assembly from Build 2. It was subjected to 320 hours of steady-state endurance testing, which was split into a 120-hour segment and a 200-hour segment. Test conditions for both segments are tabulated below.

	First Segment	Second Segment
Air Temperature (°F)	1000	1000
Oil-in Temperature (°F)	285	280
Seal Pressure Differential (psi)	200	200
Seal Velocity (ft/sec)	400	400
Spring Load (lbs)	15.4	15.4
Number of Springs	18	18

During the first segment of testing, seal leakage averaged approximately 11.7 scfm, as shown in Figure 29. During the second segment, leakage averaged 14 scfm for the first 100 hours, and increased at the rate of approximately 1 scfm per 20 hours for the second 100 hours (see Figure 30).

Near the end of the first segment of testing, an increase in vibration was noted at the rig's rear thrust bearings. Disassembly and inspection revealed a spalled outer race in one of the duplex thrust bearings. The spalled race is shown in Figure 31. As shown in Figure 32, the vibration did not harm the carbon nosepiece, although the leakage had increased with the vibration.

A pretest profile trace of the Build 3 carbon nosepiece face is shown in Figure 33. A trace taken at the same location after 120 hours of endurance is shown in Figure 34. The deepest scratch in the sealing dam was approximately 0.2 mil deep. The average Rayleigh pad wear for the 120-hour test was less than 0.05 mil.

After the second segment of testing the carbon nosepiece and seal seat were still in good condition. Figure 35 is a close-up view of the carbon nosepiece showing the Rayleigh pads and sealing dam. Figure 36 is a close-up of the seal seat, which had accumulated a total time of 715.3 hours. A profile trace (Figure 37) taken at the same location as the traces in Figures 33 and 34 shows more shallow scratches (50 to 100 microinches), but there was no increase in the number of deep scratches (200 microinches or more). The average wear on the Rayleigh pads for the second segment of testing was less than 0.05 mil.

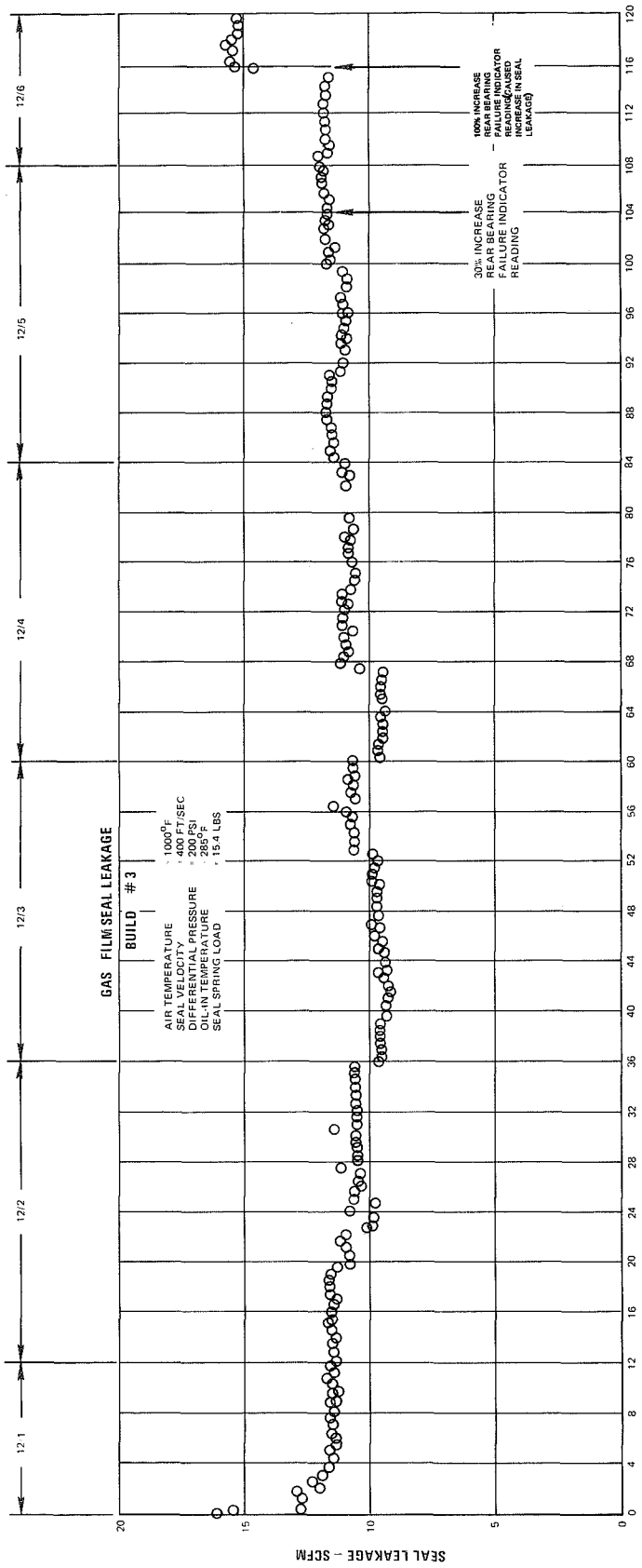

Figure 29 Build 3 Gas-Film Seal Air Leakage for 120-Hour Endurance Test

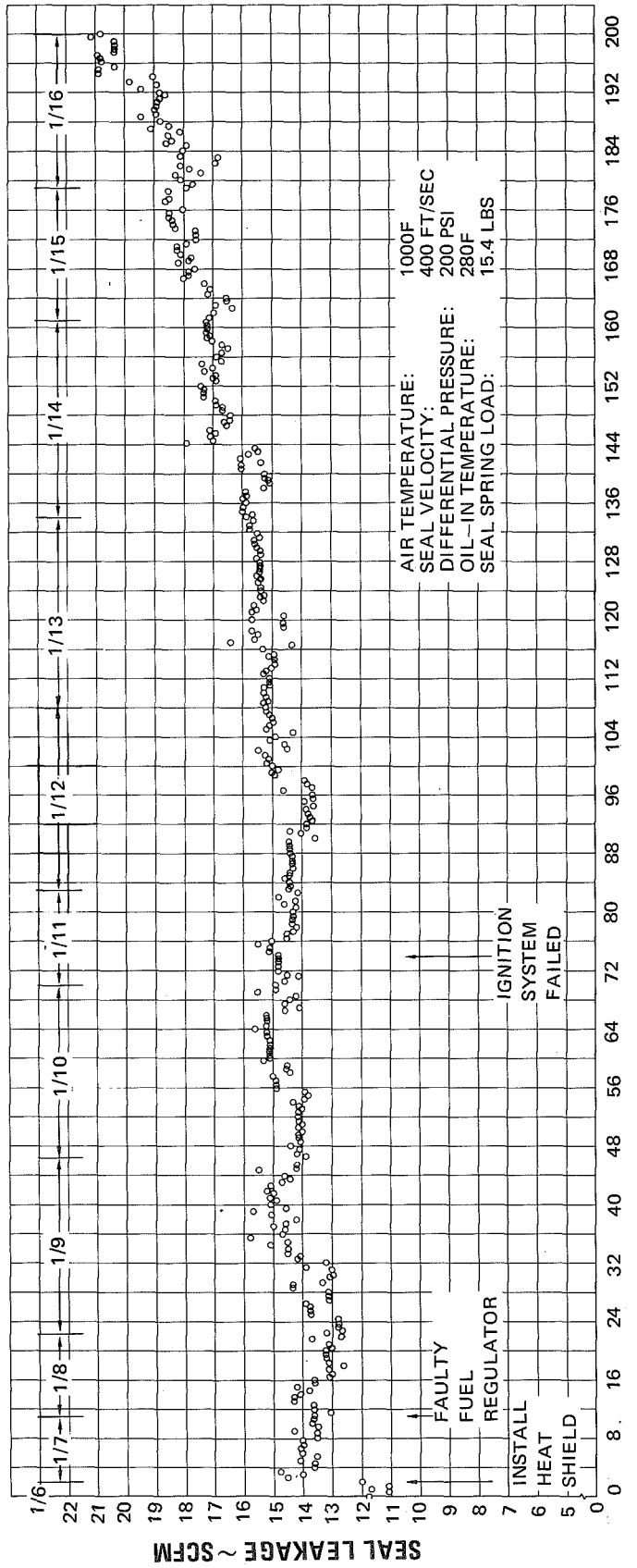

Figure 30 Measured Air Leakage During Second 200 Hours of Endurance Testing on Build 3 of the Gas-Film Seal

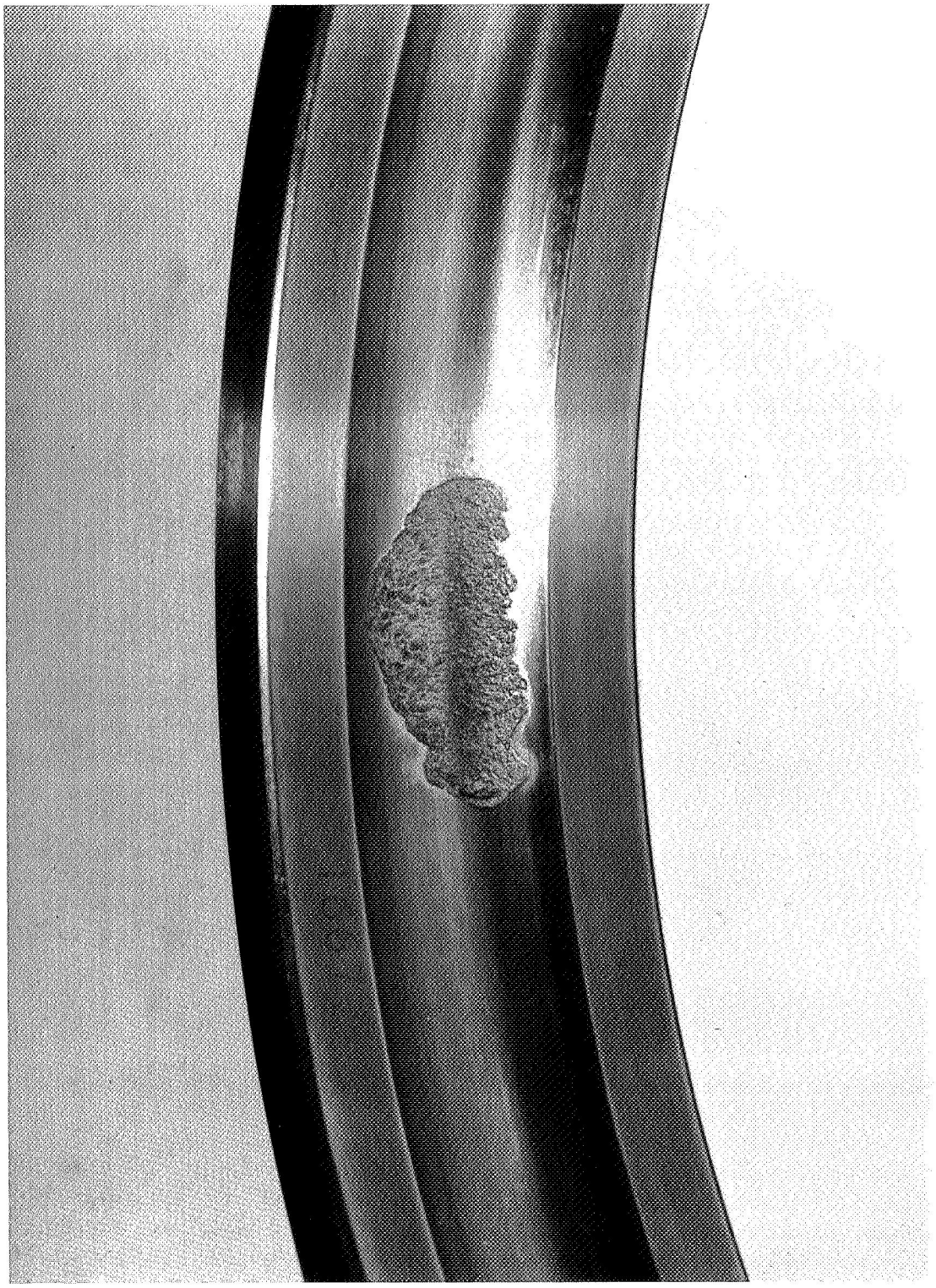

Figure 31 Spalled Outer Race (XPN-4825)

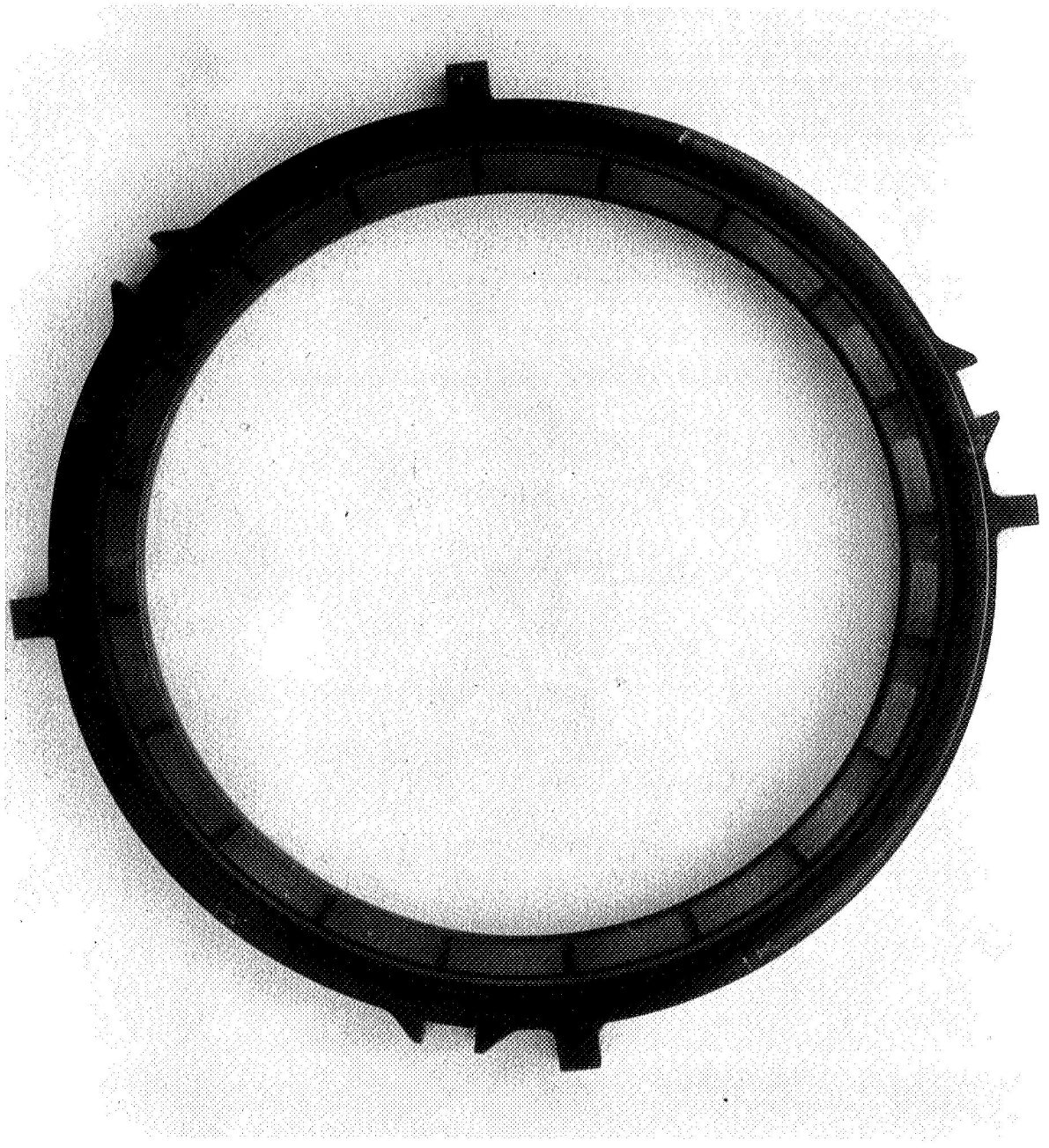

Figure 32 Condition of Build 3 Gas-Film Seal Assembly Nosepiece After 120-Hour Endurance Test. Total Time on Seal 124.5 Hours (CN-23136)

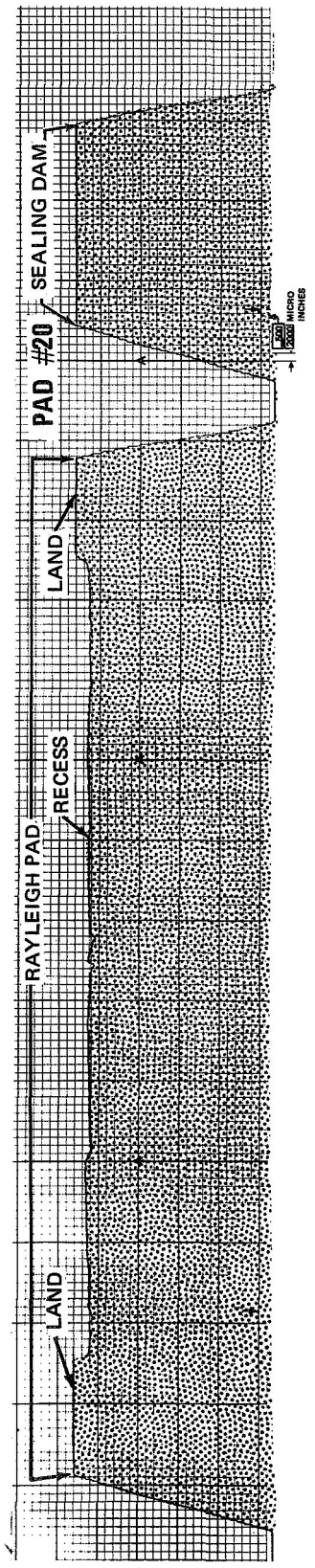

Figure 33 Representative Profile Trace Radially Across a Rayleigh Pad from Build 3 Before Testing

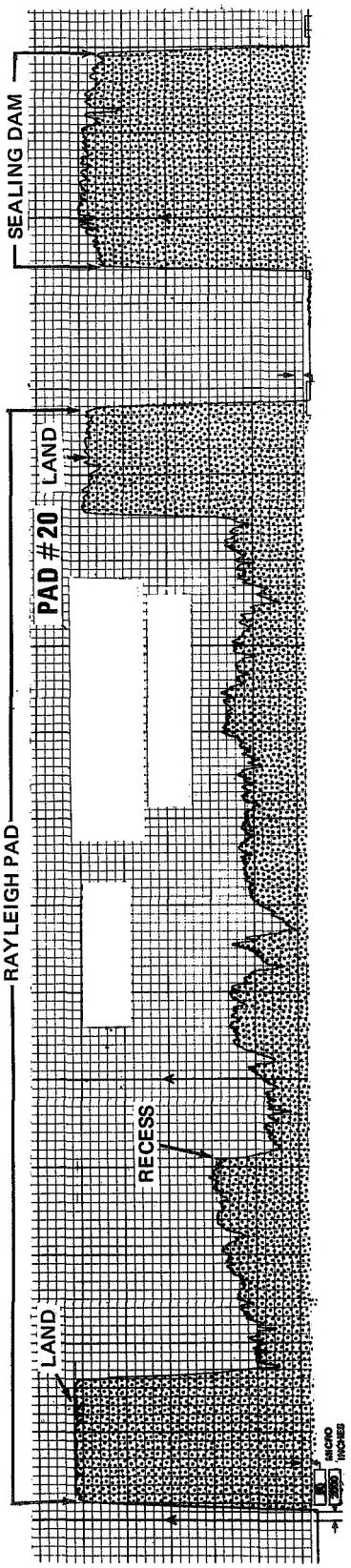

Figure 34 Representative Profile Trace Radially Across a Rayleigh Pad from Build 3 After 120 Hours of Endurance

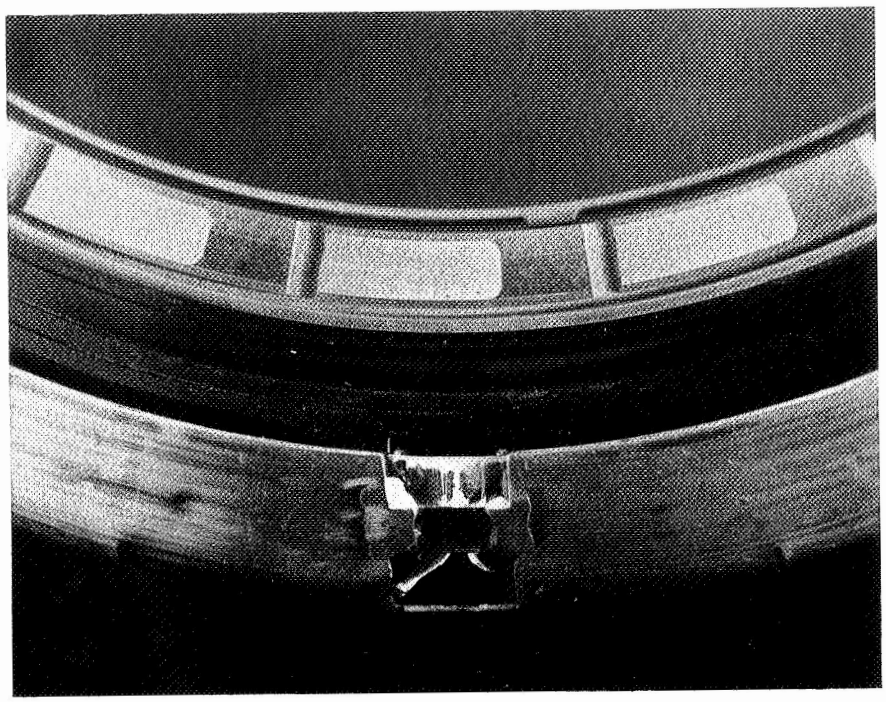

Figure 35 Close-Up of Carbon Nosepiece from Build 3 of the Gas-Film Seal After 200 Hours of Endurance Testing. Total Time on Seal: 338.5 Hours (CN-23544)

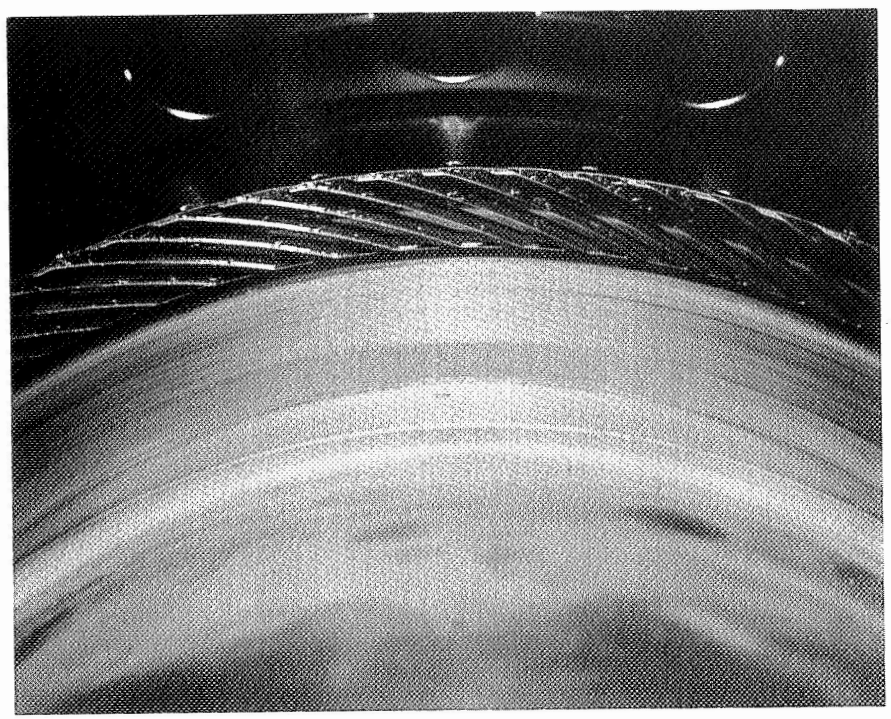

Figure 36 Close-Up of TZM Seal Seat from Build 3 of the Gas-Film Seal After 200 Hours of Endurance Testing. Total Time on Seal Seat: 715.3 Hours (CN-23541)

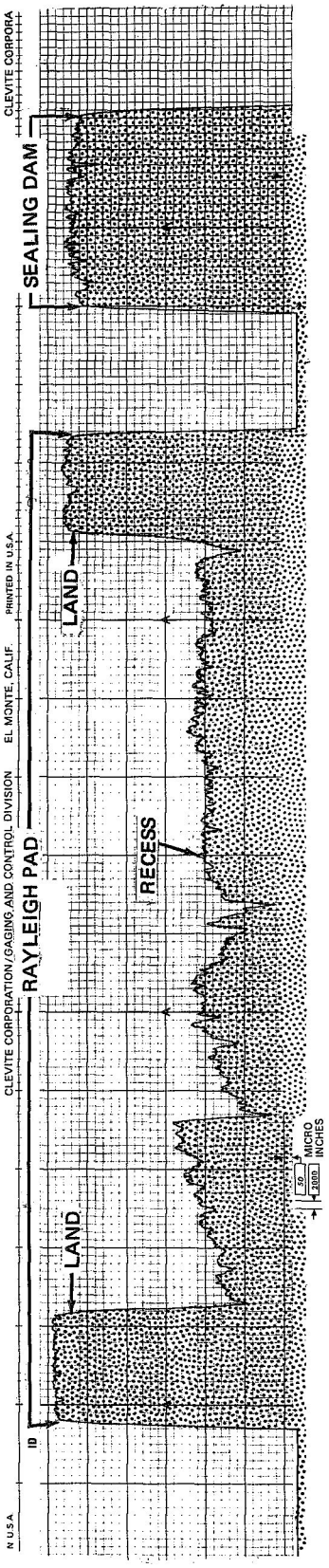

Figure 37 Representative Profile Trace Radially Across a Rayleigh Pad from Build 3 After 200 Hours of Endurance. Total Time on Seal 338.5 Hours.

A posttest check of leakage in the static fixture revealed increased leakage, as shown below:

Pressure (psi)	Pretest Air Leakage (scfm)	Posttest (after 338.5 hours) Air Leakage (scfm)
10	0.90	1.00
20	1.55	1.85
30	2.15	3.05
40	2.65	4.15
50	3.05	
60	3.55	
70	3.90	

After the static-fixture calibration, the seal assembly was disassembled. The back face of the carbon nosepiece and the face of the carrier were lapped lightly to remove deposits of oil residue, after which the seal was reassembled and pressure checked. Pressure checks with the cleaned parts were made with the piston ring in two positions: its old position and at a new position, a previously unused area on the bore of the carrier. Pressure checks were also made with a new piston ring, and the new ring gave better leakage results at both positions. The old piston ring and carrier had been used in Build 2 of the seal, and had accumulated a total time of 570.4 hours. The results of the pressure checks are presented in the tabulation below.

	Old Piston Ring Old Position	Old Piston Ring New Position	New Piston Ring Old Position	New Piston Ring New Position
Pressure (psi)	Air Leakage (scfm)	Air Leakage (scfm)	Air Leakage (scfm)	Air Leakage (scfm)
10	1.70	0.95	1.50	0.70
20	3.00	1.65	2.40	1.20
30	4.15	1.95	3.25	1.70
40		3.15	4.05	2.20
50				2.65
60		4.05		3.15
70				3.60
80				4.20

These pressure checks offer strong evidence that fretting damage to the piston ring and carrier bore caused an increase in piston-ring leakage during the 200-hour segment of endurance testing on Build 3. In order to relate the pretest and posttest static leakage measurements to the change in leakage observed during the endurance test, the static leakage data must be extrapolated to a 200-psi pressure differential and an air temperature of 600°F at the piston ring. This estimate of air temperature is based on a calculated metal temperature of about 500°F in the region of the piston ring and carrier. Extrapolation

to 200 psi yields a pretest leakage of 9.0 scfm and a posttest leakage of 21.0 scfm, while correction to 600°F reduces these rates to 4.5 scfm and 10.5 scfm, respectively. The difference of 6.0 scfm correlates well with the change in leakage observed during the endurance test. Thus it was concluded that the gradual increase in leakage during the last 100 hours was due to fretting wear of the piston ring and mating carrier bore.

7. Endurance Testing - Build 3-1

In an effort to counteract the fretting damage to the piston ring and bore, a new piston ring was installed on the seal for Build 3-1. Six hours of steady-state endurance testing were completed on Build 3-1 at an air temperature of 1000°F, a sliding speed of 400 ft/sec, a pressure differential of 200 psi, an oil-in temperature of 280°F, and a spring load of 15.4 pounds. As shown in Figure 38, the air leakage was about 22 scfm.

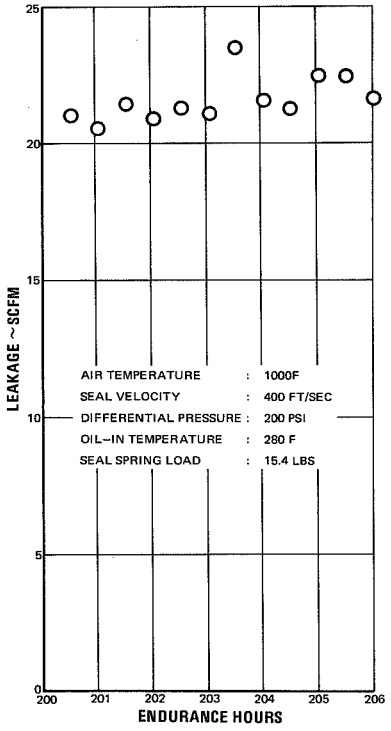

Figure 38 Measured Air Leakage During First Six Hours of Endurance Testing on Build 3-1 of the Gas-Film Seal

After the six hours of testing, the seal was removed from the rig for inspection. There was evidence that the damage to the carrier bore was severe enough to cause the new piston ring to hang up. Profile traces across the bore surface revealed that areas adjacent to the unused portion of the surface were 0.1 mil above and below it. A dynamic check of Build 3-1 at the endurance test conditions revealed an air leakage of 24 scfm. After this test, profile traces across the carbon nosepieces revealed that the seal dam had circumferential scratches 1 mil deep. The scratches on the seal dam contributed to the high primary leakage, while scratches on the carrier bore increased the piston-ring secondary leakage. A 6X magnified view of the carrier bore surface is shown in Figure 39. The contact areas for the piston-ring support land and the sealing land are clearly visible.

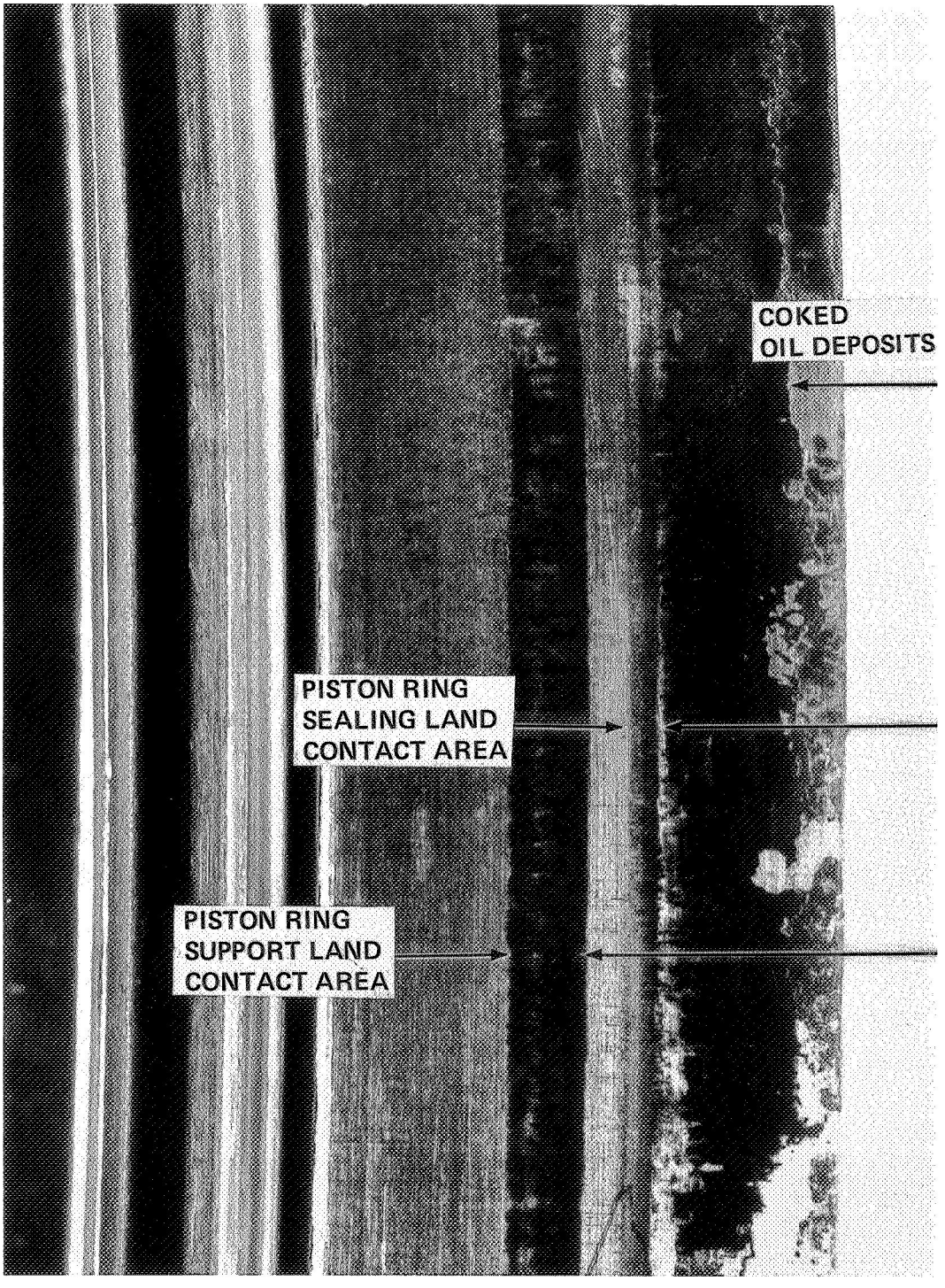

Figure 39 6X View of Carrier Piston Ring Bore Surface (XPN-6466)

8. Endurance Testing - Build 3-2

Because repairs to the spare TZM carrier (previously used in Build 1- 1) had not been completed, NASA furnished the contractor with the 410 stainless steel carrier and Inconel piston ring from the liquid-film seal assembly. These components are physically interchangeable with the comparable parts in the gas-film seal: the only significant difference is the material. Both components in the gas-film seal are made of TZM. As the start-and-stop cycles immediately planned for the gas-film seal were to be run at ambient air temperatures, the change in material would not be a factor in the seal performance. Therefore, the TZM carrier and piston ring were replaced in Build 3-2 with the 410 stainless steel carrier and Inconel piston ring.

Build 3-2 completed a program of 40 starts and stops. The cycles were carried out with ambient air at a pressure differential of 100 psi across the seal. The shaft speed was increased from 0 rpm to 8500 rpm (250 ft/sec) in approximately 15 seconds. After the seal air leakage and temperature had stabilized (approximately 15 minutes), the dynamic air leakage was recorded. After the test data was recorded, the test rig drive shaft was disengaged and the rig rotor allowed to coast down to 0 rpm, which took about 25 seconds. The static and dynamic leakages for the 40 cycles are presented in Figure 40.

Visual inspection of the test seal after the tenth and thirtieth cycles revealed that the nosepiece and seal seat were in good condition. The seal was subjected to a complete inspection after the fortieth cycle. Comparison of profile traces across the carbon nosepiece before and after the 40 cycles revealed less than 0.05 mil wear to the nosepiece face.

9. Endurance Testing - Build 3-3

As repairs to the TZM carrier were not completed, use of the 410 stainless steel carrier and Inconel piston ring was considered for the remaining 94 hours of endurance testing. Previous test data had indicated that the carrier temperatures were not so severe as originally estimated, therefore the increase in the coefficient of thermal expansion would not appreciably affect the seal balance diameter until carrier temperatures reached approximately 500°F. At 600°F, the coefficient of thermal expansion for TZM is 3.0×10^{-6} in/in-°F, while that for 410 steel is 6.2×10^{-6} in/in-°F.

After discussion with the NASA Project Manager, the program for the remaining endurance testing was modified. The sliding speed and pressure differential were to remain at 400 ft/sec and 200 psi. The seal spring load was reduced from 15.4 to 7.8 pounds to allow for the expected growth in the secondary sealing diameter at the higher air temperatures. The air temperature was to start at 200°F and be raised in increments of 100°F for each day of endurance testing until 1000°F was reached. The results of this testing are tabulated below:

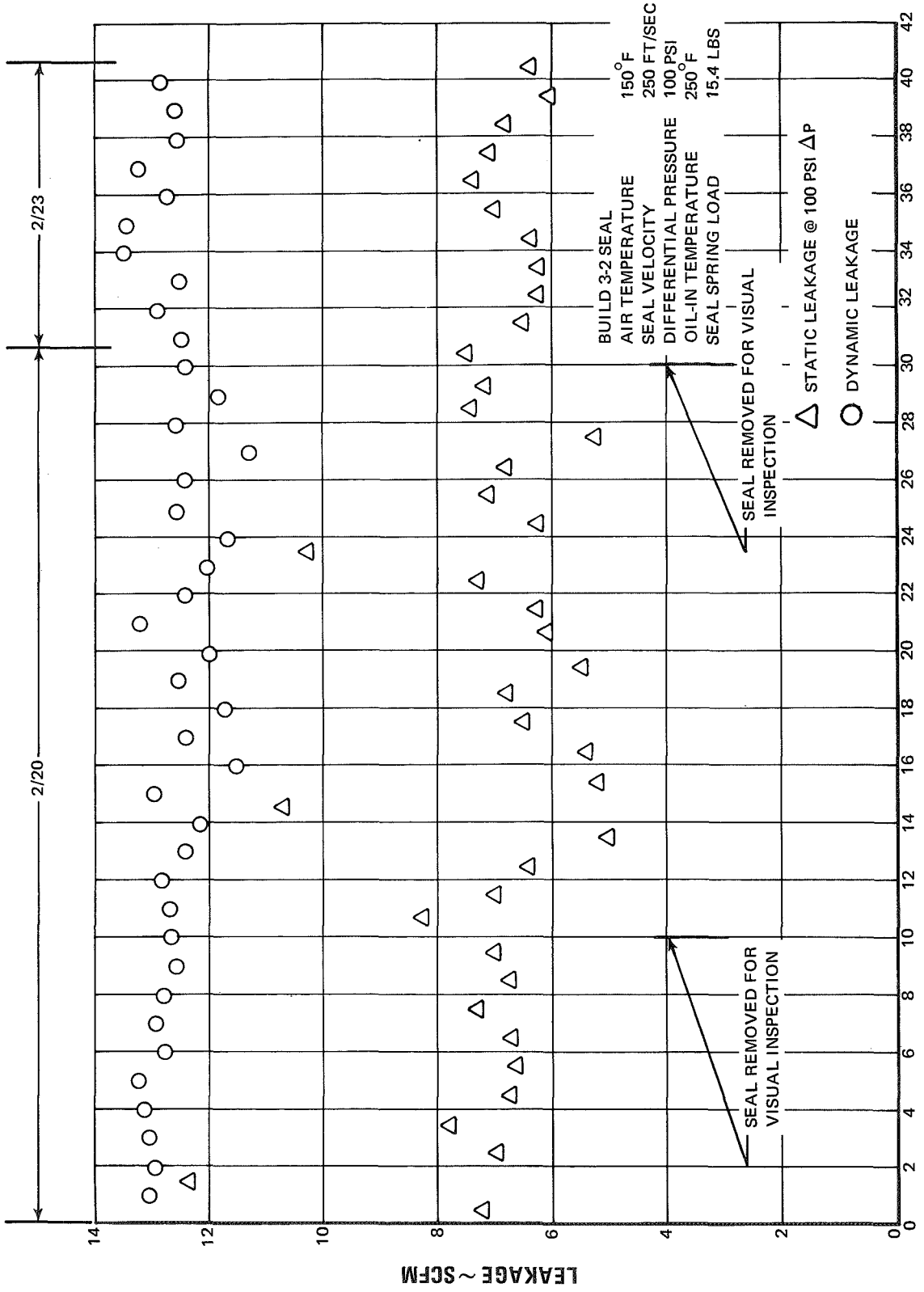

Figure 40 Static and Dynamic Air Leakage Past Build 3-2 of the Gas-Film Seal

Time (hrs)	Air Temperature (°F)	Average Air Leakage (scfm)
21.0	200	32.0
11.0	400	29.5
12.0	500	30.0
8.0	600	27.0
11.0	700	25.5
9.0	800	25.5

Skin temperature (low pressure, sump side) data from the 410 stainless steel carrier (shown in Figure 41) indicated that the piston-ring gap would not be sufficient to prevent the ends of the ring from butting together at temperatures higher than 800°F. At room temperature the gap is 24 mils.

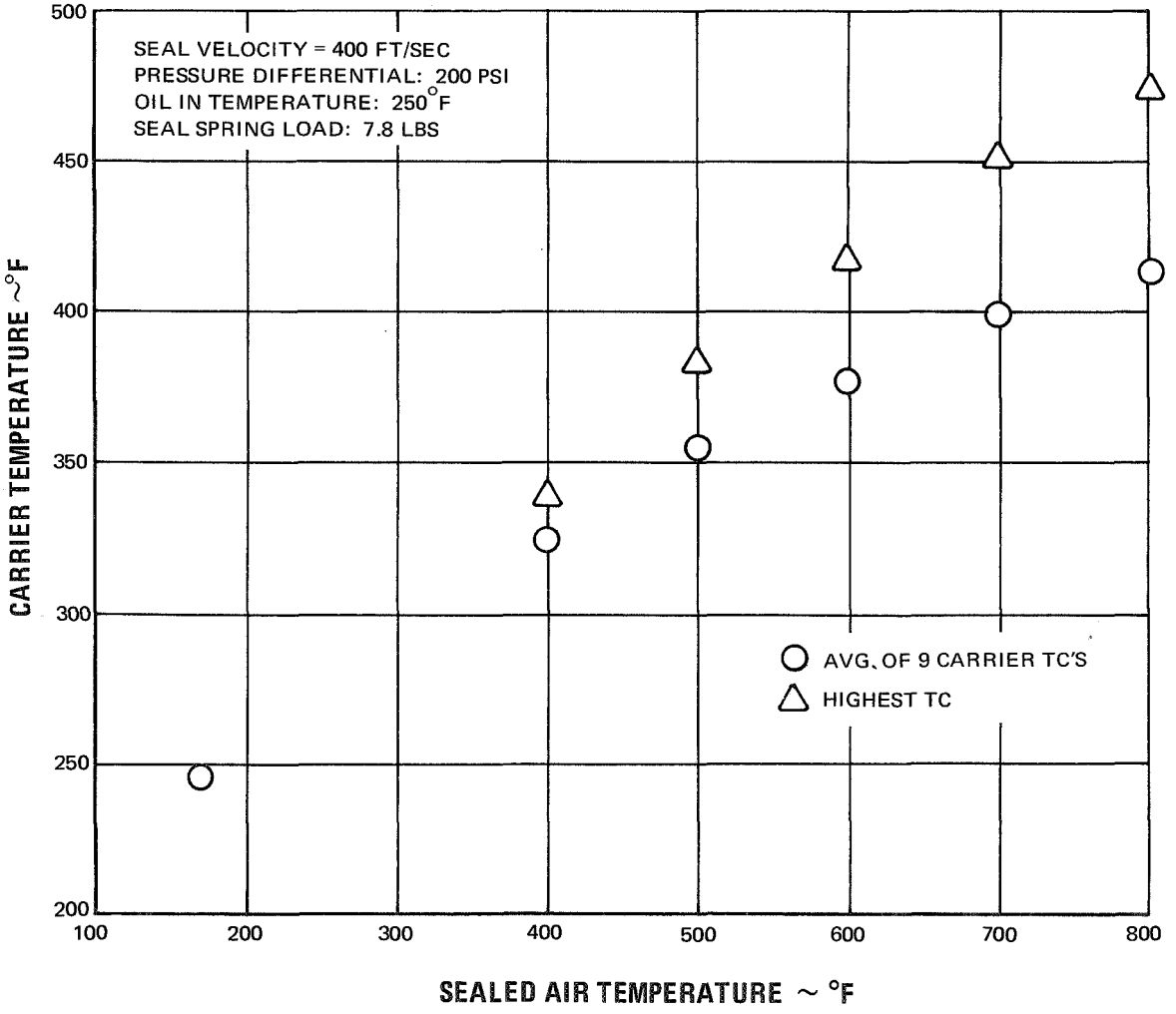

Figure 41 Skin Temperature (Low Pressure, Sump Side) Data from the 410 Stainless Steel Carrier Used in Builds 3-3 and 3-4

10. Endurance Testing - Build 3-4

To account for the higher coefficient of thermal expansion of the Inconel piston ring, a new piston ring was reoperated to increase the gap to 35 mils, and it was installed on Build 3-4. Testing was resumed at an air temperature of 900°F, a sliding speed of 400 ft/sec, and a pressure differential of 200 psi. The air leakage was approximately 27 scfm. After one half hour, the testing was halted when the pressure drop across the seal became erratic and air leakage increased. Inspection of the seal did not reveal anything abnormal other than the scored sealing dam from Build 3-2. Testing was resumed on the seal with 13.5 hours of successful operation at a 100-psi pressure differential, a 300-ft/sec sliding speed, and a 140°F air temperature. The average air leakage was 21.5 scfm.

11. Endurance Testing - Build 3-5

After discussion with the NASA Project Manager, the spring load was increased back to 15.4 pounds to reduce the seal air leakage caused by the scored condition of the seal dam. Testing was resumed at the following conditions: a pressure differential of 150 psi, a sliding speed of 400 ft/sec, and an air temperature of 1000°F. During the remaining 17.0 hours of testing, the average air leakage was 24 scfm.

Total time on the Build 3 seal carbon nosepiece was 503.4 hours. A closeup view of the nosepiece is shown in Figure 42. A profile trace taken across the nosepiece after the test is shown in Figure 43. At this location the pad wear was 0.09 mil and the seal dam wear was 0.49 mil. Average pad wear was 0.09 mil. The average seal dam wear was 0.41 mil. Profile traces were also taken across the seal seat and piston ring bore surface on the carrier. The trace of the seal seat (which had a total time of 880.2 hours) revealed that the only sign of wear was a 0.25-mil deep circumferential groove approximately 60 mils wide in the seal dam track. The trace of the carrier shown in Figure 44, revealed a 0.50 mil deep groove in the area that mated with the piston ring seal dam. Figure 45 shows the seal seat after removal from the test rig. From these inspection measurements it was concluded that increase in gas leakage was due to the erosion of the sealing dam and fretting wear of piston ring mating surfaces.

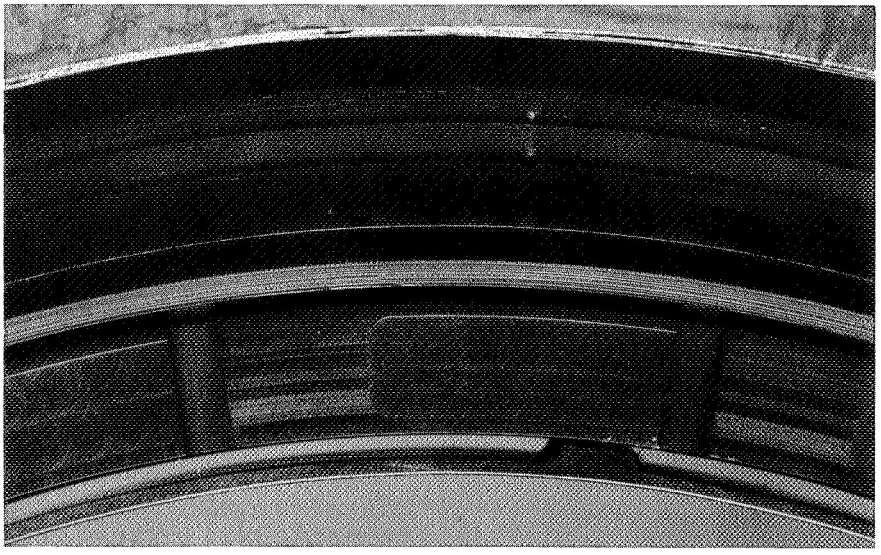

Figure 42 Close-Up of Carbon Nosepiece from Build 3-5 of the Gas-Rilm Seal After 503.4 Hours of Testing

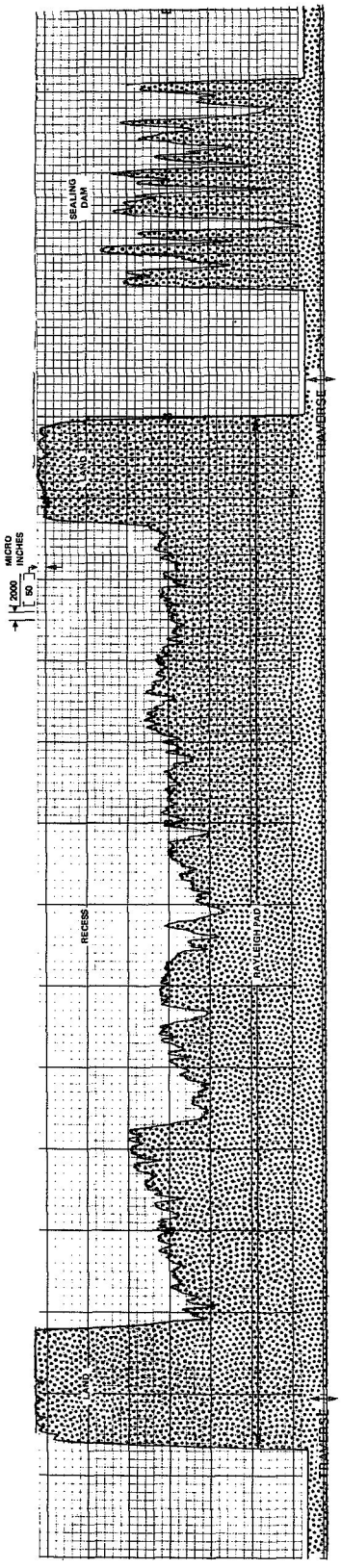

Figure 43 Representative Profile Trace Across the Nosepiece from Build 3-5 After 503.4 Hours of Testing

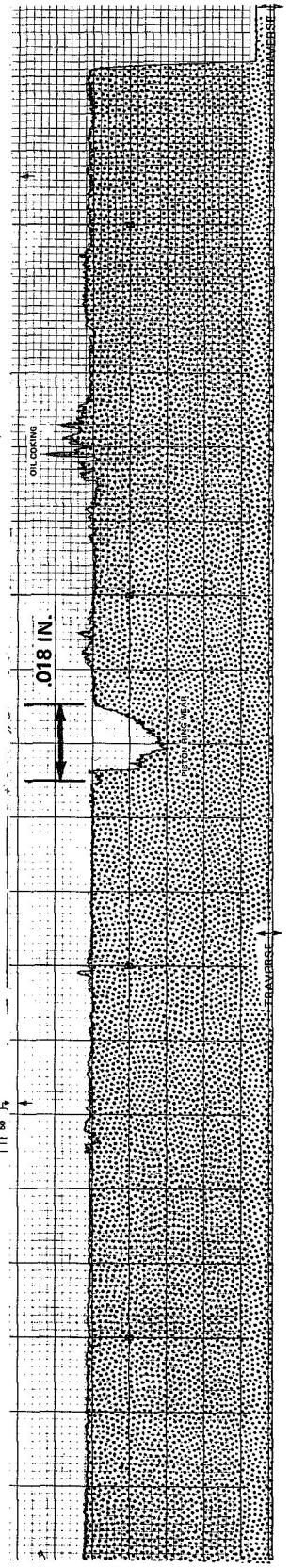

Figure 44 Representative Profile Trace Across the Carrier Piston Ring Bore Surface from Build 3-5. Total Time on Carrier 146.5 Hours

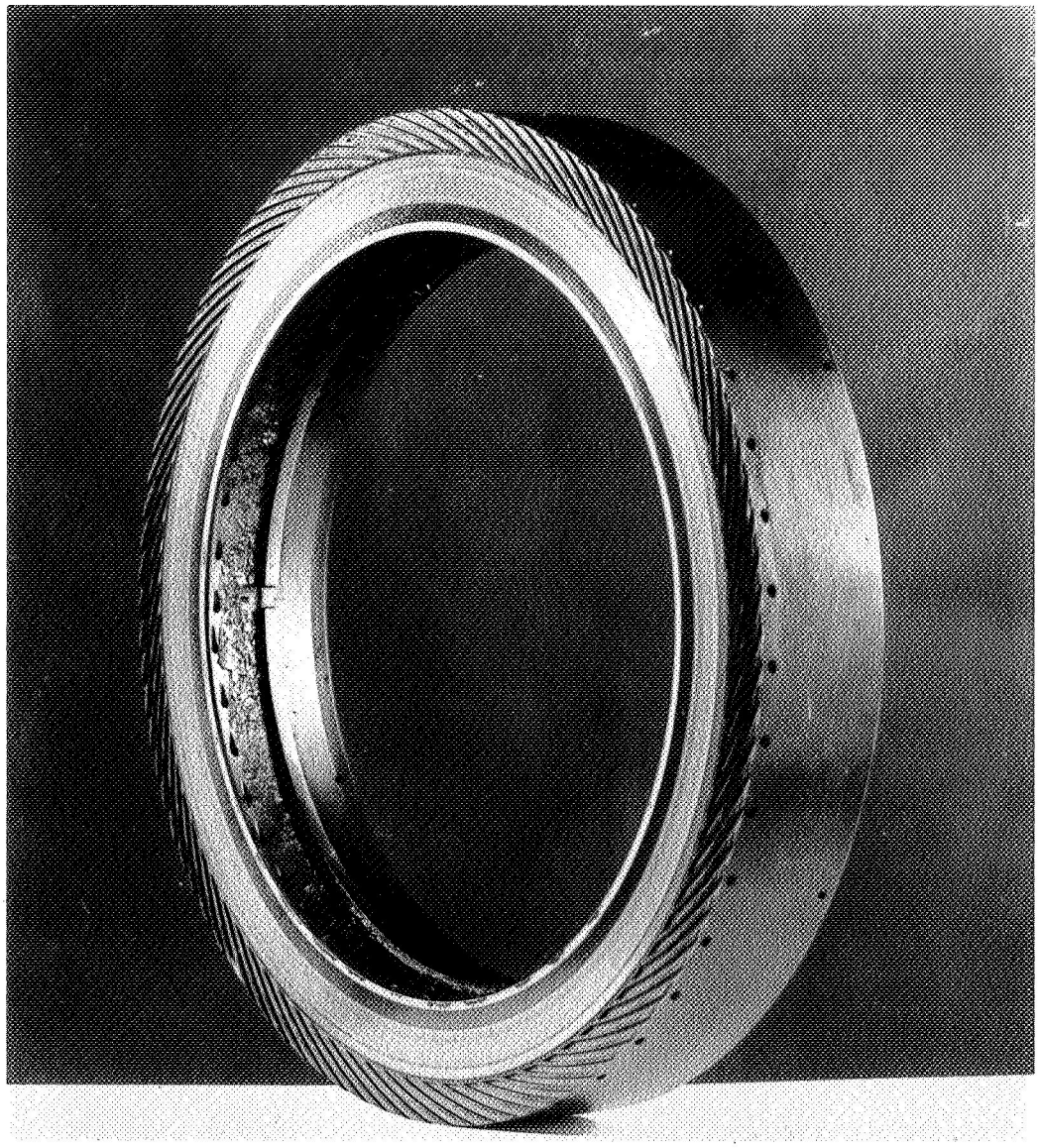

Figure 45 Seal Seat from Build 3 of the Gas-Film Seal. Total Time on Seal Seat 880.2 Hours (CN-25089)

D. EXPERIMENTAL EVALUATION OF THE OIL-FILM SEAL (TYPE B)

1. Preliminary Dynamic Checkout - Build 1

The initial static check of the oil-film seal in the test rig showed that there was excessive leakage. These leakages are compared with a static check by the vendor below.

Pressure (psi)	Vendor Fixture Measurement (scfm)	P&WA Rig Measurement (scfm)
50		10.1
100	3.0	18.4
150		28.5
200	7.8	36.3
250		46.7
300	13.6	

The nosepiece assembly was checked in the static pressure check fixture (seal fixture) and it was found that the total leakage past the primary seal face and secondary piston ring seal was 4.0 scfm at 60 psig. When an O-ring was substituted for the single piston ring, the leakage dropped to a level less than 0.8 scfm at 80 psig. The reason for the reduced leakage is that the piston ring has an end gap clearance of 0.024 inch, which provides a rather large leakage path at ambient temperature. This gap is necessary to prevent complete closure of the piston ring at operating temperatures.

The rig fixture (see Figure 11) was installed in the rig to determine the cause of excessive air leakage. With the rubber gasket and both O-rings in place, the initial check showed that the air leakage past the rig gaskets at 75 psig was less than 1.5 scfm (the minimum flow which can be measured on the rotometer). For the second check, the inner O-ring was removed, allowing the bellows spacer to be pressurized. The spacer provides the seal between the shaft and the seat. When the rig cover was repressurized, the air leakage at 75 psig was found to be 8.4 scfm. Further checks at the stand pinpointed the leak in the bellows.

A zyglo inspection showed that there were several circumferential cracks in the convolutions of the Inconel-X machined bellows. All other parts of the assembly were in excellent condition. Sectioning of the bellows by NASA revealed that one of the bellows walls was undersize resulting in an overstressed condition at assembly.

2. Preliminary Dynamic Checkout - Build 1-1

The seat assembly was reassembled with a new machined bellows which had undergone a Zyglo inspection and was found free of cracks. A pressure check of this assembly with the rig fixture at 75 psig showed that the total leakage, including that past the bellows, was less than 1.5 scfm. The nosepiece assembly was also checked again in the seal fixture; after lapping the seal carrier and positioning the piston ring in its optimum position, the leakage was found to be 4.1 scfm at 80 psig.

The assembled test rig was remounted on the test stand and a pretest static leak check was made. The results of the check compared favorably with the Phase I static seal leakage calibration experience. The leakages are tabulated below.

Pressure (psi)	Static Leakage (scfm)
50	3.2
100	6.6
150	10.6
200	15.0
250	19.7
300	24.4

It was planned to start the preliminary dynamic checkout program with ambient air temperatures and pressure differentials of 50 to 100 psi across the seal. Operation was attempted with 250°F oil at flows of 24 lb/min and 15 lb/min. However, at startup on each attempt, the seal blew open, producing seal air leakage which exceeded 100 scfm. A second static leakage calibration indicated essentially no change from the initial calibration.

Apparently the oil pressure in the region containing the oil lubricated spiral grooves was high enough to overcome the closing force and unseat the seal. To compensate for this, the oil flow was lowered to 10 lb/min at a temperature of 250°F for the second running attempt. The seal was pressurized to 100 psig, the rig was started, and the speed was raised to 7200 rpm (211 ft/sec sliding speed). During the attempt to settle out at 200 ft/sec, the seal blew open and the test was stopped. Actual running time was approximately 3 minutes, during which time the temperature of the carbon nosepiece rose rapidly to a maximum of 350°F, and then fell off to approximately 300°F. A static pressure check after the test showed a 33-percent increase in leakage at pressures up to 150 psig. At that pressure, the seal popped open repeatedly. It was concluded that the flow capacity of the seal venting system was inadequate for the combined oil flow and air flow at dynamic conditions. Therefore, testing was suspended until the carbon nosepiece could be modified.

After the test, the seal assembly was removed from the rig, and the carbon nosepiece and seat were examined. A slight discoloration of the mating ring showed that the nosepiece had rubbed on its inner lip. A profile check of the nosepiece showed that the inner lip had worn 0.1 to 0.3 mil.

3. Preliminary Dynamic Checkout - Build 2

The carbon nosepiece ring assembly used in Build 1-1 was modified for Build 2 as shown in Figure 46. The modifications were intended to reduce oil pressure forces and to increase venting capability. The circumferential annulus in the carbon was widened, and vent holes were added to connect the annulus to the low-pressure side of the seal. Additional thermocouples were installed in the back side of the carbon to permit a more complete measurement of the temperature distribution within the carbon.

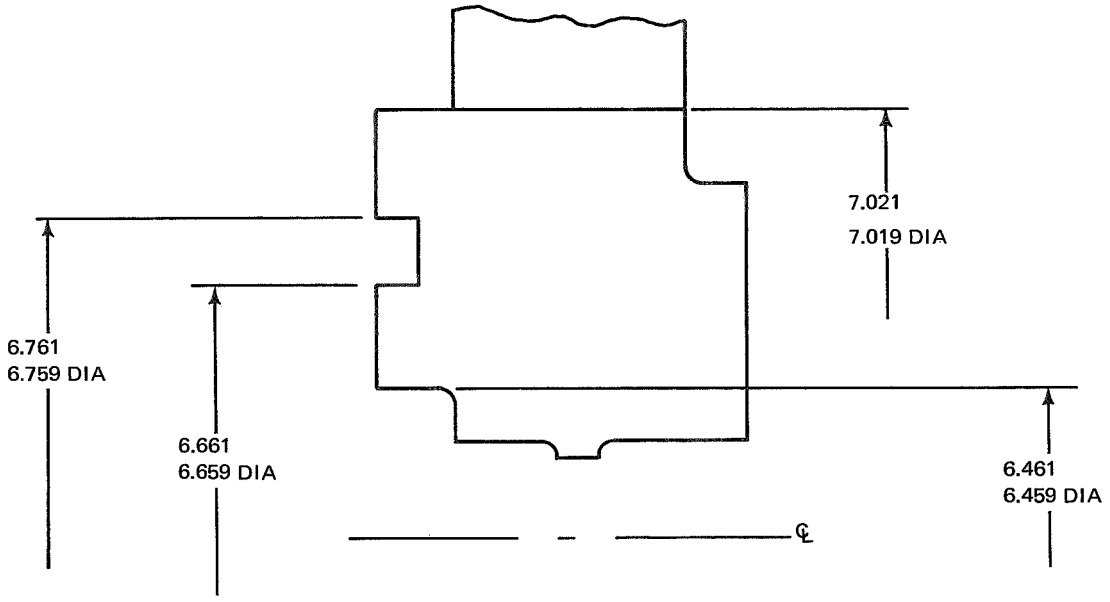

BUILD 1 AND 1-1 NOSEPIECE

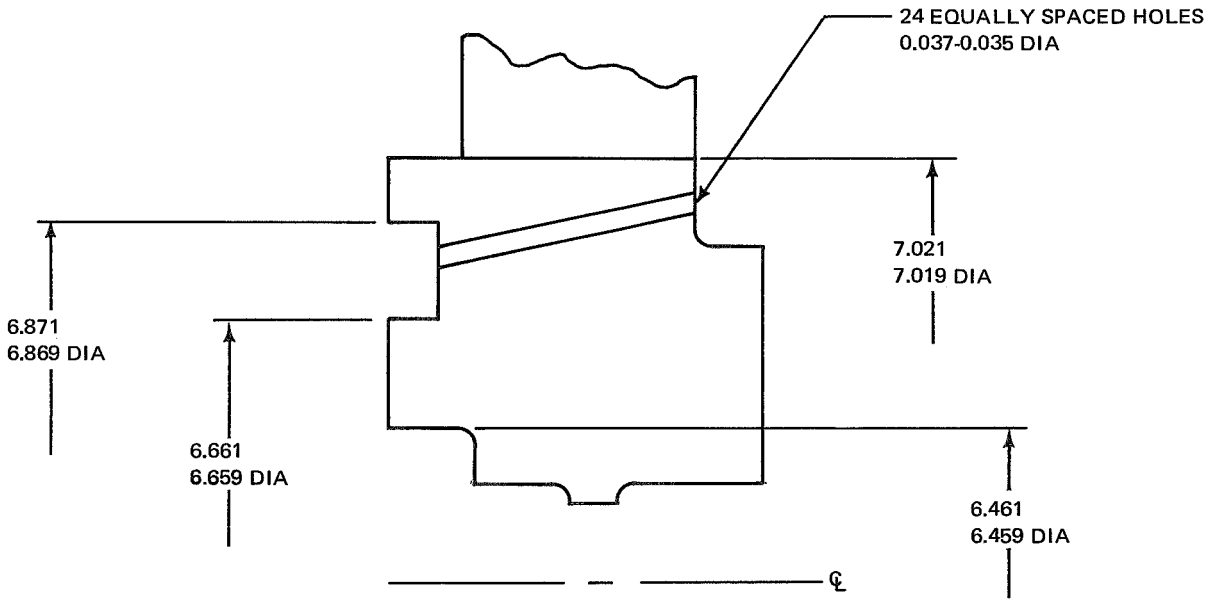

BUILD 2 NOSEPIECE

Figure 46 Modification to the Carbon Nosepiece of Oil-Film Seal

The oil-film seal assembly was installed in the test rig and a pretest static calibration was recorded. The results of the static check are tabulated below.

Pressure (psi)	Static Leakage (scfm)
50	3.5
100	6.1
150	8.7
200	11.8
250	14.7
300	18.0

For the initial run of the preliminary dynamic checkout program, ambient air was used at a pressure differential of 100 psi across the seal. The oil was kept at a temperature of 250°F and a flow rate of 15 lb/min to the seal plate. The shaft speed of 6,820 rpm provided a seal rubbing speed of 200 ft/sec. The seal air leakage dropped from 7.0 scfm at static conditions to 3.4 scfm at the dynamic conditions. After approximately 15 minutes of operation, the seal leakage had gradually increased to 4.2 scfm, and then remained steady at this level. Running was suspended after 27 minutes with no unusual occurrences, except for the fact that dynamic leakage was lower than static leakage. This reduced leakage could have been caused by heavy rubbing contact between the inner lip of the nosepiece and the seal seat, but the nosepiece thermocouples did not show the temperature rise which would be expected under such conditions.

The preliminary dynamic checkout program was continued after a static leak check showed no change in seal leakage. The dynamic operating conditions were the same as those previously, and produced similar results: seal leakage followed the same pattern at approximately the same values. After 37 minutes of operation at these conditions, the pressure differential across the seal was slowly raised. At a pressure differential of 130 psi, the seal popped open and running was suspended. A static leak check produced leakage of 21.8 scfm at a pressure differential of 100 psi, and the seal was unseated at 115 psi.

When the carbon seal assembly was removed from the rig the oil baffle was found fractured in several places. The seal is shown prior to Build 2 testing in Figures 47 and 48 and damage to the seal and oil baffle is shown in Figures 49, 50 and 51. Inspection of the nosepiece showed that the carbon was coned and warped around the circumference and displaced in the retention ring by a maximum of 0.025 inch. It was impossible to determine positively the sequence of events in the failure.

At the direction of NASA, testing on the oil-film seal was discontinued.

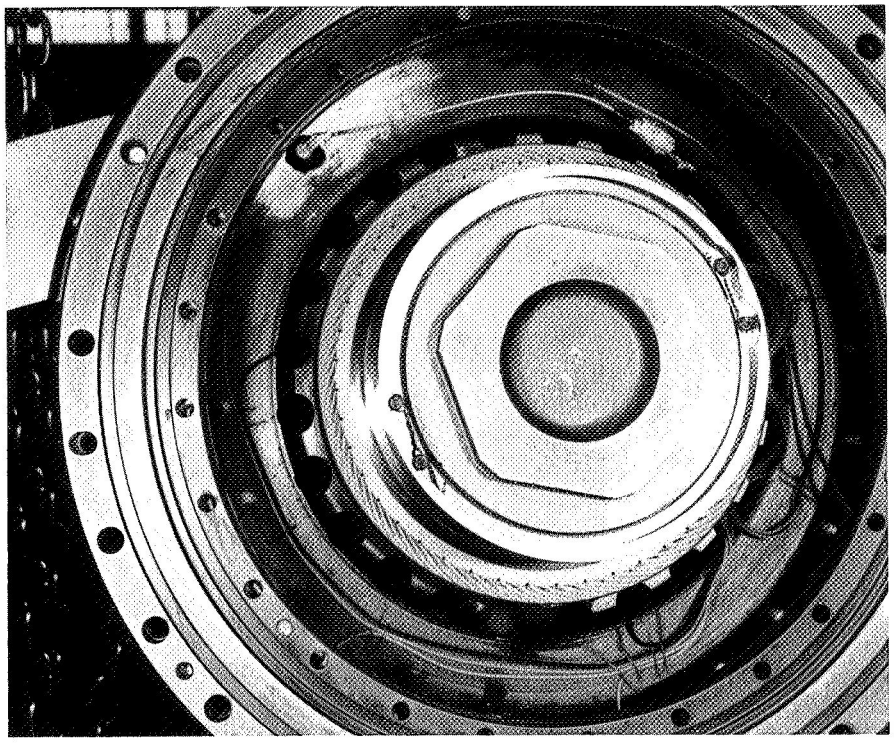

Figure 47 Seal Seat Assembly (CN-17202)

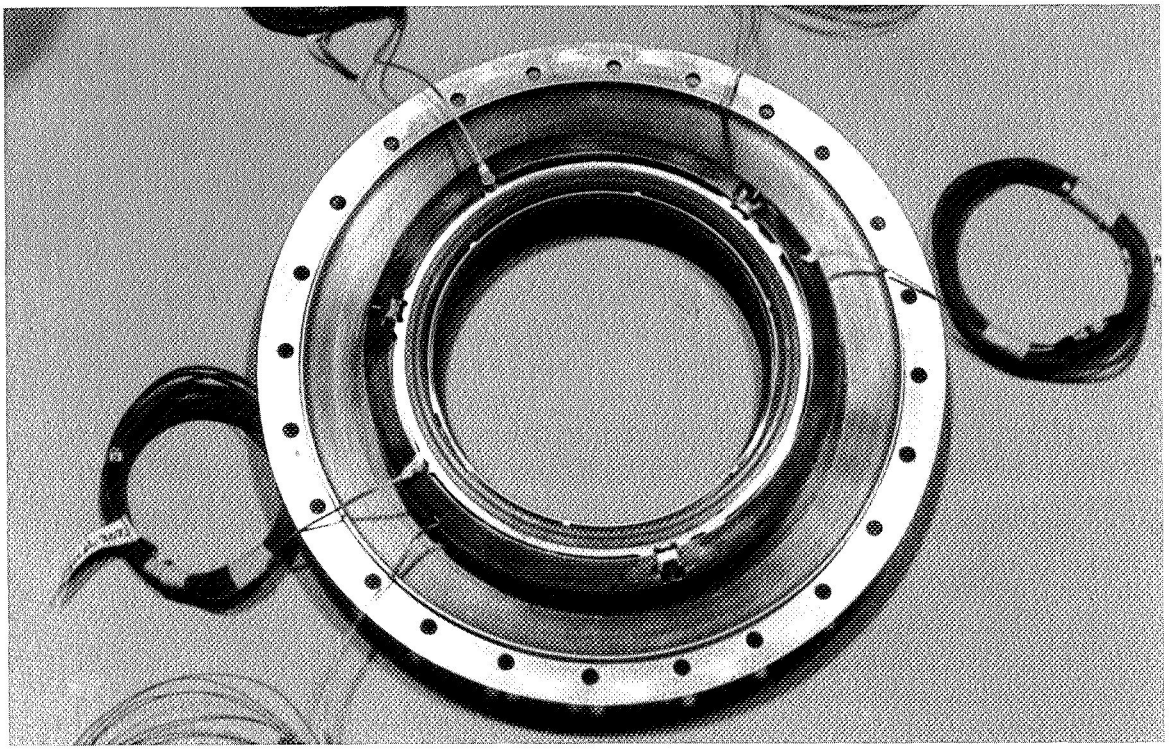

Figure 48 Seal Assembly (CN-17203)

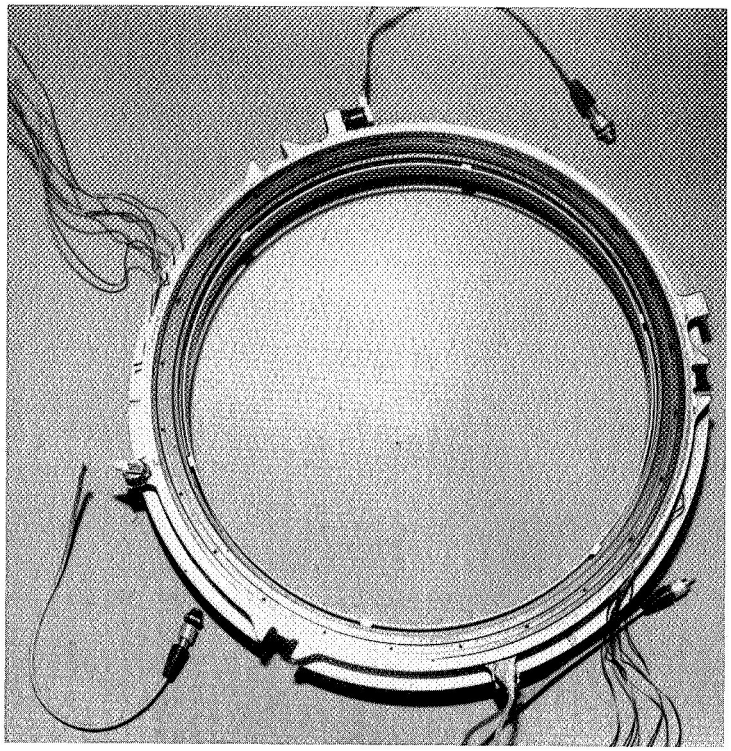

Figure 49 Oil-Film Nosepiece Assembly After Build 2 Dynamic Testing (XP-94852)

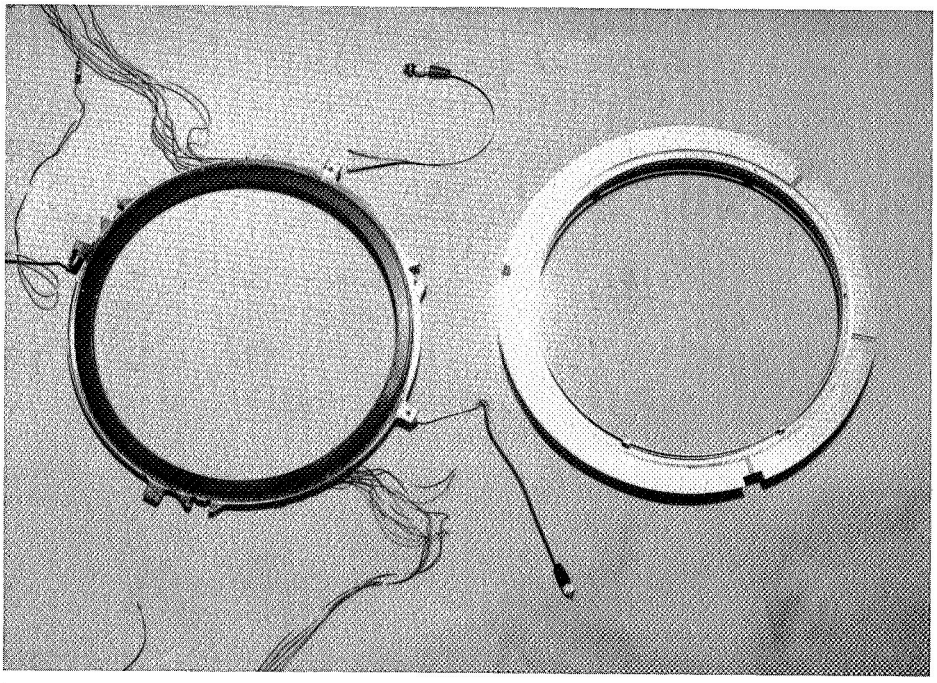

Figure 50 Rear Side of Carbon and Front of Carrier After Dynamic Testing of Build 2 of the Oil-Film Seal (XP-94853)

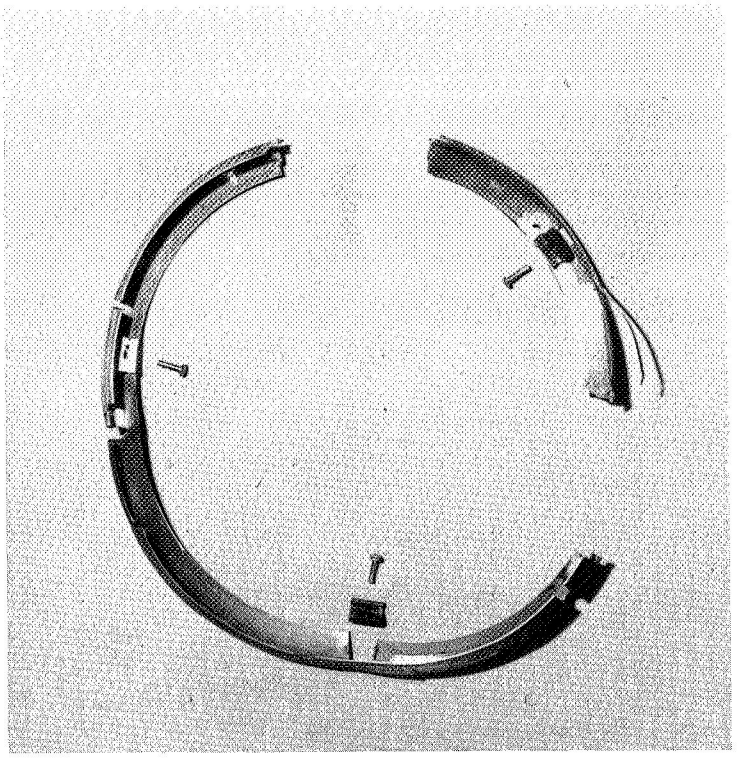

Figure 51 Oil Baffle Which Fractured During Dynamic Testing of Build 2 of the Oil-Film Seal (XP-94851)

APPENDIX A

GAS-FILM SEAL
TYPE A

by
L. P. Ludwig
Lewis Research Center
Cleveland, Ohio

National Aeronautics and Space Administration

GAS-FILM SEAL, TYPE A

INTRODUCTION

Consideration was given to a full scale type mainshaft seal of 6.6 inch (16.8 cm) mean sealing diameter. The design analysis considered design conditions at 165 psia (114 N/cm^2) sealed pressure, 500 ft/sec (153 m/sec) sliding velocity, and 800°F (700 K) sealed gas temperature. In the design analysis, calculated thermal maps, stress fields and displacement fields were used in the design refinements leading to the final seal design.

DESCRIPTION OF FACE SEAL WITH SELF-ACTING GEOMETRY FOR LIFT AUGMENTATION

Figure A1 is a cross section of the final design configuration of the face seal with self-acting lift geometry. As with a conventional face seal it consists of a rotating seat (all rotating parts are cross hatched) which is attached to the shaft and nonrotating nosepiece assembly that is free to move in an axial direction thus accommodating engine thermal expansion (axial). The piston ring type secondary seal is subjected only to the axial motion (no rotation) of the nosepiece assembly and several springs provide force to maintain contact at start and stop. In operation, the sealing faces are separated a slight amount (in the range of 0.0005 inch (0.00127 cm)) by the self-acting lift geometry, and gas leakage is from the high pressure side (I. D. of carbon nosepiece) across the sealing dam into the bearing sump. This gas leakage pressurizes the sump and assures proper scavenging of the bearing lubricant. It should be noted that although the sealed gas temperature is high, tests have shown that considerable gas temperature drop occurs in the leakage flow so that the leakage into the sump does not pose a fire hazard when the seal is operating properly. Operation to 40 SCFM (1.05 std m^3/min) and 1200°F (922 K) sealed air temperature has been obtained without a sump fire.

Seal Seat

Conventional seal seats have construction similar to that shown in Figure A2. The practice is to axially clamp the seat by such means as a bearing lock nut (not shown). Thus, the seat, in effect, becomes rigidly attached to the shaft. Experience has shown that to prevent seat face deformation the end faces of the shoulders (spacers) clamping the seat must be optically flat; the seat, of course, should be optically flat on both sides. A common assembly fault is to clamp the seat with a spacer whose end mating faces are not flat. This spacer face out-of-flatness can then be transferred into the seat face when the assembly is clamped together. It should be noted that the axial clamping can readily reach several tons of force. Further, since the seat is located on the shaft relative shaft thermal growth near one face of the seat or relative thermal growth of one spacer can cause coning deformation of the seat face as illustrated in Figure A3.

Figure A4 shows the final seal seat design for the self-acting face seal. The seat is thermally and partially structurally isolated from the shaft by the following means:

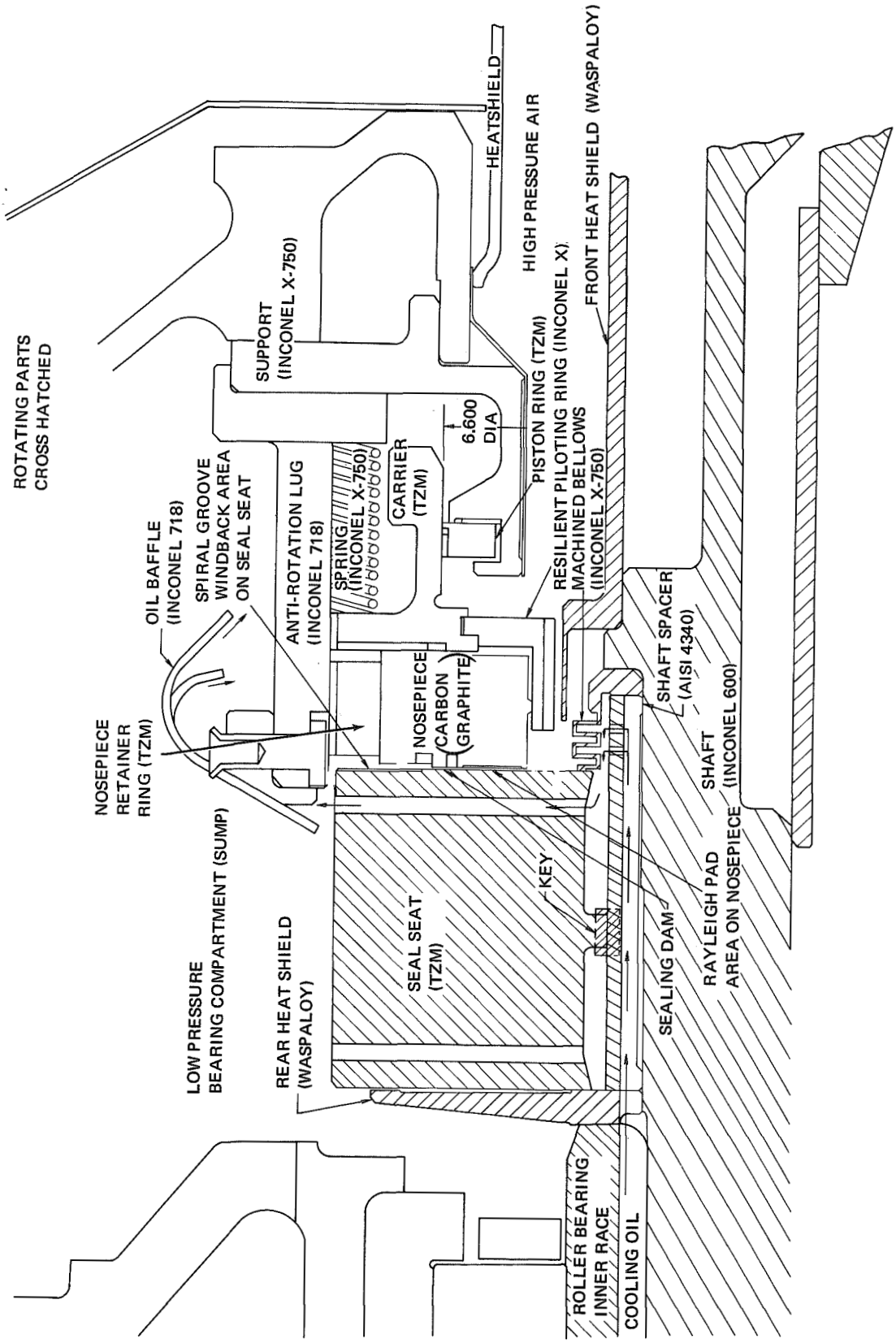

Figure A1 Shaft Face Seal With Self-Acting Lift Geometry

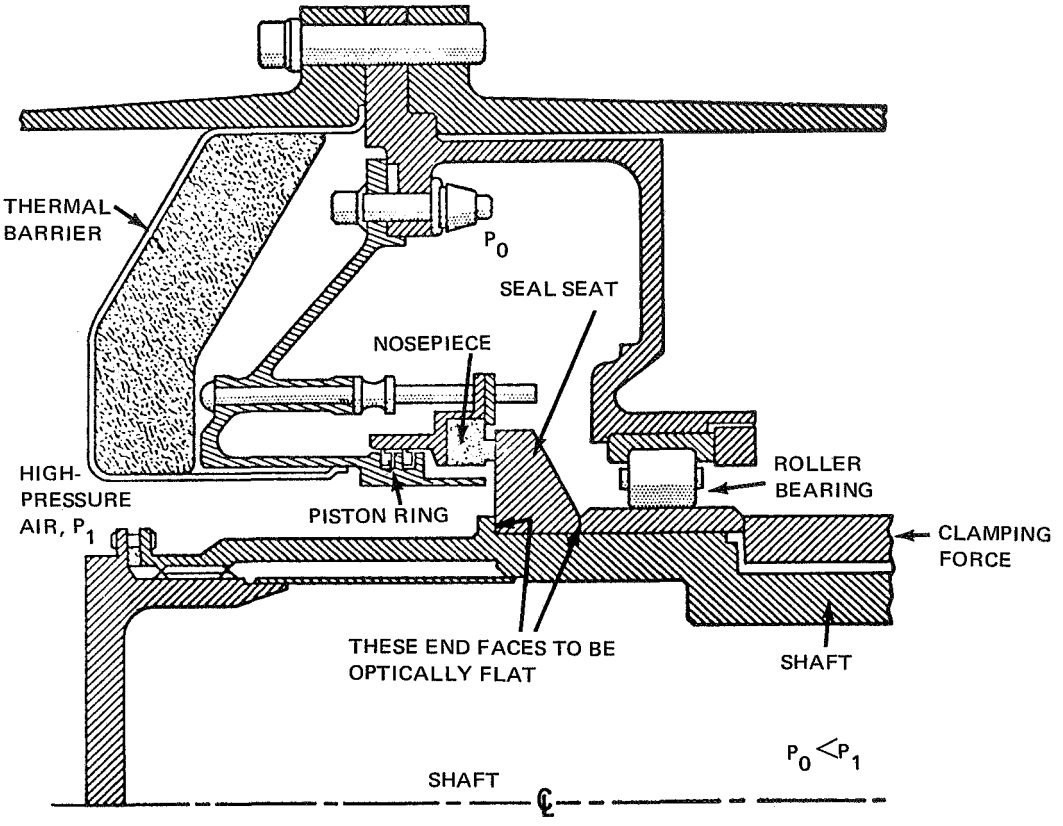

Figure A2 Conventional Seal Seat

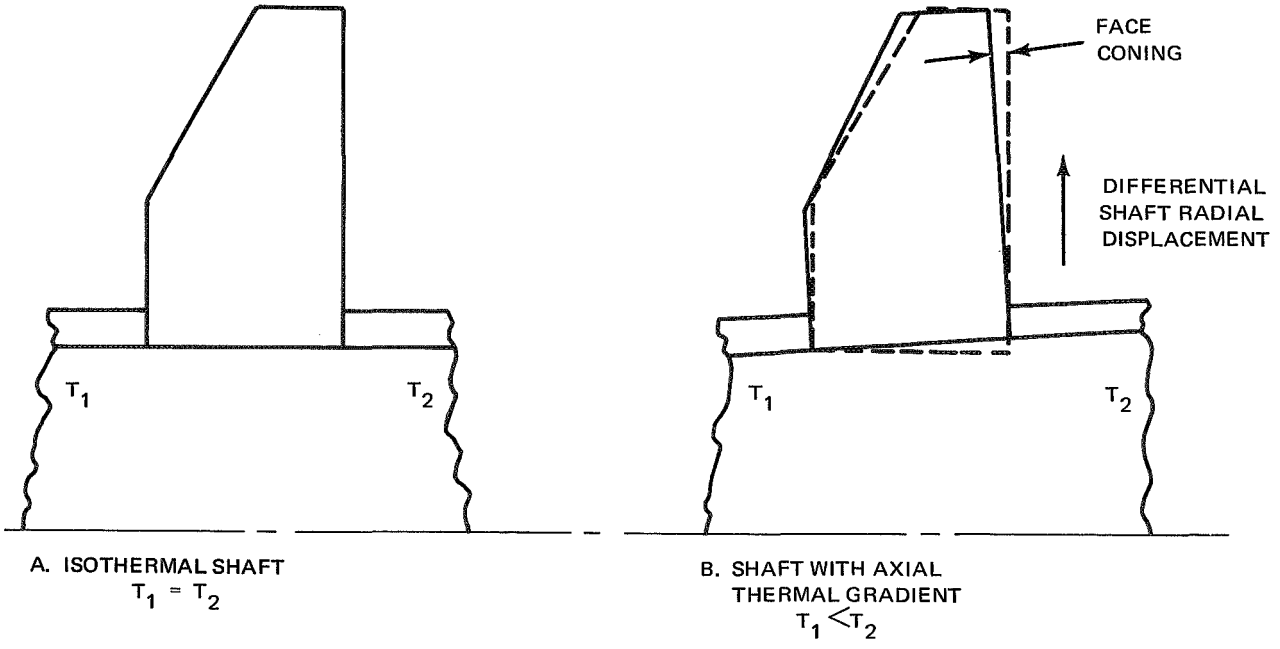

Figure A3 Coning Deformation of the Seat Face

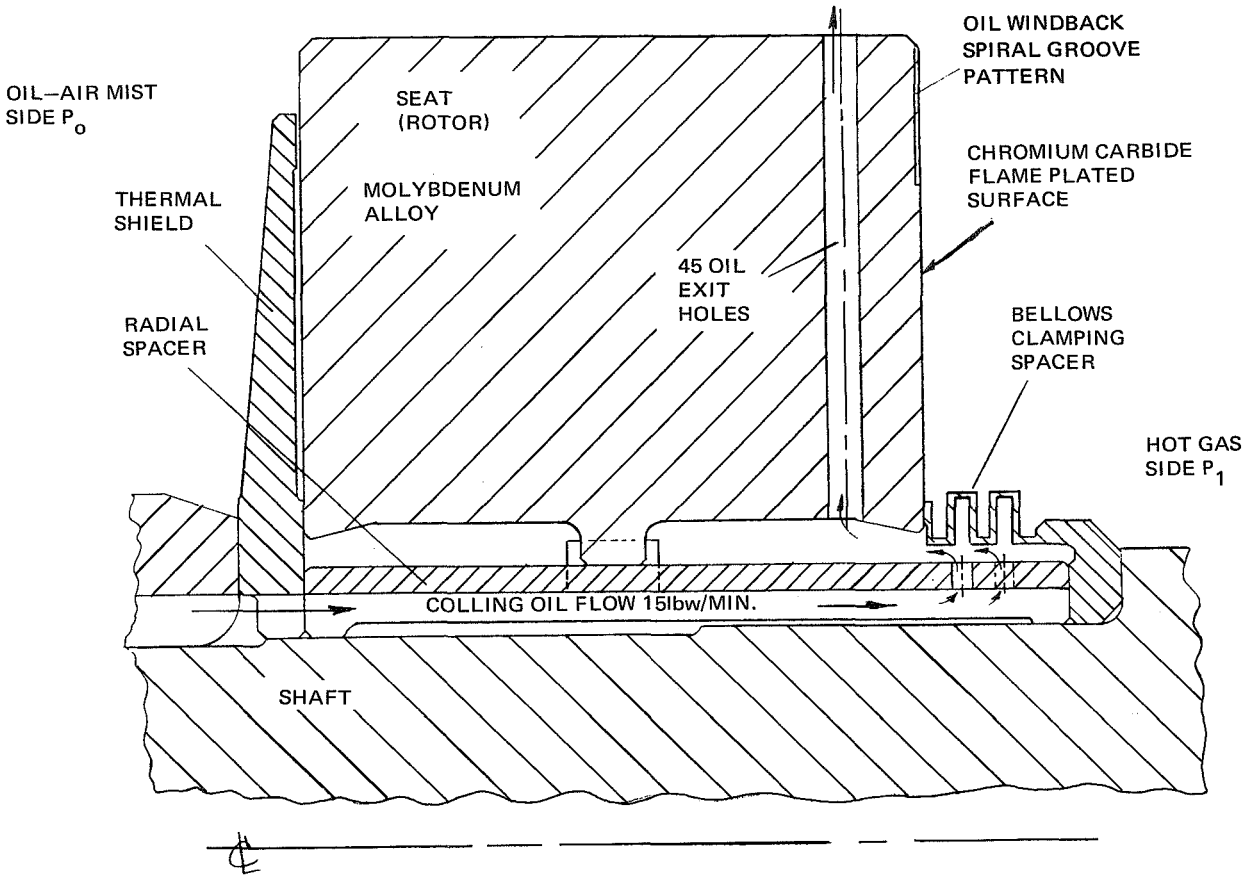

Figure A4 Seat Assembly

(1) The radial spacer between the seat and shaft serves as a radial spring that mitigates the effect of nonuniform shaft thermal growth due to the axial thermal gradient. The effect of thermal movement is further attenuated by piloting the seat over its centroid.

(2) The bellows clamping spacer applies a predetermined clamping force (approximately 2000 lbf (8896 N)). This clamping force has proven to be large enough for proper assembly of the seat, as evidenced by the fact that seat face total indicator run-outs of 0.0008 inch (0.0020 cm) are commonly obtained. The 2000 lbf (8896 N) is probably an order of magnitude less than clamping forces produced by the usual bearing lock nut assembly technique and therefore the deformation during assembly is minimized.

The seat thermal design is tailored to minimize the axial thermal gradient. Use of a molybdenum alloy, instead of the conventional SAE-8740 or heat resistant alloy, provides a relatively low deformation criterion which is defined as the ratio of thermal expansion to thermal conductivity (ref. 1). As an example, if the molybdenum is given a rating of one, SAE 8740 would have a deformation rating of 7 and the heat resistant alloys even higher. Thus, the molybdenum alloy provides a significant advantage in lower deformation as compared to the conventional seat materials.

The cooling oil flow path is also tailored to produce the minimum axial thermal gradient. By passing the cooling oil under the radial spacer, the first contact of the cooling oil with the seat is near the hotter face (face mated with nosepiece) of the seat and this produces less of a gradient than allowing first contact of the oil with the cooler seat face (face nearest to the bearing). Centrifugal pumping action due to rotation and the 45 radial exit holes near the hot face assures even distribution of the cooling oil. Figure A5 is typical thermal map (calculated by the computer program described in ref. 2) for the design operating conditions of 165 psia (114 N/cm^2 abs), 500 ft/sec (153 m/sec) and 800°F (700K) sealed gas temperature. Inspection of the temperature field reveals that the heat shields are effective in reducing the thermal gradient in the seat. As an example, the heat shield which protects the seat face from the oil passing through the bearing has a calculated temperature of 427° to 492°F (493 to 529 K) the adjacent seat face is 651° to 658°F (617 to 621 K). Without this shield the seat face would be subjected to oil cooling and the seat gradient and corresponding deformation would be significantly greater. Figure A6 gives the calculated seat assembly stresses due to combined centrifugal and thermal effects. In general, about one-half of the stress magnitude can be attributed to thermal effects, the rest arises from centrifugal effects. Thus, the thermal gradient, in addition to being a major factor in seat deformation, is also a very significant factor in stress levels. Minimization of the seat thermal gradient is, therefore, the crux of the seal design problem. Figure A7 shows the calculated seat assembly displacement due to combined centrifugal and thermal effects, as is the case of the stresses, the thermal effects are significant. The important point is that the seat face which mates to the carbon nosepiece remains

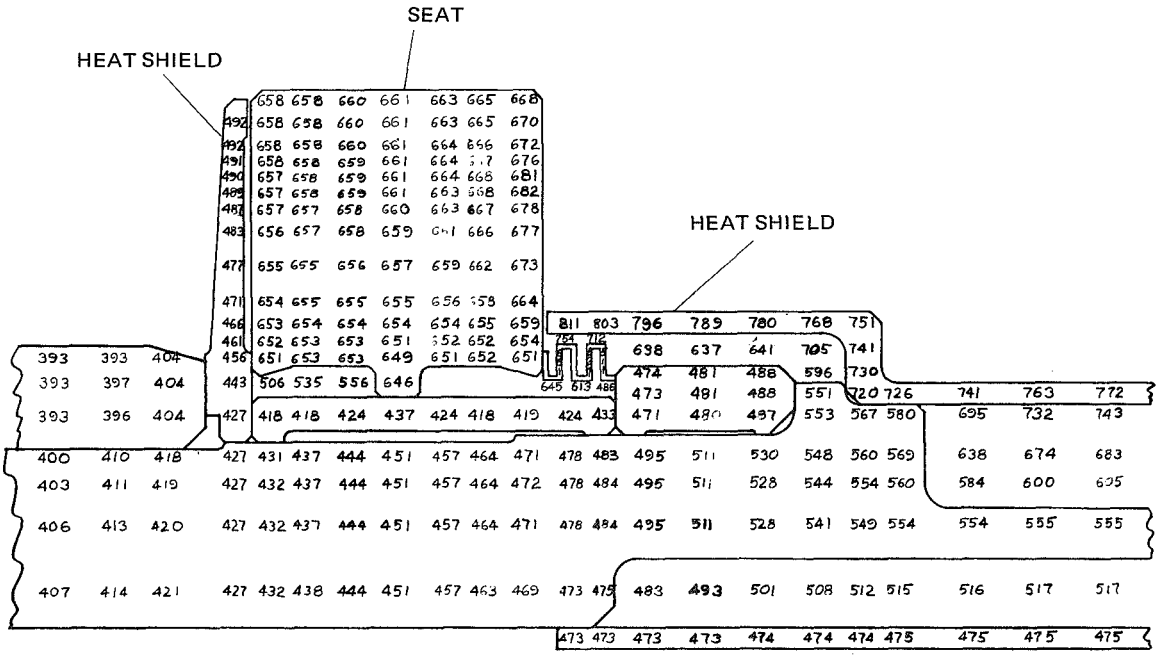

Figure A5 Calculated Temperature Field of Seal Assembly; Design Conditions: 165 psia (114 N/cm^2) Sealed Pressure, 500 ft/sec (153 m/sec) Mean Sliding Speed, 800°F (700 K) Sealed Gas Temperature. (Temperatures Are Expressed in °F.)

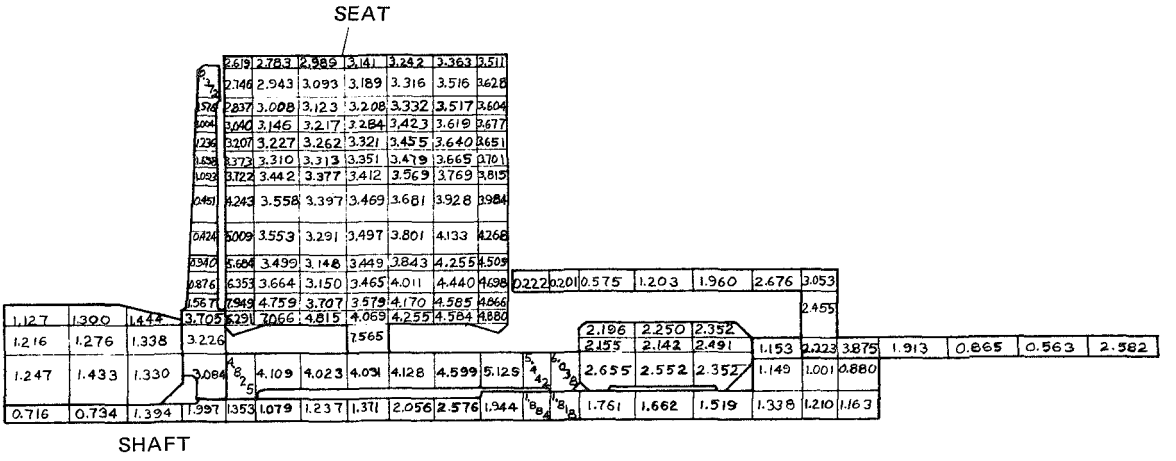

Figure A6 Calculated Stresses in Seat Assembly Due to Combined Centrifugal and Thermal Effects; Design Conditions: 165 psia (114 N/cm^2) Sealed Pressure, 500 ft/sec (153 m/sec) Mean Sliding Velocity, 800°F (700 K) Sealed Gas Temperature. (Stresses Are Expressed in psi x10^{-4}.)

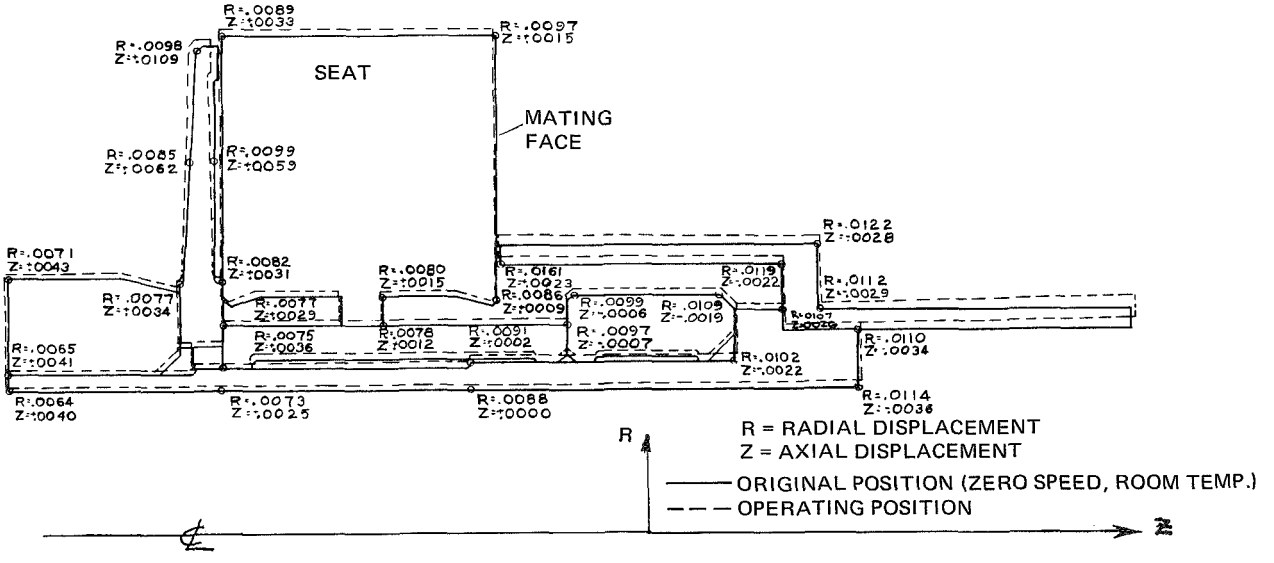

Figure A7 Displacement of Seal Assembly Due to Centrifugal and Thermal Effects; Design Conditions; 165 psia (114 N/cm^2 abs) Sealed Pressure, 500 ft/sec (153 m/sec) Mean Sliding Speed, 800°F (700 K) Sealed Gas Temperature. (Displacements Are Expressed in Inches.)

relatively square to the shaft centerline. The net calculated mating face deformation (coning) in the axial (z) direction is 0.0006 inch (0.00152 cm) and this magnitude of deformation can be accommodated by the self-acting geometry as discussed in reference 3.

A chromium carbide hard face on the molybdenum alloy seat provided wear and oxidation resistance. The final face finish was 4 to 8 rms with the face flat within 2 light bands. A spiral groove pattern (oil windback) in the face of the seat (see Figure A4) prevents oil from

leaking into the sealing dam area during operation. The spiral direction is such that relative motion of the seat induces an outward pumping action.

Nosepiece Assembly

The nosepiece assembly (see Figures A1 and A8) consists of the carbon-graphite ring which is shrink fitted into a molybdenum retainer ring and this assembly in turn is piloted (located) by a resilient ring attached to the carrier (also molybdenum alloy). Molybdenum alloy is used in the carrier and retainer ring in order to minimize thermal deformation. The relatively high density is a disadvantage in that the inertia forces associated with nosepiece movement are, therefore, higher.

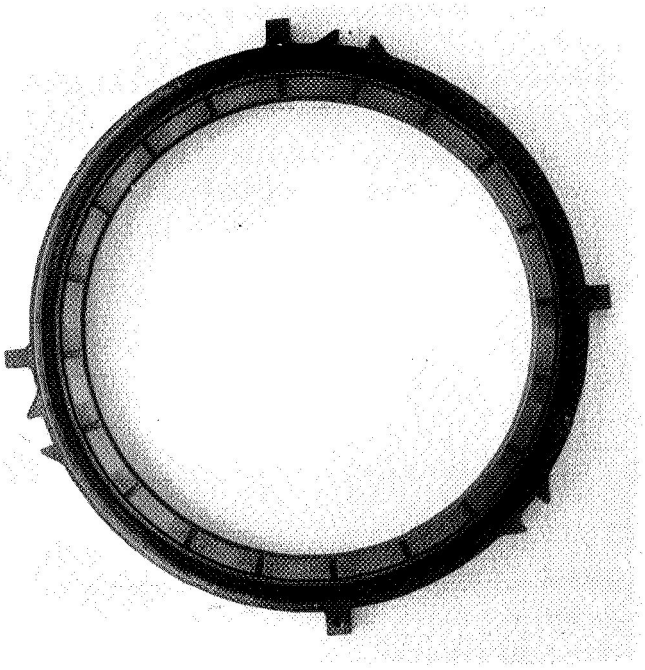

Figure A8 Gas-Film Seal Nosepiece (CN-23136)

The carbon-graphite ring contains the self-acting geometry (lift pads) that are described in reference 3. The carbon-graphite material is a small grain size high carbon content (as compared to the percent of graphite) in order to obtain maximum strength and wear resistance. Measurements by thermocouples have shown that when the sealed gas temperature is 1200°F (922K) the carbon temperature (0.06 inch (0.15 cm) from the primary face) is only 600°F (589 K); this significant drop in temperature, which is vital from an oxidation standpoint, is achieved in part by redirecting the cooling oil flow, which leaves the seat at high velocity from the 45 oil exit holes, to the nosepiece assembly O.D. (see oil baffle in Figure A1).

Figure A9 is a thermal map of the seal nosepiece assembly for the design condition of 165 psia (114 N/cm^2 abs) sealed pressure, 500 ft/sec (153 m/sec) mean seat sliding velocity, 800°F (700 K) sealed gas temperature and 370°F (461 K) oil temperature in the sump.

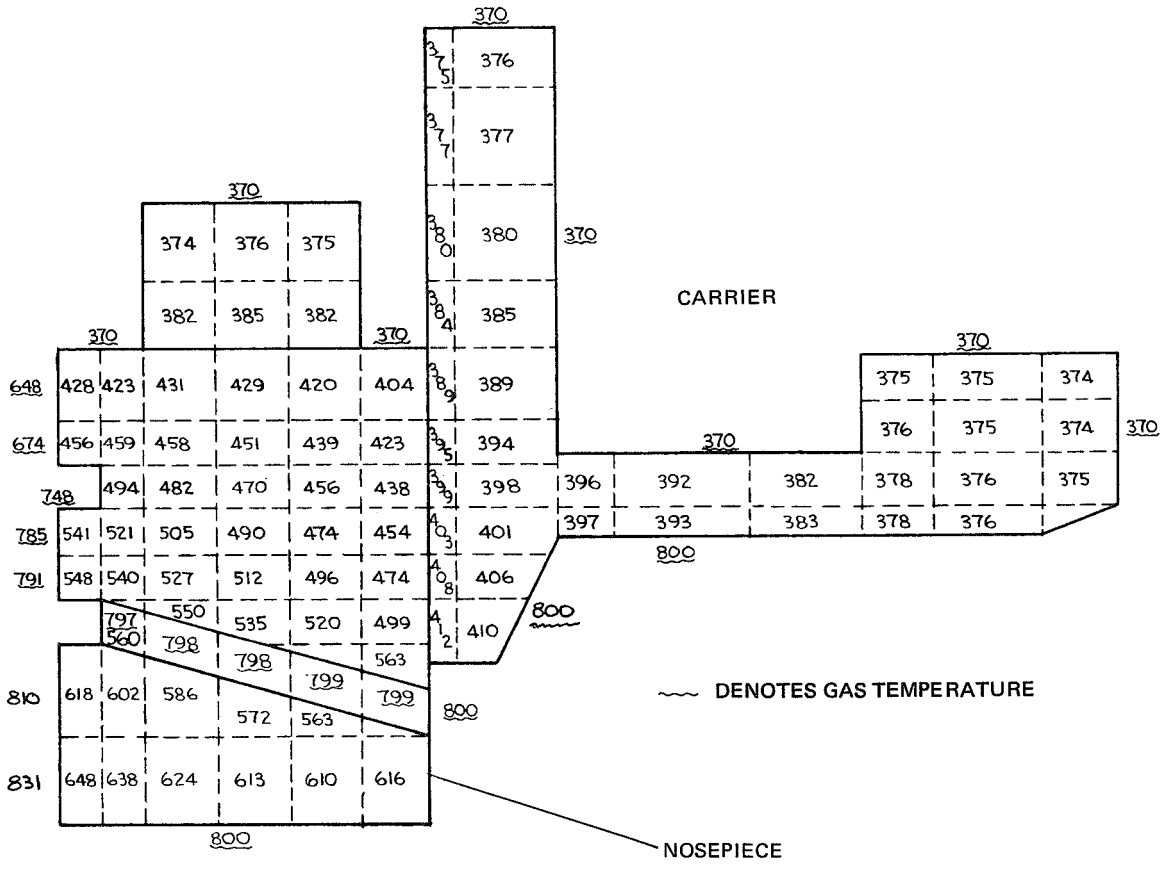

Figure A9 Calculated Temperature Field of Nosepiece Assembly; Design Conditions: 165 psia (114 N/cm^2 abs) Sealed Pressure, 500 ft/sec (153 m/sec) Mean Sliding Speed, 800°F (700 K) Sealed Gas Temperature, 370°F (461 K) Oil Sump Temperature. (Temperatures Expressed in °F.)

These thermal gradients produce relatively low stresses in the nosepiece assembly (see Figure A10); however, the sealed pressure acting on the inner diameters of the assembly is producing significant stresses.

The closing force (due to the sealed pressure) is determined in part by the relation of sealing dam inside and outside diameters to the secondary sealing diameter on the carrier. Differential thermal growth changes these diameter relations as illustrated in Figure A11. Significant changes in closing force, therefore, can be associated with differential thermal growth. Additional consideration is the force moment induced by eccentricity between the secondary sealing diameter and the sealing dam diameters. Eccentricity was minimized by the means of the resilient piloting ring which is attached to the carrier (see Figure A1) and contacts the carbon ring in the plane of the carbon ring cross section centroid.

The principal effect of the nosepiece deformation is formation of a divergent leakage gap at the sealing dam. As indicated in Figure A3 and as shown in Figure A11 the seat deformation

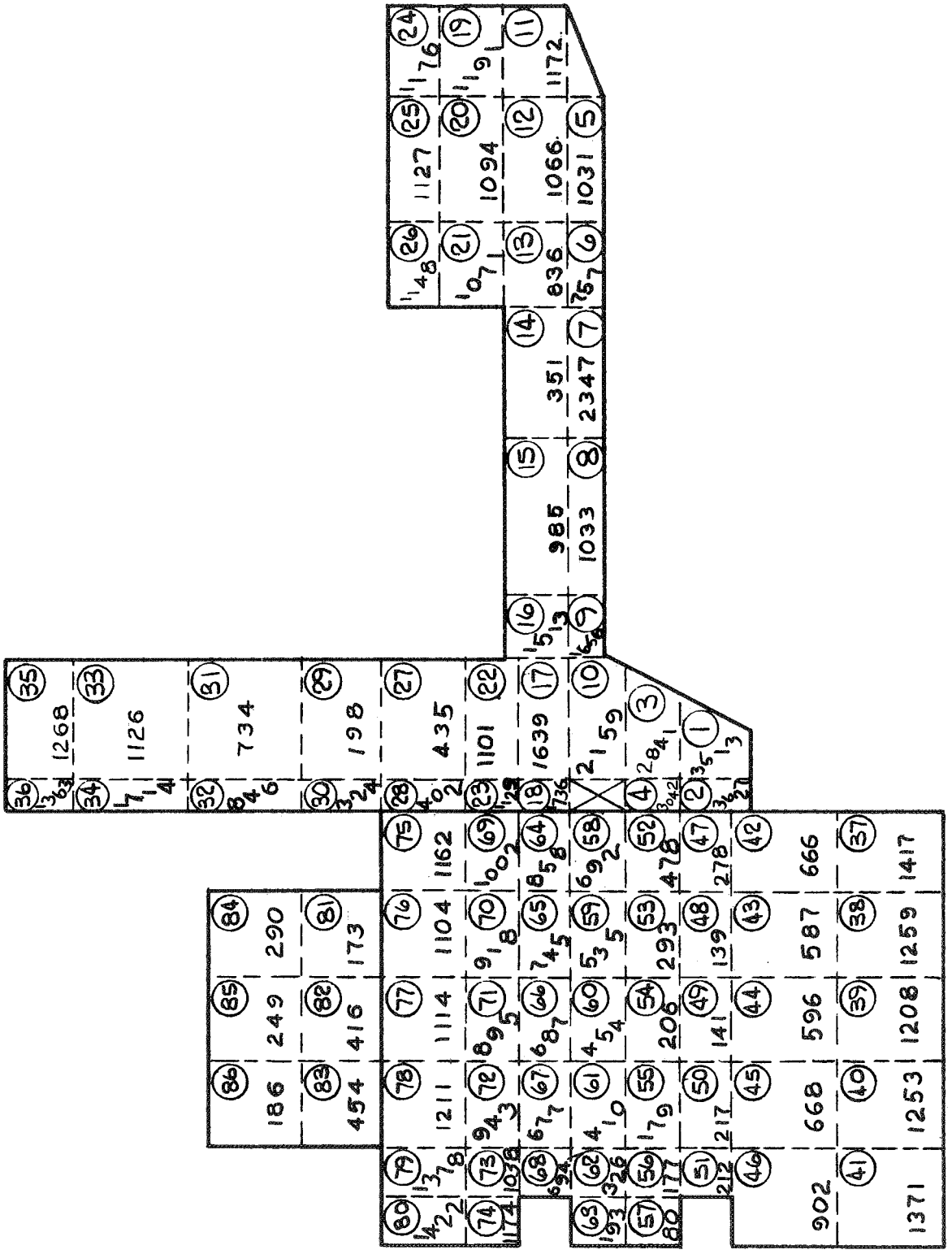

Figure A10 Calculated Stresses Due to Temperature Gradients. Design Conditions: 165 psia (114 N/cm^2 abs) Sealed Pressure, 800°F (700 K) Sealed Gas Temperature, 370°F (461 K) Oil Sump Temperature. (Stresses Expressed in psi.)

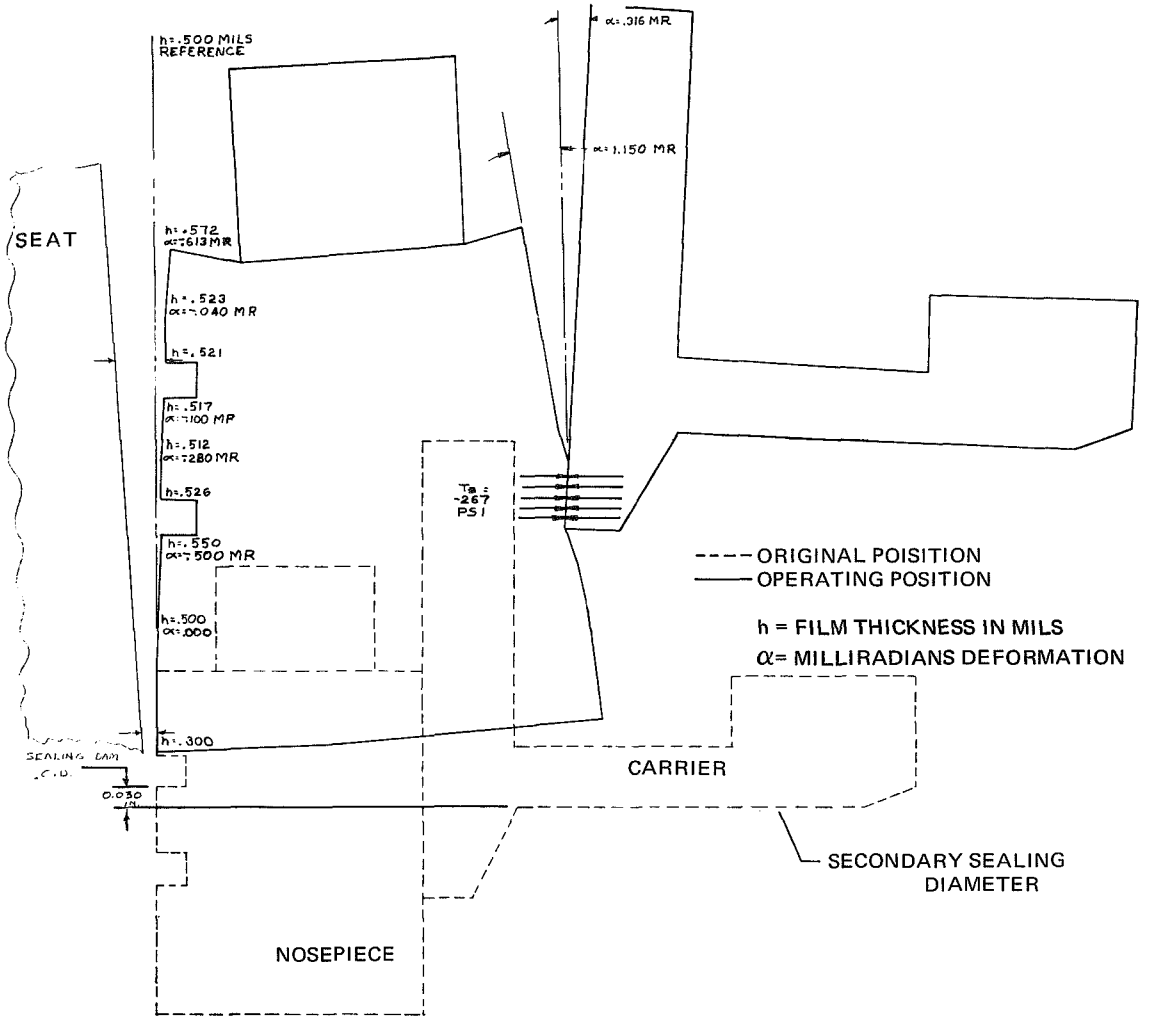

Figure A11 Calculated Displacement of Nosepiece Assembly. Design Conditions: 165 psia (114 N/cm^2 abs), 800°F (700 K) Sealed Gas Temperature. (Film Thickness (h) Expressed in Mils.)

(coning) increases the net divergence. However, the magnitude of the divergence is within practical limits as discussed and analyzed in reference 3. (Refs. 3 and 4 discuss, in detail, the effect of sealing face deformation of seal force balance.)

The carrier is made from molybdenum alloy for the purpose of matching the thermal growth of the carbon ring and for the purpose of minimizing thermal gradients which would induce detrimental deformation. The secondary seal (Figure A1) which is pressure balanced in both axial and radial directions is also made from molybdenum alloy and is chrome plated (as is the carrier bore) for oxidation and wear resistance.

SUMMARY OF APPENDIX A

A face seal with self-acting geometry was designed for operation in gas turbine engines. Because of the noncontacting feature the seal has high speed and long life potential.

Extensive use was made of molybdenum alloy in the design in order to minimize thermal gradients which cause detrimental seal deformation; in particular the seat, carbon retainer ring, carbon carrier and secondary seal were made from the molybdenum alloy.

The seat was structurally isolated from the shaft by a radial spacer in order to mitigate the deformation effects caused by shaft thermal displacement. Further, the seat was clamped through a bellows which provided a predetermined amount of axial clamping and mitigated clamping distortions.

Seat axial thermal gradients which induce undesirable deformations were minimized by thermal shielding and oil cooling. Further oil cooling the nosepiece assembly helped reduce the carbon temperature to a level at which oxidation was not a problem.

APPENDIX B

OIL-FILM SEAL
TYPE B

by
L. P. Ludwig
Lewis Research Center
Cleveland, Ohio

National Aeronautics and Space Administration

OIL-FILM SEAL, TYPE B

The design goal was to minimize: (1) thermal gradients, (2) nosepiece (and carrier) mass, and (3) distortion at the seal dam. To obtain this goal, thermal distortion studies were made of all the seal parts and materials selection was based on distortion consideration as well as strength. The seal shown in Figure B1 (Liquid Film Seal NASA drawing no. CD 847605) was designed to fit existing mainshaft seal rig developed under NAS 3-7609. The seal consists of a resiliently clamped seat which is thermally isolated by 3 heat shields. Cooling holes are located near the hot gas side, and effects of shaft expansion are minimized by piloting the seal under the seat centroid.

The shaft spacer (see Figure B1) has resilient piloting to minimize shaft expansion effects being transferred and thus casuing seat distortion.

A static seal joint exists between the carbon nosepiece and the carrier. This construction was selected in order to avoid distortions associated with integral carbon-carrier designs.

The use of only one piston ring, instead of two, permits the use of a shorter carrier. The use of short carriers alleviates distortion problems.

The seal cooling oil is directed to the seal interface from which it is expelled by centrifugal force and by the pumping action of the spiral grooves. This spiral groove and centrifugal force pumping action is sufficient to preclude a static oil pressure increase at the orifice exit. Lubrication film thickness over the spiral groove land areas determines the film thickness at the gas sealing dam. Additionally the spiral groove outward pumping action also prevents weeping of oil inward toward the gas seal dam.

The hydrodynamic effect over the land areas supports the seal unbalanced force. Film thicknesses (see Figure B2) in the order of .0001 inches have been measured when operating with oil with bulk viscosity of 10 centistokes at 130°F and at speeds between 10 and 20 ft/sec. Film thickness is expected to vary with oil flow quantity, seal geometry, oil viscosity and sliding speed.

The oil expelled from the seal interface is caught by a baffle which redirects the oil. "Punched out" tabs in the baffle redirect approximately ½ of the oil to the nosepiece and carrier; the other ½ is redirected by the main body of the baffle to cool the spring and the piston ring area.

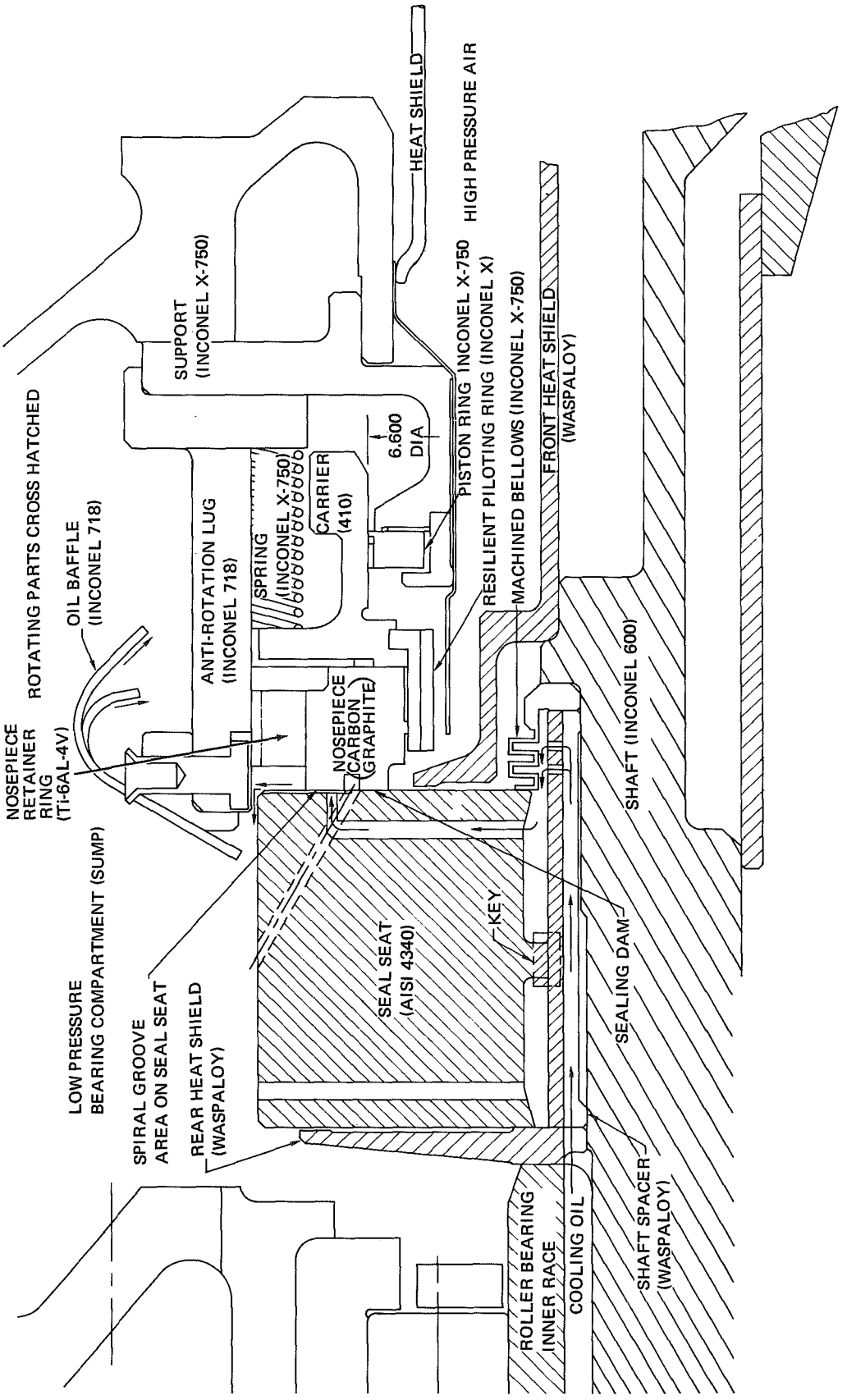

Figure B1 Oil-Film Seal Design

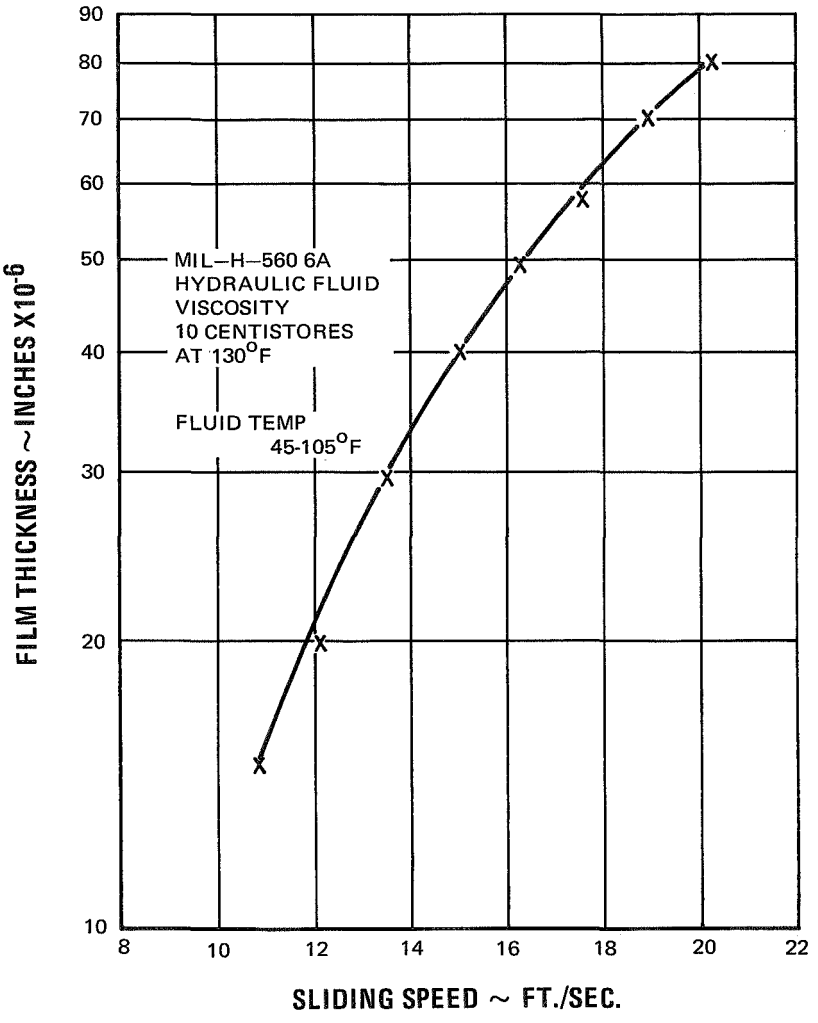

Figure B2 Film Thicknesses in the Oil-Film Seal

APPENDIX C
ANALYSIS OF SELF-ACTING GEOMETRY (RAYLEIGH STEP LIFT PAD) FOR GAS FILM SEAL

by
J. Zuk
Lewis Research Center
Cleveland, Ohio

National Aeronautics and Space Administration

DESCRIPTION OF FACE SEAL WITH SELF-ACTING GEOMETRY

Figure C1 shows a face-type seal with a self-acting pad geometry that consists of a series of shallow recesses arranged circumferentially around the seal under the sealing dam. It should be noted that the lift geometries are bounded at the inside and outside diameters by the sealed pressure P_1. This is accomplished by feed slots that connect the annular groove directly under the sealing dam with the sealed pressure in the cavity. The effect of the self-acting geometry on face seal operation is illustrated in figure C2, which shows parallel sealing faces operating without rubbing contact because of a balance between the closing force and the opening force, that is, the self-acting lift force plus the pressure acting between the sealing faces. If the seal tends to close, the gas bearing force increases to prevent rubbing contact; thus, a condition of no rubbing contact can prevail except at startup and shutdown.

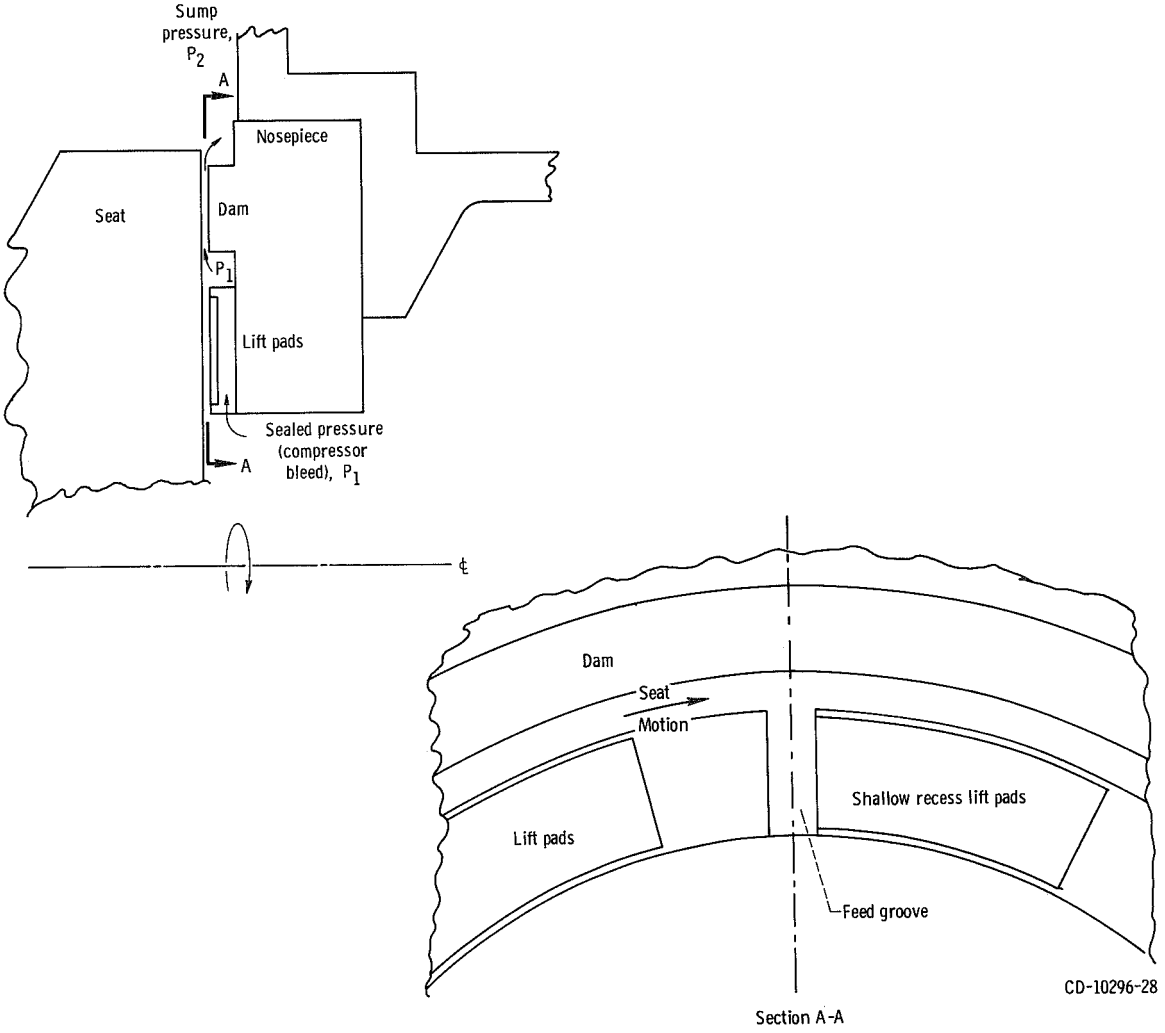

Figure C1 Face Seal With Self-Acting Lift Pads (Rayleigh Pad)

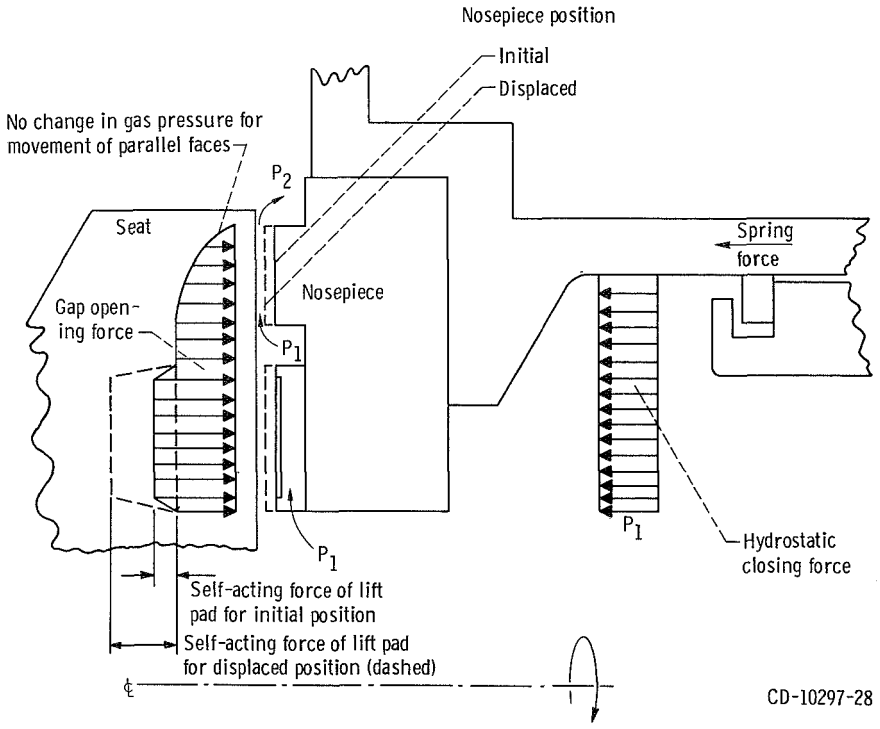

(a) Mechanical, penumatic, and self-acting forces on seal nosepiece.

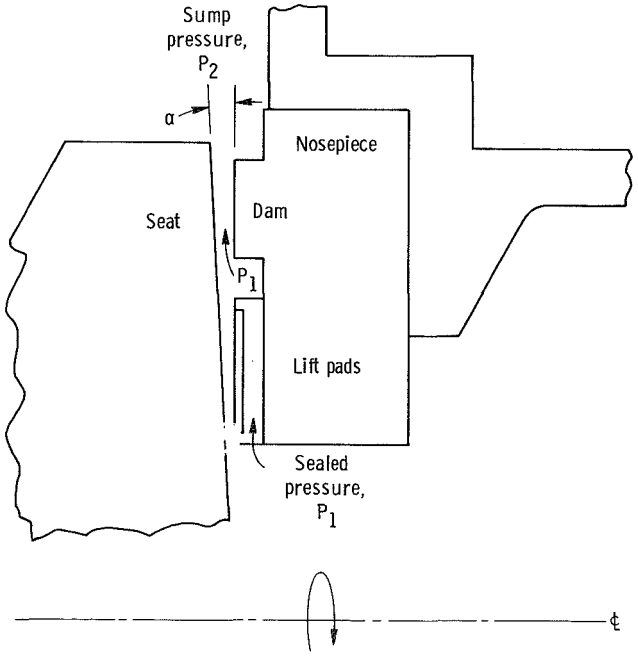

(b) Seal with divergent sealing faces

Figure C2 Self-Acting Face Seal

DESIGN POINTS

For the purpose of analysis, three design points were selected as representative of operating conditions in the advanced gas turbine (see table C1).

MODEL OF SELF-ACTING LIFT GEOMETRY

A single self-acting pad (shrouded step-type), which served as the mathematical model, is shown in figure C3. The radial width b of all pads was 0.20 inch (0.507 cm), and the length c was determined by the number of pads arranged circumferentially under the sealing dam. Because of the large radius-to-pad width ratio r/b, the curvature was neglected in the mathematical model. Thus, the pad boundaries conform to a Cartesian coordinate system. The feed-groove width f was held constant for all pads. The recess length-to-land length ratio R/L was varied between 0.4 and 1.8. Also, the effect on load capacity of the ratio of recess depth to film thickness Δ/h_m was determined over the range of $(\Delta + h_m)/h_m = 1.52$ to 6.0. Calculations of load capacity were made for the parallel film case and for the case with a 2-milliradian angular deformation. This angular deformation was chosen as a practical case that might occur as the result of thermal gradients. Figure C4 shows the actual dimensions of one of the pad designs.

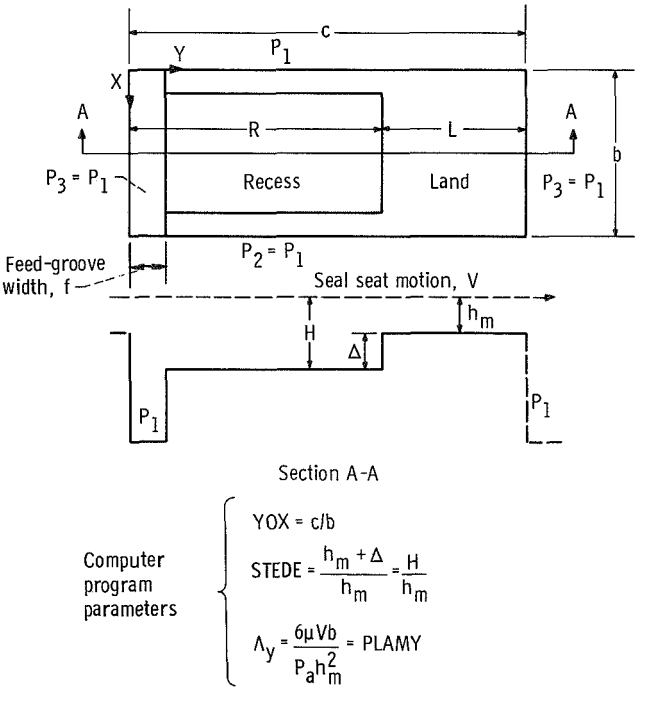

Figure C3 Model of Single Self-Acting Pad (Shrouded Rayleigh Step Type)

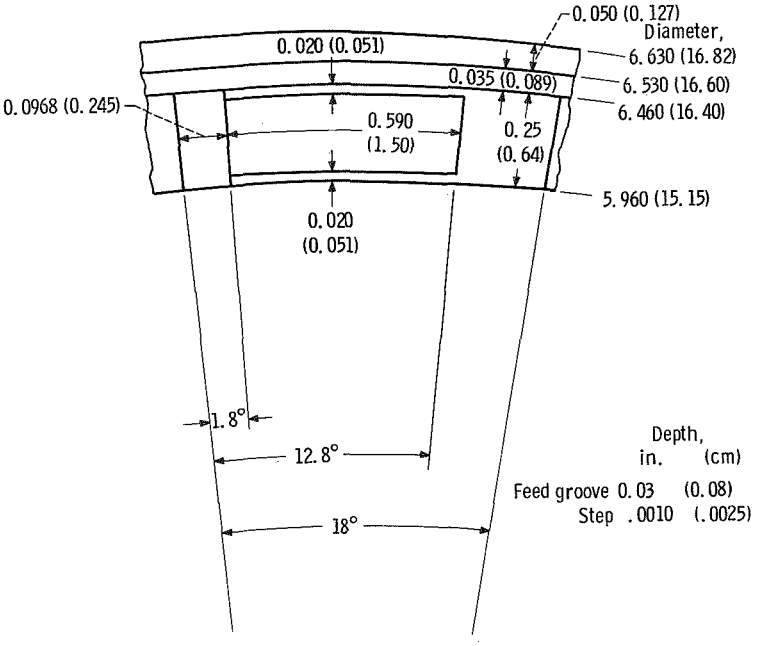

Figure C4 Details of Sealing Dam and Self-Acting Pad Geometry. All Dimensions Are in Inches (cm).

The computer program listing in reference 5, which is valid for a shrouded lift pad, is used for this study. This computer program has been modified (as shown in reference 3) so that it can be used on the Lewis Research Center computer, and the input has been modified for NAME LIST to facilitate parametric design studies. The program solves the complete two-dimensional compressible flow Reynolds lubrication equation written in the P^2 form

$$\frac{\partial}{\partial X}\left(\frac{H^3}{2}\frac{\partial P^2}{\partial X}\right)+\frac{\partial}{\partial Y}\left(\frac{H^3}{2}\frac{\partial P^2}{\partial Y}\right)=\Lambda_x\frac{\partial(PH)}{\partial X}+\Lambda_y\frac{\partial(PH)}{\partial Y}$$

where

$$\Lambda_x=\frac{6\mu Ub}{P_a h_m^2} \qquad \Lambda_y=\frac{6\mu Vb}{P_a h_m^2}$$

The formulation of this analysis is given in reference 6. For details of the solution of the foregoing equation, see appendix B in reference 7. A discussion of the use of the program for a nonparallel film is given in appendix A of reference 5. The following assumptions or restrictions apply in the present analysis:

(1) The fluid is Newtonian and viscous. A laminar flow regime is assumed. It should be noted that it is possible for the seal assembly to be operated in the transition or slip flow regime for clearances less than 0.0001 inch (0.00025 cm), and the analysis is not valid in this slip regime.

(2) The bulk modulus, $3\lambda + 2\mu = 0$, is Stokes idealization and is valid since local shocks are not present and the flow is analyzed for the continuum flow regimes.

(3) The body forces are negligible.

(4) The flow is laminar for a maximum film thickness of 0.001 inch (0.003 cm). The maximum Reynolds number is 658, which is considerably less than the minimum transition rotational Reynolds number of about 1900.

(5) The modified or reduced pressure flow Reynolds number is much less than 1. For example, at design point 3 in table CI, the modified Reynolds number is in the range of 0.023. Thus, the Reynolds equation should be valid for the model of the self-acting lift pad.

TABLE CI DESIGN POINTS

	DESIGN POINT		
	1	2	3
Velocity, V, ft/sec (m/sec)	200 (61)	500 (153)	450 (137)
Sealed gas pressure, P_1, psia (N/cm^2 abs)	65 (45)	215 (148)	315 (217)
Sealed gas temperature, T_1, °F (K)	100 (311)	800 (700)	1300 (977)
Sump pressure, P_2, psia (N/cm^2 abs)	15 (10.3)	15 (10.3)	15 (10.3)
Viscosity, μ, (lb)(sec)/$in.^2$ ((N)(sec)/cm^2)	2.7×10^{-9} (1.9×10^{-10})	4.87×10^{-9} (3.36×10^{-10})	6.00×10^{-9} (4.14×10^{-10})
Operating condition	Descent	Takeoff and climb	Cruise

The compressibility number Λ_y was calculated for each of the three design points (see table CI) at various film thicknesses (see Ref. 3) by using the following relations:

Design point 1:

$$\Lambda_y = \frac{15.2 \times 10^{-8}}{h_m^2}$$

Design point 2:

$$\Lambda_y = \frac{20.4 \times 10^{-8}}{h_m^2}$$

Design point 3:

$$\Lambda_y = \frac{15.4 \times 10^{-8}}{h_m^2}$$

EFFECT OF NUMBER OF SELF-ACTING LIFT PADS

The load capacity of the self-acting pads as a function of the number of pads is shown in figure C5. As the number of pads increases, the circumferential length of each pad

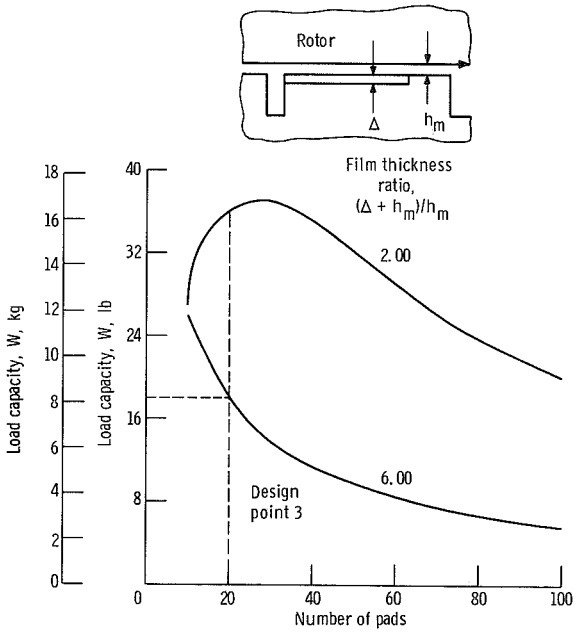

Figure C5 Load Capacity of Shrouded Self-Acting Lift Pads as Function of Number of Pads. Sealed Pressure, 315 psia (217 N/cm^2 abs); Sealed Gas Temperature, 1300°F (977 K); Sliding Velocity, 450 Feet Per Second (137 m/sec).

necessarily decreases in order to fit the available region under the sealing dam. The calculations were made at design point 3, which has a pressure differential of 300 psi (206 N/cm^2) and a sealed gas temperature of 1300°F (977 K). The sliding velocity was 450 feet per second (137 m/sec). At a film thickness ratio of $(\Delta + h_m)/h_m = 2$, which is a practical ratio for a large operating film thickness, an optimum is indicated at 28 pads. However, at a film thickness ratio of $(\Delta + h_m)/h_m = 6$, which is a practical ratio for a small operating thickness, no optimum is indicated and the load capacity increases as the number of pads decreases. Since the seal is expected to operate at various film thicknesses, a compromise in the number of pads must be sought, and the number selected was 20.

EFFECT OF RECESS LENGTH-TO-LAND LENGTH RATIO

The load capacity as a function of recess length-to-land length ratio R/L for symmetric and asymmetric designs is shown in Figure C6. The calculation was made for design point 3 of Table I with the film thickness ratio of $(\Delta + h_m)/h_m = 6$. A symmetric design has a slightly greater load capacity than an asymmetric design, and the curve trend suggests that a recessed land length ratio R/L of 1.8 or greater will provide near optimum capacity. Because of wear considerations, it is desirable to have the land length as long as practical; therefore, a recess-to-land length ratio of 1.4 was selected as a compromise between wear and load capacity considerations.

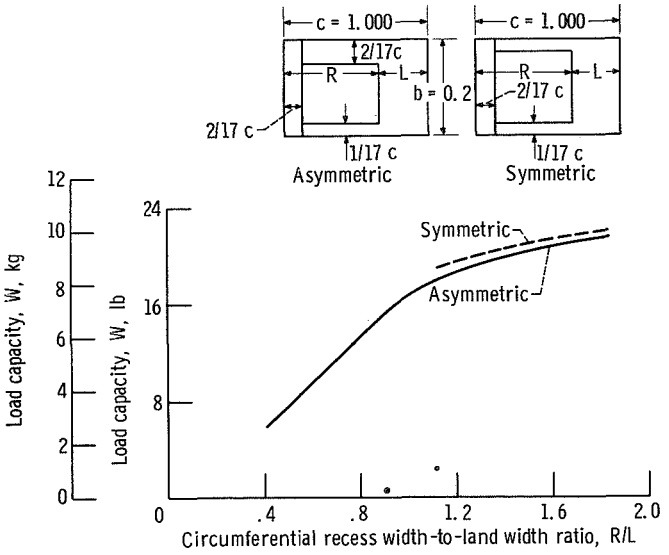

Figure C6 Load Capacity of Shrouded Self-Acting Lift Pads as Function of Recess Length-to-Land Length ratio. Sealed pressure, 315 psia (217 N/cm^2 abs); sealed gas temperature, 1300°F (977 K); sliding velocity, 450 feet per second (137 m/sec); number of pads, 20; film thickness ratio, 6; compressibility number in circumferential direction, 1.78.

EFFECT OF RECESS DEPTH-TO-FILM THICKNESS RATIO

The load capacity as a function of film thickness ratio $(\Delta + h_m)/h_m$ is shown in Figure C7. The optimum film thickness ratio is near $(\Delta + h_m)/h_m = 2$. However, under dynamic opera-

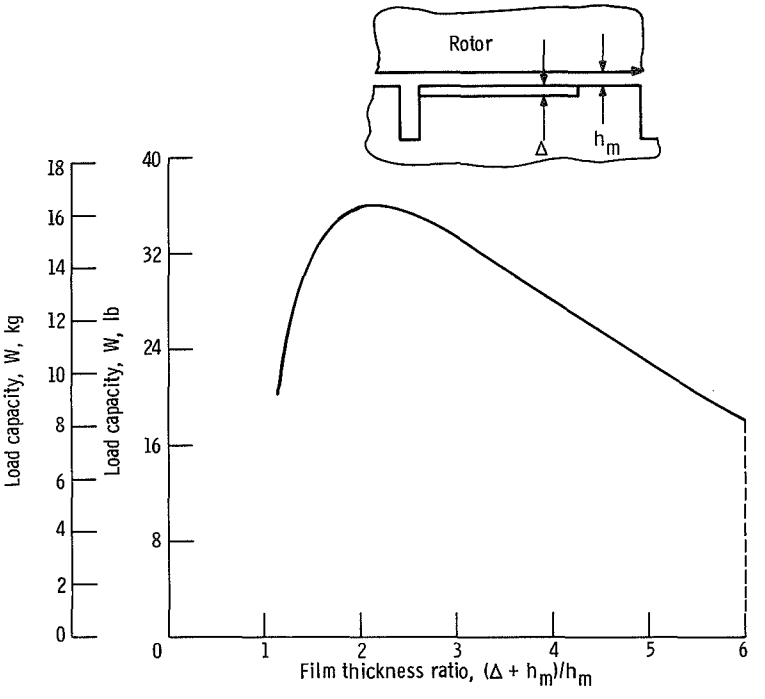

Figure C7 Load Capacity of Shrouded Self-Acting Lift Pads as Function of Film Thickness Ratio. Sealed pressure, 315 psia (217 N/cm^2 abs); sealed gas temperature, 1300°F (977 K); sliding velocity, 450 feet per second (137 m/sec); number of pads, 20 (h_m was fixed, recess depth was varied, $\Lambda = 1.7$)

tion, the film thickness is expected to vary because of the inherent runout of the seal seat face. Thus, in operation, a range of film thickness ratios is expected. Because of leaking considerations, the film thickness of 0.0004 inch (0.0010 cm) is a practical average operating condition; and for this case, the recess depth would be 0.0004 inch (0.0010 cm) to achieve the optimum value of $(\Delta + h_m)/h_m = 2$. However, in order to provide increased wear capability, a recess depth of 0.001 inch (0.00254 cm) was selected. Thus, for a film thickness of 0.0004 inch (0.0010 cm), the film thickness ratio is $(\Delta + h_m)/h_m = 3.5$.

LOAD CAPACITY AS FUNCTION OF FILM THICKNESS

The load capacity for the three design points listed in Table C1 is shown in Figure C8.

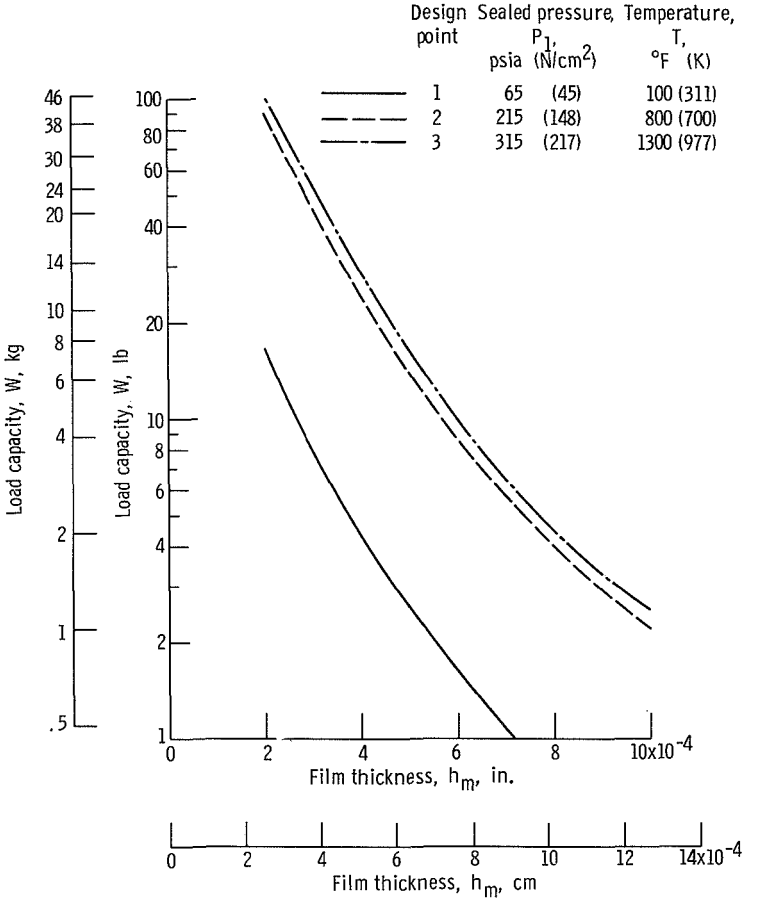

Figure C8 Load Capacity of Shrouded Self-Acting Lift Pads as Function of Film Thickness. Number of pads, 20; recess length-to-land length ratio, 1.4.

The calculations are for 20 pads and a recess depth of 0.001 inch (0.003 cm). The curves reveal a high film stiffness that is advantageous for seal operations; that is, at low film thicknesses, a high lift force is produced to prevent rubbing contact and at high film thicknesses, which would have high leakage, only a low lift force is produced. Thus, if the seal opens, the pad lift force drops off sharply, and the closing force acts to return the nose to the equilibrium condition.

EFFECT OF FACE ANGULAR DEFORMATION

The effect of face angular deformation on load capacity is shown in Figure C9. A deformation of 2 milliradians was selected as a practical value that might occur as a result of axial thermal gradients in the seal faces. This angular deformation results in a loss in load capacity. For example, Figure 9 shows a 27-pound (12-kg) load capacity for parallel faces and a 21-pound (9.5-kg) load capacity for faces with a mean film thickness of 0.0004 inch (0.0010 cm) and a 2-milliradian deformation. This loss in load capacity is not excessive and indicates that the self-acting geometry can accommodate some face deformation. (See ref. 5 for discussion of techniques in minimizing deformations in seals.)

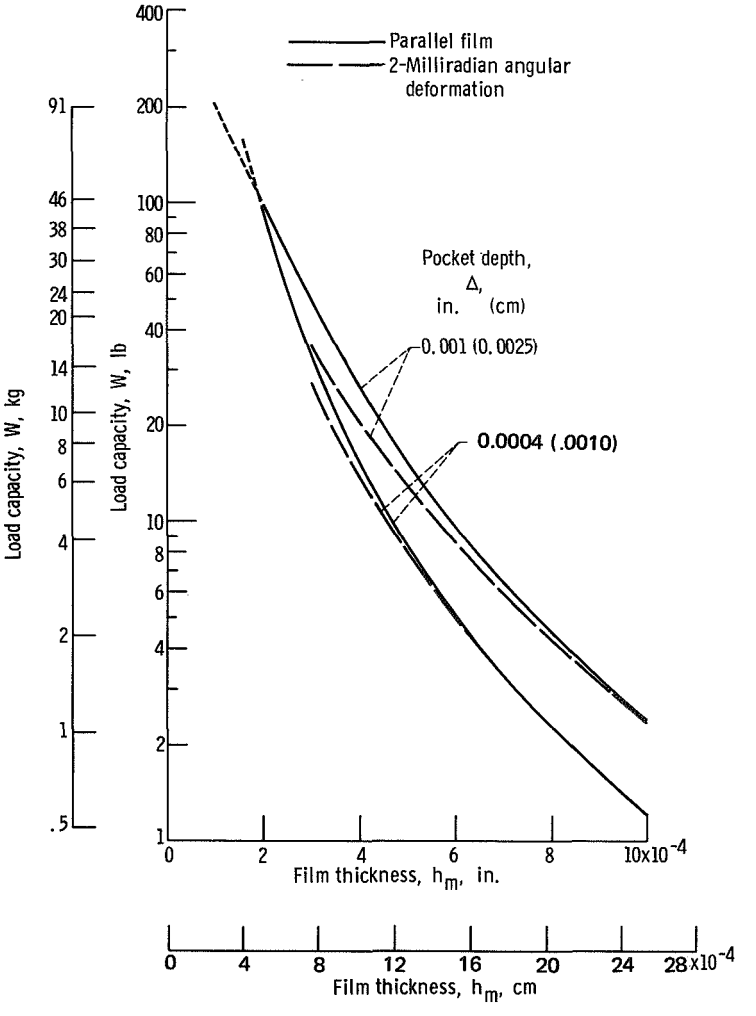

Figure C9 Load Capacity of Self-Acting Geometry as Function of Angular Deformation. Sealed pressure, 315 psia (217 N/cm^2 abs); sealed gas temperature, 1300°F (977 K); sliding velocity 400 feet per second (122 m/sec); number of pads, 20; recess length-to-land length ratio, 1.4; recess depths, 0.0010 inch (0.0025 cm) and 0.0004 inch (0.0010 cm).

EFFECT OF RECESS DEPTH ON FILM STIFFNESS

The 0.001-inch (0.003-cm) recess depth was selected as a practical value because a compromise between wear and load capacity was necessary. A comparison of the 0.001-inch (0.003-cm) depth with the 0.0004-inch (0.0010-cm) depth demonstrates the penalty paid for the compromise. Figure C10 shows load capacity as a function of film thickness for each of the two recess depths. The 0.001-inch (0.003-cm) recess depth has a greater load capacity except at very small film thicknesses, that is, at 0.0002 inch (0.0005 cm) and below. The important point is that the shallow recess has a higher film stiffness (curve of steeper load against film height), and this higher film stiffness is desirable in seal operation; that is, if the seal tends to open, the self-acting force drops off rapidly and, hence, the closing force increases rapidly. If the seal tends to close, the opposite effect occurs.

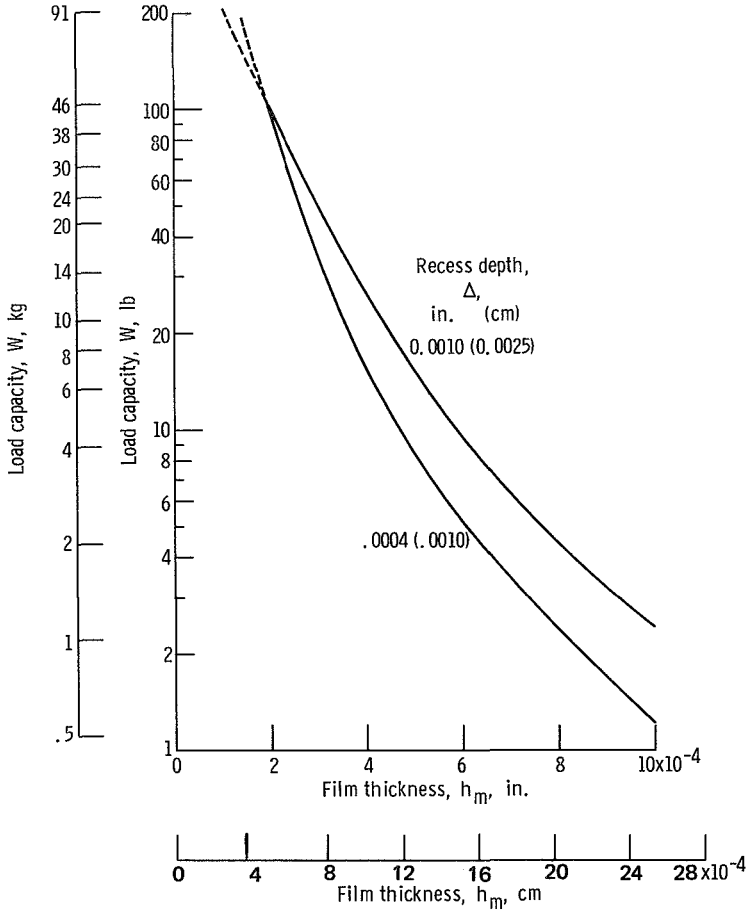

Figure C10 Effect of Recess Depth on Load Capacity of Self-Acting Lift Pads. Sealed pressure, 315 psia (217 N/cm^2 abs); sealed gas temperature, 1300°F (977 K); sliding velocity, 450 feet per second (137 m/sec); number of pads, 20; recess length-to-land length ratio, 1.4.

SUMMARY OF RESULTS OF APPENDIX C

A parametric study was made on a face seal with a self-acting lift geometry having a 6.5-inch (16.5-cm) nominal diameter. Sealed gas pressures of 65, 215, and 315 psia (45, 148, and 217 N/cm^2 abs) were considered. The load carrying capacity of the self-acting geometry was calculated for various recess depths, film thicknesses, angular deformations, and numbers of self-acting pads. A self-acting geometry was placed on a high-pressure side of the seal dam inside diameter. The analysis yielded the following results:

1. The characteristic steep gradient of lift force against gap height of the self-acting geometry was responsible for maintaining the small sealing gap height necessary for low leakage. That is, if the seal tends to open, the lift force drops off rapidly; hence, the closing force increases rapidly. If the seal tends to close, the opposite effect occurs. Thus, the self-acting geometry provides a high gas film stiffness, which is necessary if the nosepiece is to track dynamically the face runout of the seal seat.

2. The gradient of self-acting lift force against film thickness was affected by the recess pad depth; the shallower recesses produced a steeper gradient.

3. For faces with angular deformation (e.g., due to thermal gradients), the self-acting lift force was less than that for parallel faces. Calculations for practical values of angular deformation indicated that the self-acting geometry produces a useful load.

4. The self-acting pad geometry selected was a compromise between wear and load capacity considerations; that is, the recess depth selected was deeper than the optimum, and the recess length-to-land length ratio was smaller than the optimum.

SYMBOLS FOR APPENDIX C

A pad area, $in.^2$; cm^2

b self-acting pad radial width, in.; cm

c self-acting pad circumferential length, in.; cm

f feed-groove circumferential length, in.; cm

H recess depth plus film thickness, in.; cm

h film thickness, in.; cm

L land circumferential length, in.; cm

P static pressure, psi; N/cm^2

R recess circumferential length, in.; cm

r radius, in.; cm

T temperature, °F; K

U moving seal seat radial surface speed, ft/sec; m/sec

V moving seal seat circumferential surface speed, ft/sec; m/sec

W load capacity, lb; kg

X radial coordinate direction

Y circumferential coordinate direction

α relative inclination angle of surface, milliradians

Δ recess or pocket depth, in.; cm

Λ_x compressibility number in radial direction, $6 \mu Ub/P_a h^2_m$

Λ_y compressibility number in circumferential direction, $6 \mu Vb/P_a h^2_m$

λ second viscosity coefficient or coefficient of bulk viscosity

μ absolute or dynamic viscosity, (lb)(sec)/$in.^2$; (N)(sec)/cm^2

Subscripts:

a ambient conditions

m mean

1 sealed conditions

2 sump conditions

APPENDIX D
SEALING DAM DESIGN ANALYSIS

by
J. Zuk
Lewis Research Center
Cleveland, Ohio

National Aeronautics and Space Administration

SEALING DAM DESIGN ANALYSIS

The sealing dam analysis is based on a sealing dam model described in references 8 and 9. The model consists of two parallel, co-axial, circular rings in relative rotation at a constant speed separated by a very narrow gap (Fig. D1). A pressure differential exists between the ring's inner and outer radii. The cavities on either side (i.d. and o.d.) of the sealing dam are assumed to be constant pressure reservoirs.

Refer to references 8 and 9 for details of the assumptions; however, the following pertinent comments should be noted:

1. The effect of the rotational flow on the hydrostatic radial flow is neglected. This assumption is justified by using equation (39) from reference 10. For the range of film thickness considered the increase in leakage due to rotation would only be 2.6 percent, 7.9 percent and 4.3 percent for design points 1, 2 and 3, respectively (see table DI).

2. For subsonic flow, Mach number $\leq 1/\sqrt{\gamma}$, the analysis of reference 8 will be used. This analysis finds an exact solution for this case when the viscous friction is balanced by the pressure drop. For this condition the entrance pressure drop is small, hence $P_1 = P'_1$ and $P_2 = P'_2$ (see fig. D1). The flow is basically isothermal for the film thickness range studied. Neglecting rotation, theoretically it can be shown that the isothermal and adiabatic flow solutions are identical. This analysis yields the classical cubic dependence of mass flow on film thickness. Also this analysis enables small tilts of the sealing dam surfaces to be studied. These small tilts simulate seal face deformation which can occur due to thermal, centrifugal, etc., effects. The equations used for this analysis are summarized in table DII.

3. For flow approaching Mach 1 where the flow chokes, the inertia force neglected in reference 8 becomes important. Also the flow behaves more as an adiabatic flow rather than isothermal. The mathematics is very complex because of the nonlinearity of the inertia terms; thus an approximate analytical model must be used. In this model the flow is analyzed as a quasi-one dimensional flow utilizing a control volume integral analysis. The viscous effect is represented by a mean friction factor which has been observed to be almost invariant under many an ensemble of fluid mechanics experiments, geometries, and conditions. See reference 9 for details. For the purposes of this analysis a mean friction factor of 24/Re will be used. This friction factor can be derived from the exact analysis of reference 8 for subsonic flow. Figure D2 shows that the leakage flow rate analysis of references 8 and 9 coincide until the Mach number exceeds 0.845 where the isothermal viscous flow model loses its validity. This model is valid for choked flow. The flow is choked at the exit. The area expansion is negligible in this design (i.d./o.d. = 0.985). For purposes of this design study the effect of different surface temperatures and the heat source in the fluid film due to rotation will be neglected. In this case it will be shown that there is a pressure drop at the entrance ($P'_1 \neq P_1$) and due to choking at the exit $P'_2 \neq P_2$.

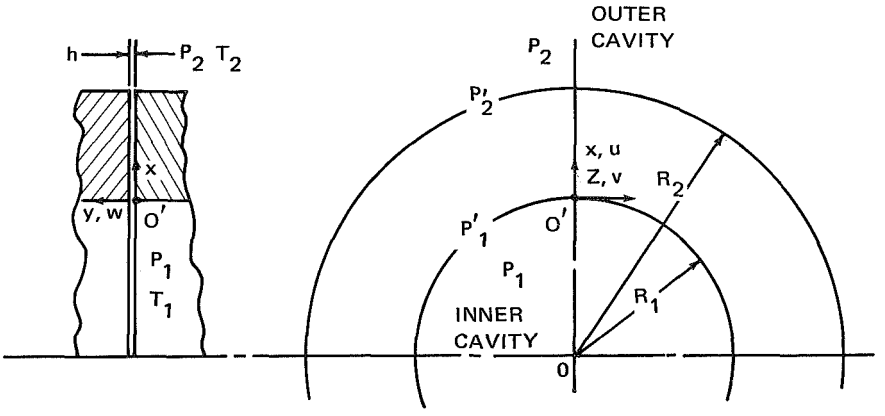

A. PARALLEL SEALING FACES

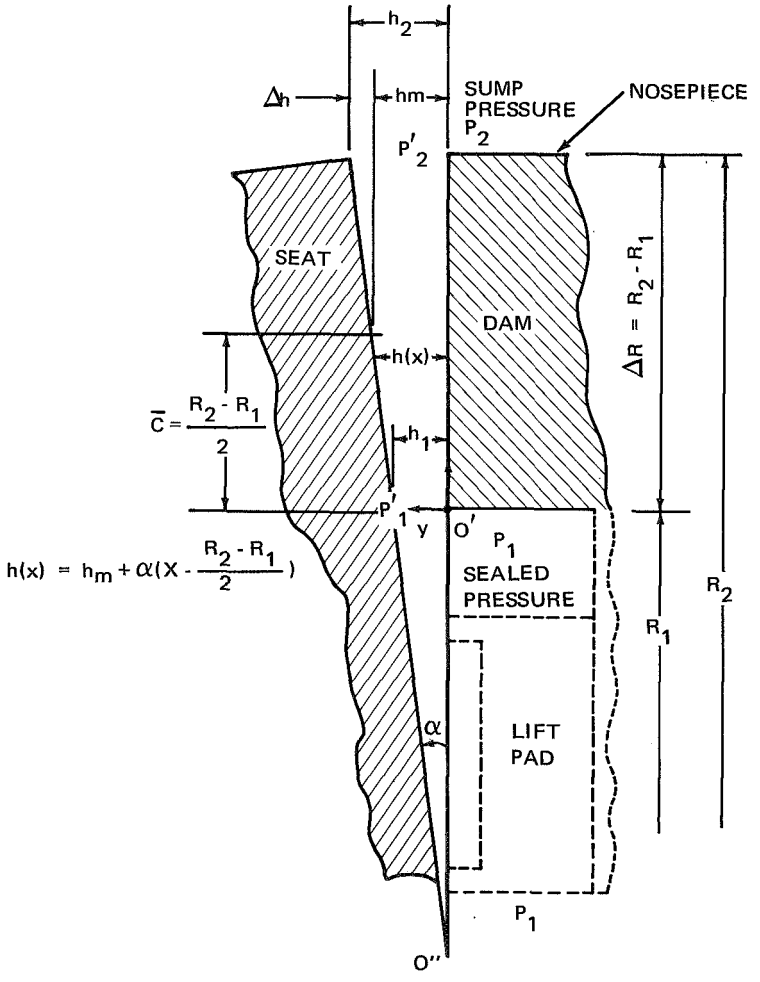

B. SEALING FACES WITH SMALL TILT
(FACE DEFORMATION)

Figure D1 Model and Notation of Sealing Faces (Dam)

TABLE DI - DESIGN POINTS - REPRESENTATIVE OF ADVANCED AIRCRAFT GAS TURBINE OPERATION

	Design Points		
	1	2	3
Operating condition simulated	Descent	Takeoff and Climb	Cruise
Velocity, V, ft/sec (m/sec) (mean relative surface speed of seal dam surfaces)	200 (61)	500 (153)	450 (137)
Sealed gas pressure, P_1, psia (N/cm^2 abs)	65 (45)	215 (148)	315 (217)
Sealed gas temperature, T_1, °F (K)	100 (311)	800 (700)	1300 (977)
Sump pressure, P_2, psia (N/cm^2 abs)	15 (10.3)	15 (10.3)	15 (10.3)
Viscosity of air, (lb)(sec)/in.^{2} ((N) (sec)/cm^2)	2.75×10^{-9} (1.9×10^{-10})	4.87×10^{-9} (3.3×10^{-10})	6.00×10^{-9} (4.14×10^{-10})

TABLE DII
SUMMARY OF SUBSONIC FLOW EQUATIONS
FROM REF. 8

Leakage Flow Rate

$$Q = \left\{ \begin{matrix} 2.726 \\ 0.001287 \end{matrix} \right\} \frac{h^3_{char}\, L\, (P_1^2 - P_2^2)}{\mu RT\, (R_2 - R_1)} \left\{ \begin{matrix} \text{S.C.F.M.} \\ \text{S.C.M.S.} \end{matrix} \right\}$$

Pressure Distribution

Parallel Film Case

$$P = P_2 \left[1 - \left(1 - \frac{P_1^2}{P_2^2} \right) \left(\frac{R_2 - r}{R_2 - R_1} \right) \right]^{1/2}$$

Small Deformation Case

$$P = P_1 \left[1 + \frac{\left[\left(\frac{P_2}{P_1} \right)^2 - 1 \right] h_2^2\, X\, (2B + \alpha X)}{2 (R_2 - R_1)\, h_m\, (B + \alpha X)^2} \right]^{1/2}$$

Sealing Dam Force

Parallel Film Case

$$F = \frac{2P_1 L (R_2 - R_1) \left[1 - \left(\frac{P_2}{P_1} \right)^3 \right]}{3 \left[1 - \left(\frac{P_2}{P_1} \right)^2 \right]}$$

Small Deformation Case

$$F = L \int_0^{R_2 - R_1} (P - P_{min})\, dX$$

(Evaluated Numerically)

Radial Center of Pressure

Parallel Film Case

$$R_c = \frac{L\, (R_2 - R_1)^2}{F} \left\{ \frac{P_1 \left[\frac{2}{5} \left(\frac{P_2}{P_1} \right)^5 - \frac{2}{3} \left(\frac{P_2}{P_1} \right)^3 + \frac{4}{15} \right]}{\left[1 - \left(\frac{P_2}{P_1} \right)^2 \right]^2} - \frac{P_{min}}{2} \right\}$$

Small Deformation Case

$$R_c = \frac{L}{F} \int_0^{R_2 - R_1} (P - P_{min})\, x dx,$$

(Evaluated Numerically)

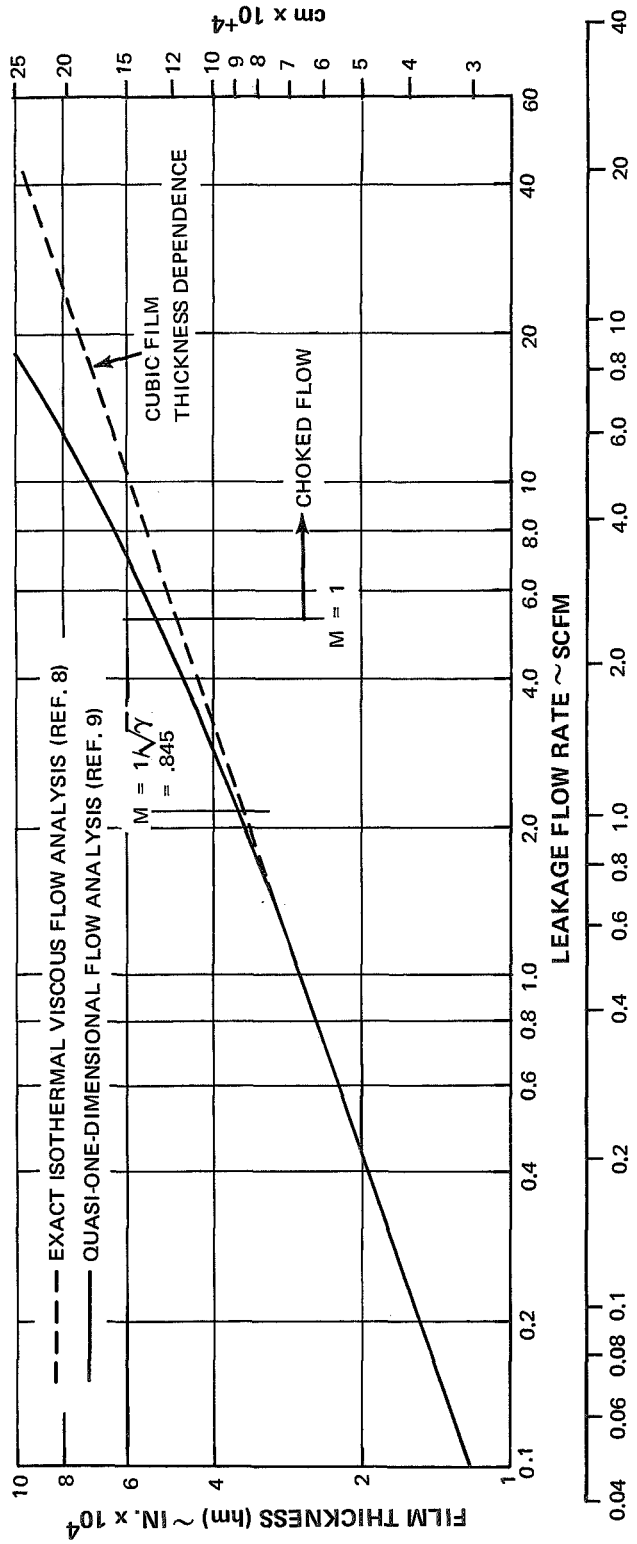

Figure D2 Seal Gas Leakage as a Function of Film Thickness for Parallel Sealing Dam Surfaces and Design Point No. 1. Radial Dam Width, ΔR = 50 Mils (0.127 cm); Sealed Air Pressure, P_1 = 65 psia (45 N/cm² abs); Sump Pressure, P_2 = 15 psia (10.3 N/cm² abs); Sealed Gas Temperature, T_1 = 100°F (311 K)

RESULTS

The results that are found were obtained by using the computer programs found in references 8 and 9. These two references appeared to be the best available models simulating the actual gas film seal.

The design of the gas film seal required finding the smallest film thickness so the leakage is a minimum but yet a large enough film thickness such that both the power dissipation and subsequent shear heating is tolerable and potential seal face deformations can be accomodated. A rough calculation showed that the gap must be at least 0.1 mil for parallel surfaces. A larger gap than a 0.1 mil (.00254 cm) is necessary to accommodate deformation of the sealing faces. The effect of the sealing dam radial width (ΔR) on force balance suggested that radial widths of 20 mil (0.051 cm), 50 mil (0.127 cm), 80 mil (0.203 cm) and 100 mil (0.254 cm) be investigated in detail. Leakage flow rates of less than 25 SCFM (1.18×10^{-3} SCMS) were desired for all three design points.

Leakage Flow Rates

Figure D2 shows the relationship between film thickness and gas leakage flow from the high pressure side into the sump (low pressure side). The calculations for 65 psia (45 N/cm^2 abs) and 100°F (311 K) (design point 1, table DI) were obtained from the seal analysis computer programs (refs. 8 and 9) and are for parallel surfaces and a sealing dam of 50 mils (0.127 cm) in radial width. For small film thickness 0.2 mil (0.0005 cm) the leakage is small, in the range of 0.43 SCFM (2.06×10^{-4} SCMS), but because of the cubic dependence of leakage on film thickness, a slight change in film thickness significantly affects leakage. Even though the pressure ratio is approximately 4 to 1, choking occurs for a film thickness of 0.52 mil (0.00131 cm). Note that for gaps larger than 0.3 mil (0.000756 cm) the leakage has a less than cubic dependence on gap. The limiting case would be a linear dependence which would be achieved when the film thickness is on the order of the sealing dam radial width of 50 mils. This would be a choked orifice flow which linearly varies with film thickness.

Figure D3 shows the effect of operating pressure and temperature on seal leakage for parallel sealing surfaces for the three design points. Note that choking occurs at film thicknesses of 0.52 mils (0.00131 cm), 0.22 mils (0.00054 cm), and 0.17 mils (0.000429 cm) for design points 1, 2, and 3, respectively. Also notice that transition to turbulence has occurred for design points 2 and 3 at a film thickness of 0.9 mils (0.00227 cm); the radial flow Reynolds number has exceeded 2300. This Reynolds number, based on hydraulic diameter, has been chosen to be the critical transition Reynolds number.

Figure D4 shows the effect of sealing dam radial width on leakage flow at design point 2. The four radial widths of 20 mils (0.051 cm), 50 mils (0.127 cm), 80 mils (0.201 cm) and 100 mills (0.254 cm) are those used in this study. Also shown are 5-mil (0.0127-cm) and 10-mil (0.0254 cm) radial width dams. These plots illustrate that from strictly a leakage point of view the longest leakage path possible is most desirable. However, the leakage path length must be compromised from a force balance point of view when surface deformations occur.

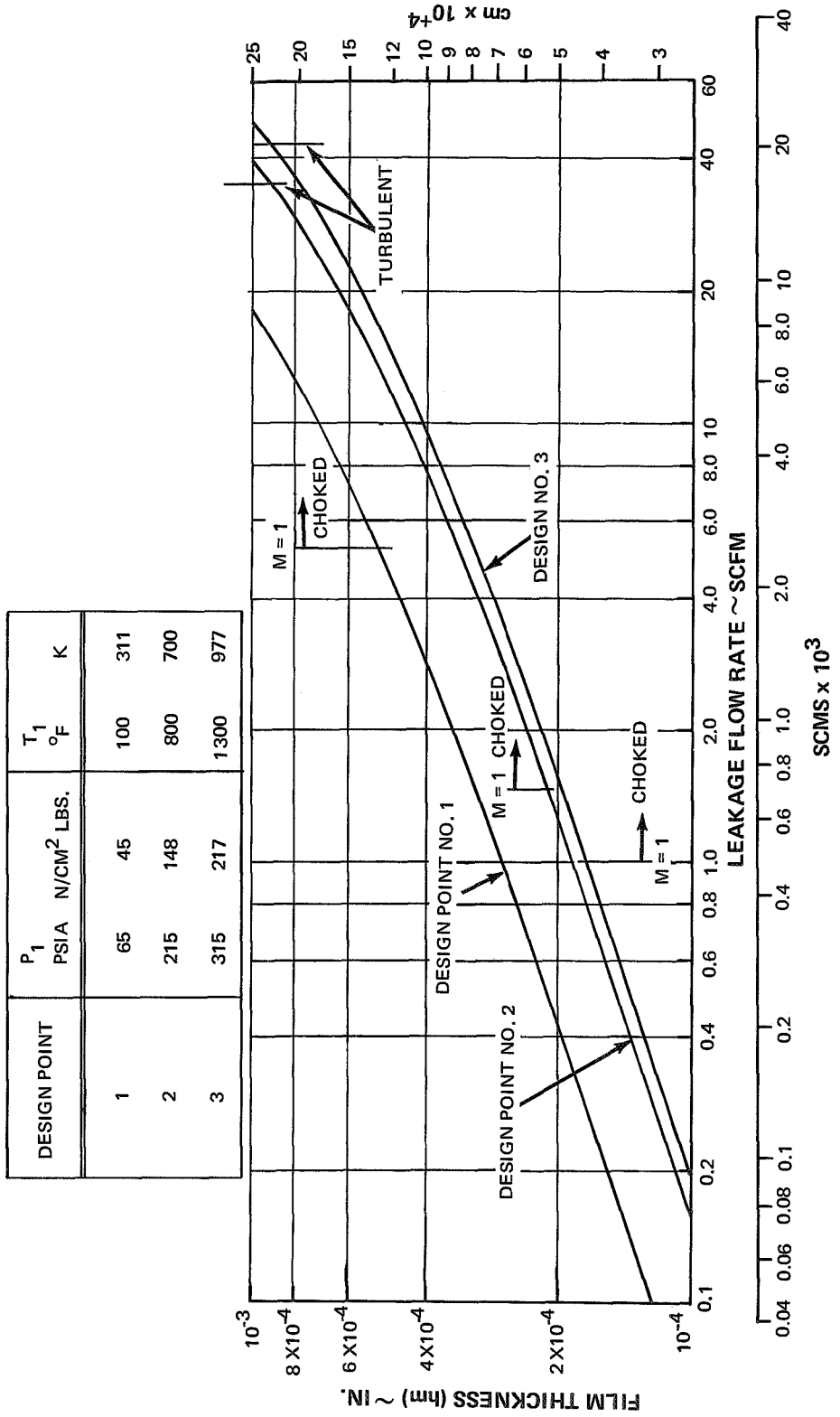

Figure D3 Effect of Operating Point (Pressure and Temperature) on Seal Gas Leakage; Parallel Sealing Surfaces ($\alpha = 0$); Sealing Face Radial Length, 50 Mils (0.127 cm); Sump Pressure, P_2 = 15 psia (10.2 N/cm^2 abs); Sealed Fluid, Air

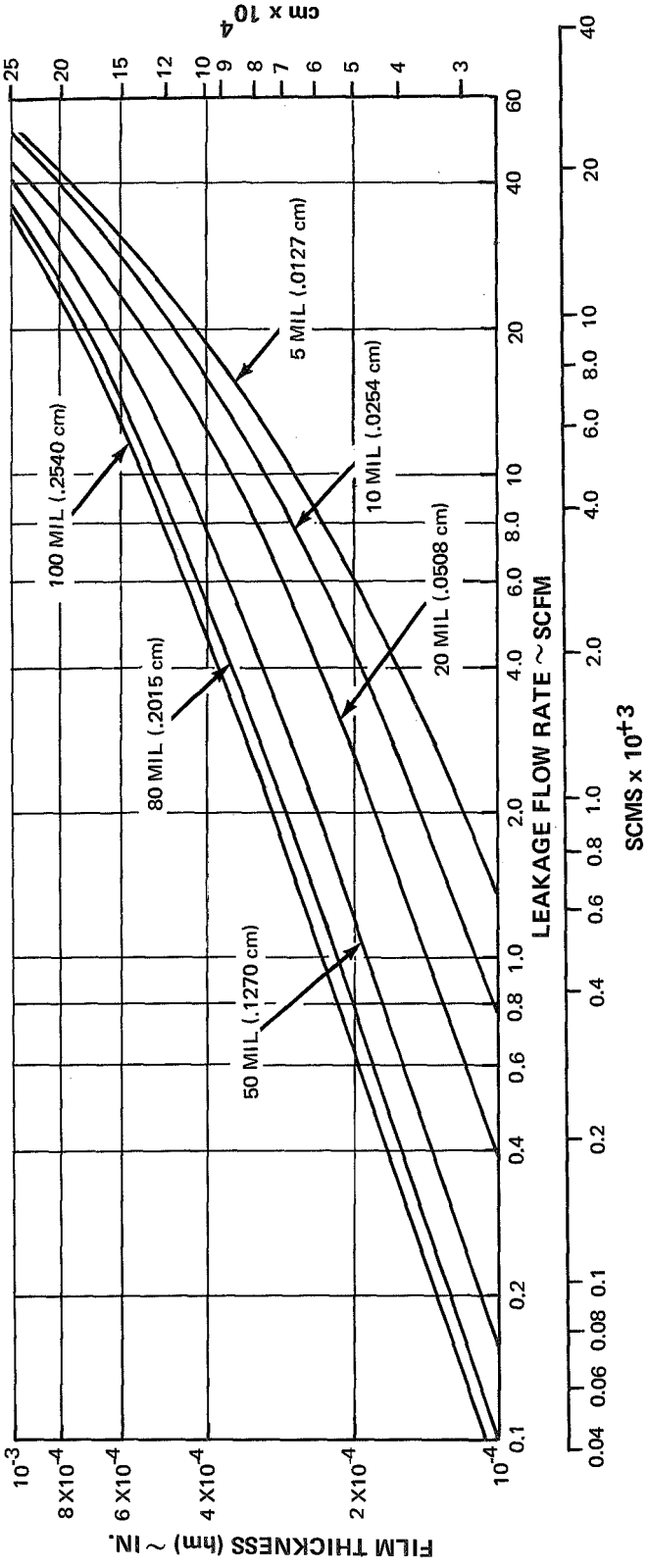

Figure D4 Effect of Seal Face Radial Length on Seal Leakage; Parallel Sealing Faces for Design Point 2. Sump Pressure, P_2 = 15 psia (10.3 N/cm^2 abs) Sealed Pressure, P_1 = 215 psia (148 N/cm^2 abs); Sealed Gas Temperature, 800°F (700 K); Sealed Fluid, Air

Figure D5 shows, for parallel sealing faces, the normalized pressure as a function of radial position within the sealing gap: The normalized pressure gradient for the three operating design points (see table DI) are shown; and since the faces are parallel, the profile is independent of film thickness. However, the profiles shown are valid only below the choking points (Mach no. <0.845).

For nonparallel sealing surfaces the pressure gradients are dependent on film thickness and ref. 11 has the details of the nonparallel analysis as well as calculated sealing dam opening force and center of pressure.

GROSS SEAL CHARACTERISTICS

The gas film seal operating film thicknesses can be found by equating the closing forces with the opening forces. The closing forces are comprised of the spring (mechanical) force and a hydrostatic (pneumatic) closing force. (A spring force of 6.6 pounds was chosen.) The hydrostatic closing force is determined by the bore diameter against which the secondary seal (piston ring) mates (Figure C2(a)).

The results are summarized on Table DIII. Note that a leakage of 25 SCFM (1.18×10^{-3} SCMS) or less can be expected for the three design points shown. This is about an order of magnitude less than that achieved by conventional labyrinth seal practice.

TABLE DIII

SUMMARY OF GROSS SHAFT FACE SEAL (WITH SELF-ACTING LIFT AUGMENTATION) CHARACTERISTICS DETERMINED FROM A FORCE BALANCE (PARALLEL FILM)

Design point	Closing force, lbf (kg)		Total force, lbf (kg)	Opening force, lbf (kg)		Operating gap, mils (μm)	Leakage flow rate, SCFM (SCMS)
	Hydrostatic	Spring		Sealing dam	Pad		(Primary Face)
1	36.1 (16.4)	6.6 (3.0)	42.7 (19.4)	31.3 (14.2)	11.4 (5.18)	0.25 (6.30)	0.83 (3.92×10^{-4})
2	144.4 (65.6)	6.6 (3.0)	151 (68.7)	141.8 (64.5)	9.2 (4.19)	0.59 (14.9)	17.5 (8.26×10^{-4})
3	216.7 (98.5)	6.6 (3.0)	223.3 (101.5)	214.8 (97.6)	8.5 (3.87)	0.63 (15.9)	25 (1.18×10^{-3})

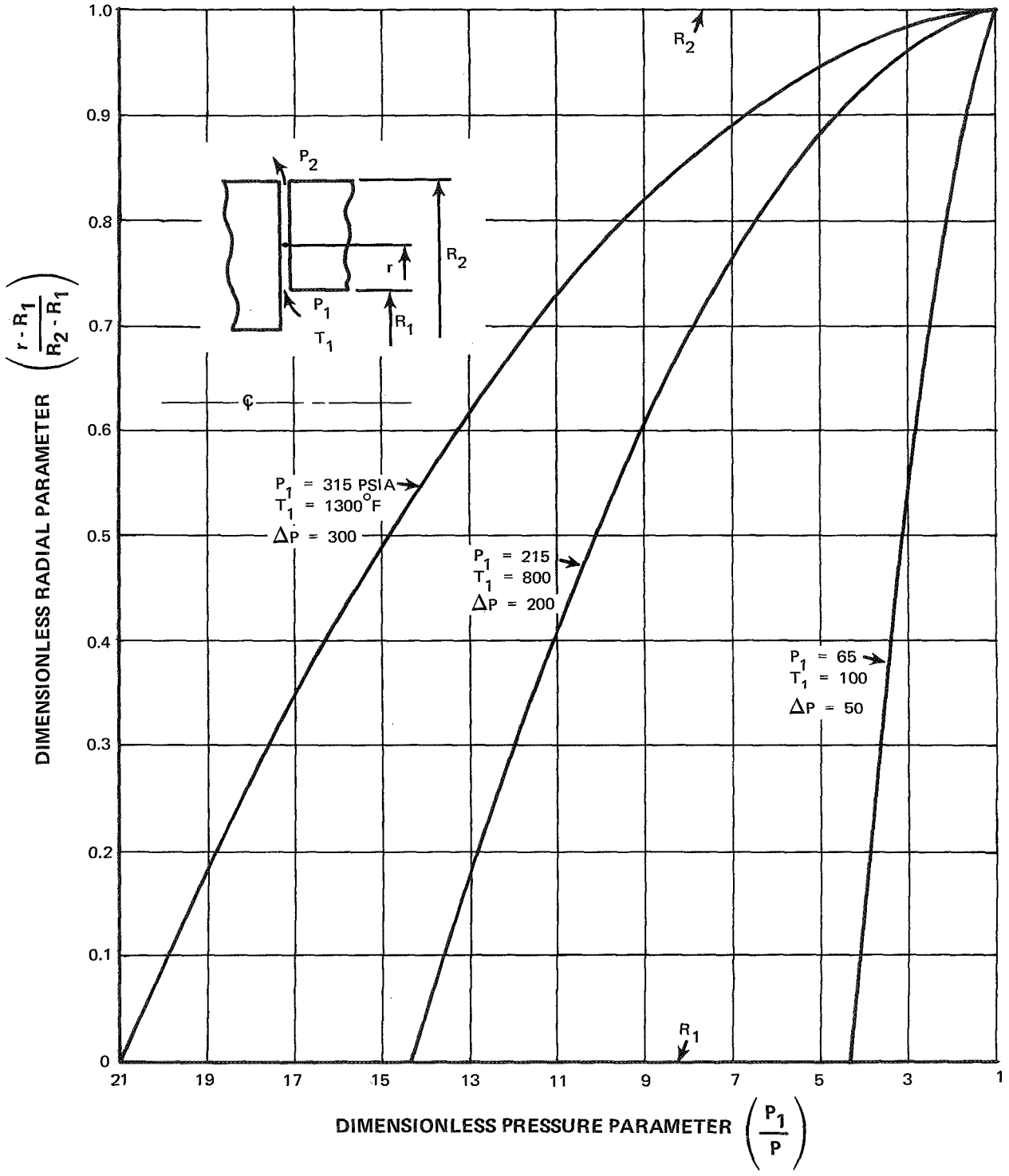

Figure D5 Gas Pressure Gradient (Profile) within Sealing Faces; Parallel Sealing Faces ($\alpha = 0$); Sump Pressure, P_2 = 15 psia (10.3 N/cm² abs); Non-choked Flow

SYMBOLS FOR APPENDIX D

B	constant = $h_m - \frac{\alpha(R_2-R_1)}{2}$
F	sealing dam force , lbf; N
$\bar{f}$	mean friction factor
h	film thickness, in.; cm
h_{char}	characteristic film thickness = $\left(\frac{h_1^2\ h_2^2}{h_m}\right)^{1/3}$, in.; cm
L	sealing dam circumferential length, in.; cm
M	Mach number
P	pressure, psi; N/m^2
P_1	sealed pressure
P'_1	static pressure at sealing dam entrance
P_2	sump pressure
P'_2	static pressure at sealing dam exit
Q	net leakage (volume) flow rate, SCFM; SCMS
R	radius, in.; cm
ΔR	sealing dam radial width, $R_2 - R_1$, in.; cm
R	gas constant, universal gas constant/molecular weight,
a	ft-lbf/(lbm) (°R); J/kg - K
Re	Reynolds number
R_c	center of pressure in radial or x-direction, in.; cm (referenced from inner diameter)
r	radial direction coordinate
T	temperature, °F; K

V	mean relative surface speeds of seal dam surfaces, ft/sec; m/sec
x	coordinate in pressure gradient direction (radial direction)
y	coordinate across film thickness
z	shear flow coordinate in Cartesian system
α	relative inclination angle of sealing dam surfaces, rad
γ	specific heat ratio, C_p/C_v
μ	absolute or dynamic viscosity, (lbf-sec)/ft^2; N-sec/m^2
ρ	density, (lbf) (sec^2)/ft^4; kg/m^3

Subscripts

av	average
char	based on characteristic film thickness
h	based on film thickness
m	mean
r	based on radius
1	inner cavity
2	outer cavity

REFERENCES

Details of the calculation methods and considerations used to design the seals are found in the following references.

1. L. P. Ludwig, T. N. Strom, G. P. Allen, and R. L. Johnson; *Improving the Performance of Face-Contract Seal in Liquid Sodium (400°F to 1000°F) by Incorporation of Spiral-Groove Geometry;* NASA TN D-3942

2. T. Russell, G. P. Allen, L. P. Ludwig, and R. L. Johnson; *Gas Turbine Face Seal Thermal Deformation and Computer Program for Calculation of Axisymmetric Temperature Field;* NASA TN D-5606; December 1969

3. J. Zuk, L. P. Ludwig, and R. L. Johnson; *Study of Shaft Face Seal with Self-Acting Lift Augmentation;* "I. Design of Self-Acting Geometry"

4. R. L. Johnson and L. P. Ludwig; *Shaft Face Seal with Self-Acting Lift Augmentation for Advanced Gas Turbine Engines;* NASA TN D-5170

5. R. M. Hawkins; *Development of Compressor End Seals, Stator Interstage Seals, and Stator Pivot Seals in Advanced Air Breathing Propulsion Systems;* Ref. PWA-2875, Pratt & Whitney Aircraft (NASA CR-83786); July 20, 1966

6. H. S. Cheng, V. Castelli, and C. Y. Chow; "Performance Characteristics of Spiral-Groove and Shrouded Rayleigh-Step Profiles for High-Speed Non-Contacting Gas Seals"; *Journal of Lubrication Technology,* vol. 91, no. 1; January 1969; pp. 60-68

7. R. M. Hawkins and C. A. Knapp; *Development of Compressor End Seals, Stator Interstage Seals, and Stator Pivot Seals in Advanced Air Breathing Propulsion Systems;* Ref. PWA-2752, Pratt & Whitney Aircraft (NASA CR-54625); January 20, 1966

8. J. Zuk and P. J. Smith; *Computer Program for Viscous, Isothermal Compressible Flow Across a Sealing Dam With Small Tilt Angle;* NASA TN D-5373; August 1969

9. J. Zuk and P. J. Smith; *Computer Program for Quasi-One-Dimensional Flow Across a Sealing Dam;* Proposed NASA TN

10. J. Zuk and L. P. Ludwig; *Investigation of Isothermal Compressible Flow Across a Rotating Sealing Dam;* "I - Analysis"; NASA TN D-5344; September 1969

11. J. Zuk, L. P. Ludwig, and R. L. Johnson; *Design Study of Shaft Face Seal with Self-Acting Lift Augmentation;* "II - Sealing Dam"; Proposed NASA TN D-7006

Distribution List

Addressee	Number of Copies
NASA Headquarters Washington, D.C. 20546	
Attention: N. F. Rekos (RAP)	1
A. J. Evans (RAD)	1
J. Maltz (RRM)	1
J. J. Gangler (RRM)	1
NASA-Lewis Research Center 21000 Brookpark Road Cleveland, Ohio 44135	
Attention: A. Ginsburg, MS 5-3	1
E. E. Bisson, MS 5-3	1
R. L. Johnson, MS 23-2	1
W. R. Loomis, MS 23-2	1
L. P. Ludwig, MS 23-2	6
M. A. Swikert, MS 23-2	1
E. Schiopota, MS 77-3	1
J. E. Dilley, MS 500-309	1
J. H. Childs, MS 60-4	1
Report Control Office, MS 5-5	1
Library, MS 60-3	1
Technology Utilization Office, MS 3-19	1
Dr. B. Lubarsky, MS 3-3	1
NASA-Scientific and Technical Information Facility P.O. Box 33 College Park, Maryland 20740	
Attention: NASA Representative	6
NASA-Langley Research Center Langley Station Hampton, Virginia 23365	
Attention: Mark R. Nichols	1
United States Air Force Wright-Patterson Air Force Base AF Systems Command USAF Wright-Patterson AFB, Ohio 45433	
Attention: AFAPL (APDL), K. L. Berkey	1
and L. DeBrohum	1
AFAPL (AFTC), C. Simpson	1
APTP, I.J. Gershon	1
SEJDF, S. Prete	1
MANL, R. Adamczak	1
MANE, R. Headrick	1
MANE, P. House	1
FAA Headquarters 800 Independence Avenue, S.W. Washington, D.C. 20553	
Attention: General J. C. Maxwell	1
F. B. Howard	1

Addressee	Number of Copies
U.S. Naval Air Material Center Aeronautical Engine Laboratory Philadelphia, Pennsylvania 19112	
Attention: A.L. Lockwood	1
U.S. Naval Research Laboratory Washington, D.C.	
Attention: Charles Murphy	1
Department of the Navy Bureau of Naval Weapons Washington, D.C.	
Attention: A.D. Nehman, RAAE-3	1
C.C. Singletorry, RAPP-4	1
Department of the Navy Bureau of Ships Washington, D.C. 20525	
Attention: Harry King, Code 634A	1
Department of Navy Naval Air Systems Command AIR-330 Washington, D.C. 20360	1
U.S. Navy Marine Engineering Laboratory Friction and Wear Division Annapolis, Maryland	
Attention: R. B. Snapp	1
Department of the Army U.S. Army Aviation Materials Labs. Fort Eustis, Virginia 23604	
Attention: John W. White, Chief Propulsion Division	1
U.S. Army Ordnance Rock Island Arsenal Laboratory Rock Island, Illinois	
Attention: R. LeMar	1
Aerospace Corporation Building A-2 P.O. Box 95085 Los Angeles, California 90045	
Attention: James Todd	1
AVCOM AMSAVEGTT Mart Building 405 South 12th Street St. Louis, Missouri 63100	
Attention: E. England	1
Aerojet-General Corporation 20545 Center Ridge Road Cleveland, Ohio 44116	
Attention: W. L. Snapp	1

Addressee	Number of Copies
Advance Carbon Products, Inc. Hampshire & Mariposa Streets San Francisco, California 94110 Attention: W. J. Crader	1
Avco Corporation Lycoming Division 550 South Main Street Stratford, Connecticut 06497 Attention: R. Cuny	1
Battelle Memorial Institute 505 King Avenue Columbus, Ohio 43201 Attention: C.M. Allen	1
Bendix Corporation Fisher Building Detroit, Michigan 48202 Attention: L. B. Young	1
B.F. Goodrich Company Aerospace & Defense Products Division Troy, Ohio Attention: L. S. Blalkowski	1
Boeing Aircraft Company 224 N. Wilkinson Dayton, Ohio 45402 Attention: H. W. Walker J. D. Raisbeok	1 1
Borg-Warner Corporation Roy C. Ingersoll Research Center Wolf and Algonquin Roads Des Plaines, Illinois 60018	1
Carborundum Company Graphite Products 2050 Corry Drive Sanborn, New York 14132 Attention: R. M. Markel	1
Cartiseal Corporation 634 Glenn Avenue Wheeling, Illinois 60090 Attention: R. Voltik	1
Chicago Rawhide Manufacturing Company 900 North State Street Elgin, Illinois 60121 Attention: R. Blair	1
Clevite Corporation Cleveland Graphite Bronze Division 17000 St. Clair Avenue Cleveland, Ohio 44110 Attention: Thomas H. Koenig	1
Continental Aviation & Engineering 12700 Kercheval Detroit, Michigan 48215 Attention: A. J. Follman	1
Crane Packing Company 6400 W. Oakton Street Morton Grove, Illinois 60053 Attention: Harry Tankus	1
Defense Ceramics Information Center Battelle Memorial Institute Columbus Labs, Room 11-9021 505 King Avenue Columbus, Ohio 43201	1
McDonnell Douglas Corporation 333 West First Street Dayton, Ohio 45402 Attention: R. G. Donmoyer	1
Durametallic Corporation Kalamazoo, Michigan Attention: H. Hummer	1
E.I. DuPont de Nemours & Company 1007 Market Street Wilmington, Delaware 19898 Attention: N.W. Todd	1
Fairchild Hiller Corporation Stratos Group Orinoco Drive Bay Shore, New York 11706	1
Fairchild Hiller Corporation Republic Aviation Division Farmingdale, L.I., New York 11735 Attention: D. Schroeder	1
Franklin Institute Laboratories 20th and Parkway Philadelphia, Pennsylvania 19103 Attention: V. J. Gordon W. Shapiro	1 1
Garlock, Incorporated Palmyra, New York 14522 Attention: E.W. Fisher	1
Garrett Corporation AiResearch Manufacturing Division 9851-9951 Sepulveda Blvd. Los Angeles, California 90009 Attention: A. Silver	1

Addressee	Number of Copies
General Dynamics Corporation 5100 West 164 Street Cleveland, Ohio 44142 Attention: W.J. Gkudtner, Jr.	1
Hitco 1600 West 135 Street Gardena, California 90249 Attention: Mrs. Sherril Hisaw	1
General Electric Company Advanced Engine & Technology Department Cincinnati, Ohio 45215 Attention: L.B. Venable G. J. Wile C. C. Moore H-25 W. McCarty	1 1 1 1
General Motors Corporation Allison Division Plant #3, Department 7339 Indianapolis, Indiana 46206 Attention: E.M. Deckman	1
Great Lakes Carbon Corporation 229 Park Avenue New York, New York 10017 Attention: J. P. Sachs R. Hillier	1 1
Gulf General Atomic Inc. P.O. Box 608 San Diego, California 92112 Attention: J. C. Bokros	1
IIT Research Foundation 10 West 35 Street Chicago, Illinois 60616 Attention: Dr. Strohmeier M.A. Schwartz	1 1
Kendall Refining Company Bradford, Pennsylvania 16701 Attention: F.I.I. Lawrence	1
Keystone Carbon Corporation 1935 State St. Marys, Pennsylvania 15857 Attention: B. R. Reuscher	1
Koppers Company, Inc. Metal Products Division Piston Ring and Seal Department P.O. Box 298 Baltimore, Maryland 21203 Attention: F.C. Kuchler E. Taschenburg J. Heck	1 1 1

Addressee	Number of Copies
Lockheed Aircraft Company 118 West First Street Dayton, Ohio 45402 Attention: R.R. Witte	1
Los Alamos Scientific Laboratory University of California Los Alamos, New Mexico Attention: M.C. Smith	1
Martin Marietta Corporation 1700 Needmoor Road Dayton, Ohio 45414 Attention: Z.G. Horvath	1
Mechanical Technology Incorporated 968 Albany-Shaker Road Latham, New York 12110 Attention: Donald F. Wilcock	1
Midwest Aero Industries Corporation 4834 Delemere Avenue Royal Oak, Michigan 48073 Attention: J. Sherlock D. Ramadanoff	1 1
Midwest Research Institute 425 Volker Blvd. Kansas City, Missouri 64110 Attention: V. Hopkins	1
Monsanto Company 800 North Lindbergh Blvd. St. Louis, Missouri 63166 Attention: Dr. W. R. Richard R. Hatton	1 1
Morganite, Incorporated 401 N. Ashe Avenue P.O. Box 347 Dunn, North Carolina 28334 Attention: S. A. Rokaw	1
North American Rockwell Corporation 5100 West 164 Street Cleveland, Ohio 44142 Attention: George Bremer	1
Northrop Corporation 1730 K Street N.W. Suite 903-5 Washington, D.C. 20006 Attention: S.W. Fowler, Jr.	1
Pesco Products Division Borg-Warner Corporation 24700 N. Miles Bedford, Ohio 44146 Attention: W. J. Cieslik	1

Addressee	Number of Copies
Pressure Technology Corporation of America 326 W. Beaver Avenue Boalsburg, Pennsylvania 16827 Attention: Dr. A. Bobrowsky	1
Poco Graphite Incorporated P.O. Box 1524 Garland, Texas 75040 Attention: Dr. R.F. Wehrmann	1
Pure Carbon Company, Inc. 441 Hall Avenue St. Marys, Pennsylvania 15857 Attention: Dr. R. R. Paxton	1
North American Rockwell Corporation Rocketdyne Division 6633 Canoga Avenue Canoga Park, California 91304 Attention: M. Butner	1
Sealol Incorporated P.O. Box 2158 Providence, Rhode Island 02905 Attention: Justus Stevens	1
Sinclair Oil Corporation 600 Fifth Avenue New York, New York 10020 Attention: C. W. McAllister	1
Sinclair Research Incorporated 400 E. Sibley Blvd. Harvey, Illinois Attention: M.R. Fairlie	1
SKF Industries, Incorporated 1100 Frist Avenue King of Prussia, Pennsylvania 19406 Attention: L. B. Sibley	1
Socony Mobil Oil Company Research Department Paulsboro Laboratory Paulsboro, New Jersey Attention: E. Oberright	1
Space Craft Incorporated 5670 Markdale Drive Dayton, Ohio Attention: J.W. Sharp	1
St. Marys Carbon Company 1939 State Road St. Marys, Pennsylvania 15857 Attention: J. E. Lanzel	1

Addressee	Number of Copies
Director Government Research Laboratory Esso Research & Engineering Company P.O. Box 8 Linden, New Jersey 07036	1
Southwest Research Institute P. O. Drawer 28510 San Antonio, Texas 78228 Attention: P.M. Ku	1
Stanford Research Institute 333 Ravenwood Avenue Menlo Park, California 94025 Attention: R. C. Fey	1
Stein Seal Company 20th Street and Indiana Avenue Philadelphia, Pennsylvania 19132 Attention: Dr. P.C. Stein	1
Sun Oil Company Automotive Laboratory Marcus Hook, Pennsylvania 19061 Attention: J. L. Griffith	1
Stackpole Carbon Company St. Marys, Pennsylvania 15857 Attention: Dr. E.I. Shobert	1
Ultra Carbon Corporation 1300 N. Madison Avenue Bay City, Michigan 48706 Attention: Del Hughes	1
United Aircraft Corporation Pratt & Whitney Aircraft Division Engineering Building EB2B-2 East Hartford, Connecticut 06108 Attention: R. Shevchenko	3
United States Graphite Company 1621 Holland Saginaw, Michigan Attention: F. F. Ruhl	1
Westinghouse Electric Corporation 5100 W. 164 Street Cleveland, Ohio 44142 Attention: Lynn Powers	1
Wright Aeronautical Division Curtiss-Wright Corporation 333 West First Street Dayton, Ohio 45402 Attention: D. Lombardo	1

Addressee	Number of Copies
Pennsylvania State University Department of Chemical Engineering University Park, Pennsylvania 16802 Attention: Dr. E. E. Klaus	1
The University of Tennessee Department of Mechanical and Aerospace Engr. Knoxville, Tennessee 37916 Attention: Professor W. K. Stair	1
Dr. C. Fisher	1